Coral species-specific loss and physiological legacy effects are elicited by extended marine heatwave

Strand, E.L.[1*], Wong, K.H.[1,2], Farraj, A.[1], Gray, S.[1], McMenamin, A.[1], Putnam, H.M.[1]

[1] University of Rhode Island
[2] Department of Marine Biology and Ecology, University of Miami Rosenstiel School of Marine and Atmospheric Science, 4600 Rickenbacker Causeway, Miami, FL, 33149, USA.
[*]corresponding author

Key Words

- Physiological legacy
- Double-stressor experiment
- Thermal and ocean acidification tolerance
- Coral-algal symbiosis
- Multivariate statistics
- Symbiodiniaceae communities
- Stress and recovery periods

Abstract

Marine heatwaves are increasing in frequency and intensity, with potentially catastrophic consequences for marine taxa and ecosystems such as coral reefs. Environmentally realistic, extended heatwave and recovery time-series in a multi-stressor experimental framework can therefore provide enhanced predictive capacity for the performance of such systems under climate change. We exposed two common reef-building corals in Hawai‘i, *Montipora capitata* and *Pocillopora acuta*, to a two-month period of high temperature and high pCO_2 conditions (29.5 °C, ~1100 ppm) or ambient conditions (27.5 °C, ~500 ppm) in a factorial design, followed by two months of return to ambient conditions. In response to high temperature, but not high pCO_2, multivariate physiology shifted through time in both species, driven by decreases in respiration rates and endosymbiont density. *P. acuta* exhibited more significantly altered physiology, and substantially higher bleaching and mortality than *M. capitata*. The species-specific sensitivity of

P. acuta appears to be driven by higher baseline rates of photosynthesis and lower initial host antioxidant capacity and thus sensitivity to reactive oxygen species under thermal stress. Thermal tolerance of *M. capitata* may be due in part to harboring a mixture of *Cladocopium* and *Durusdinium spp.*, while *P. acuta* was dominated by other distinct *Cladocopium spp.,* but there was no evidence of Symbiodiniaceae shuffling due to treatment or time. Only *M. capitata* survived the exposure and recovery period, but physiological state in heatwave-exposed *M. capitata* remained significantly diverged at the end of the recovery period relative to *M. capitata* that experienced ambient conditions. In extended heatwave and climate change stressor scenarios, our results indicate a species-specific loss of corals that are driven by baseline differences in both host and symbiont physiology. Notably, the species that survive climate change conditions exhibit lasting physiological legacies that are likely to influence future stress responses.

Introduction

Coral holobionts, organisms composed of an animal coral host, endosymbiont dinoflagellates, and associated microbial community (Rohwer et al. 2002), make up the structure of one of the most ecologically diverse and economically valuable ecosystems in the world: coral reefs. The function and health of the coral holobiont, and therefore coral reefs, is dependent on this multi-partner symbiotic relationship that cycles nutrients and provides each partner with otherwise limited or unavailable nutritional resources (Bourne et al. 2016). However, climate change is impacting the marine environment through increasing ocean temperatures (Masson-Delmotte et al. 2018), specifically marine heatwaves (Oliver et al. 2021), and ocean acidification (Gattuso et al. 2015), among other stressors, challenging the symbiotic function, physiological processes, and ultimately the survival of reef building corals. While ocean acidification will place a chronic energetic strain on coral calcification (Mollica et al. 2018) and cellular acid-base balance (Tresguerres et al. 2017; Gibbin et al. 2014), the dominant physiological stress is currently in the form of increased temperature and increasingly frequent, intense marine heatwaves (Oliver et al.

57 2018; Sweet and Brown 2016). This thermal stress triggers dysbiosis known as “coral bleaching”,
58 or the disruption of the symbiotic relationship between a coral host and their endosymbionts that
59 results in the coral host expelling the endosymbionts, leaving a stark white (“bleached”)
60 appearance and the coral host depleted of their primary carbon source (Gates et al. 1992; Boilard
61 et al. 2020). Mass coral bleaching events due to marine heatwaves have increased in frequency
62 and intensity in recent years (Oliver et al. 2021), and this trend is on track to continue with
63 catastrophic consequences projected for coral reef ecosystems (Heron et al. 2016; Le Nohaïc et
64 al. 2017; Robert van Woesik and Kratochwill 2022).

65 The current understanding of the mechanistic cascade of bleaching is linked to the host
66 and/or symbionts’ response to increased reactive oxygen species (ROS) levels produced under
67 higher temperature that consequently increase oxidative stress and cause a breakdown of
68 photosynthetic processes within the symbiont cells (Weis 2008; Gates et al. 1992). This
69 breakdown causes the symbiont cells to be either digested or expelled via several mechanisms
70 including exocytosis, apoptosis, necrosis, and host cell detachment (Weis 2008; Lesser 2004;
71 Gates et al. 1992). A review of recent studies has shown that oxidative stress can occur in the
72 host first (Oakley and Davy 2018), suggesting that host antioxidant capacity may be critical in
73 tolerating higher levels of temperature stress. However, host response to changing environment
74 conditions has been shown to be highly species-specific (Bahr et al. 2016). In Kaneʻohe Bay,
75 Oʻahu, Hawaiʻi, two common reef-building coral species display differential thermal tolerance:
76 *Montipora capitata* is more resistant and *Pocillopora acuta* is more sensitive to environmental
77 stress (Bahr et al. 2015; Gibbin et al. 2015). The underlying mechanisms to differential tolerance
78 are known to be complex, ranging from genetic influences, epigenetic patterns, and associated
79 endosymbiont and bacterial communities (Putnam 2021), to host morphological structure and
80 tissue thickness differences (Loya et al. 2001), but are not fully understood. Thus multivariate
81 analyses of key processes and traits can provide the capacity to quantify temporal variation in

host, symbiont, and holobiont responses are necessary to more fully elucidate the bleaching cascade (Gardner et al. 2017; Wall et al. 2021; McLachlan et al. 2021).

Although extensive research has been conducted on the effects of increased temperature on coral (Mydlarz et al. 2010; Sweet and Brown 2016; McLachlan et al. 2020; Cziesielski et al. 2019; Lesser 2011; van Oppen and Lough 2018), there are fewer experimental studies that simultaneously address critical environmentally-relevant aspects. Specifically, that concurrently address: 1) mimic daily and seasonal environmental fluctuations (Woesik et al. 2022; Ziegler et al. 2021; Putnam and Edmunds 2011), while 2) accounting for simultaneous, multivariate stressors (Pendleton et al. 2016; Robert van Woesik et al. 2022), 3) sampling with high frequency to capture short and long-term temporal stress and recovery dynamics (Claar et al. 2020; Gardner et al. 2017), 4) occur during environmentally realistic times of the year (Robert van Woesik et al. 2022; Ziegler et al. 2021) and 5) track the survivors following the stress exposure (Claar et al. 2020; Gardner et al. 2017). These factors are particularly important, as exposure to diurnal temperature and pCO_2 fluctuations elicit different responses than stable, or less variable conditions (Putnam and Edmunds 2011; Dufault et al. 2012; Schoepf et al. 2022; Barshis et al. 2013). Further, high frequency sampling of a variety of variables was able to elucidate that symbiont expulsion and bleaching precedes severe holobiont physiological responses and health decline in later stress time points (Gardner et al. 2017). Additionally, seasonal studies of influences on coral physiology (Jurriaans and Hoogenboom 2020; Scheufen et al. 2017; Thornhill et al. 2011; Edmunds and Putnam 2020), highlight the variation in traits based on recent environmental conditions, supporting the need to study bleaching under seasonally realistic conditions to more accurately predict an organism's stress response (e.g., conducting bleaching studies at the timing of the peak of temperature for that region). Thus, increased sampling frequency during long-term studies of exposure and recovery will further our understanding of the mechanisms and sequential timing of the symbiotic state during stress and subsequent recovery.

Considering the need for data from environmentally-relevant, high frequency studies with

multiple response variables under increased temperature and pCO_2 condition projections to improve our understanding of coral biology and forecasting reef futures, we tested the effect of an environmentally realistic extended heatwave in the context of diurnally fluctuating temperature and ocean acidification on coral physiology. Specifically, we conducted a four-month multi-stressor time-series experiment during the fall warming season in Kaneʻohe Bay, Oʻahu, Hawaiʻi to assess the temporal dynamics during exposure to increased temperature and pCO_2 in addition to seasonal change, compare differential stress response in a resilient and sensitive coral species, and elucidate temporal dynamics during recovery and the potential for physiological legacies after an environmental perturbation.

Methods

Coral Collections

Coral fragments (one ~3x3 cm fragment per colony from 75 colonies of *Montipora capitata* and 75 colonies *Pocillopora acuta*) were collected from each of six reef areas ranging across the north to south span of Kāneʻohe Bay including both fringing and patch reefs (Lilipuna.Fringe : 21°25'45.9"N 157°47'28.0"W; Hawaiʻi Institute of Marine Biology (HIMB): 21°26'09.8"N 157°47'12.7"W; Reef.11.3: 21°27'02.9"N 157°47'41.8"W; Reef.18: 21°27'02.9"N 157°48'40.1"W; Reef.35.36: 21°28'26.0"N 157°50'01.2"W; Reef.42.43: 21°28'37.9"N 157°49'36.8"W) under Hawaiʻi Department of Aquatic Resources Special Activity Permit 2019-60, between 4-10 September 2018 (Fig. 1A-B). This collection approach was designed to target a diverse collection of genotypes that represent the coral population for *Montipora capitata* and *Pocillopora acuta* in Kāneʻohe Bay. Coral fragments were brought back to HIMB and affixed in an upright position to individually numbered plastic coral fragment mounting plugs by hot gluing the base of the skeleton to the plug. Coral fragments were allowed to acclimate for ~14 days in outdoor mesocosm tanks and then were randomly allocated to replicate tanks described below.

133 *Experimental Timeline*

134 Coral fragments were exposed to one of four experimental conditions: Ambient
135 Temperature - Ambient pCO_2 (ATAC), Ambient Temperature - High pCO_2 (ATHC), High
136 Temperature - Ambient pCO_2 (HTAC), and High Temperature - High pCO_2 (HTHC) for ~two
137 months (22 September - 17 November 2018; Fig. 1C). Once sampling and treatments were
138 completed, the pCO_2 injections were shut off immediately and the temperature gradually
139 decreased over the course of a week (Fig. 1G), and fragments were exposed to ambient
140 temperature and ambient pCO_2 conditions for ~ two months (18 November 2018 - 12 January
141 2019), identified here as the recovery period. Molecular sampling occurred at the following time
142 points: 0h, 6h, 12h, 30h, and 1, 2, 4, 6, 8, 12, and 16 weeks (Fig. 1D). At each time point, one
143 fragment was selected at random from each tank (n=1 $tank^{-1}$ x 3 tanks $treatment^{-1}$ = 3 fragments
144 $treatment^{-1}$ $species^{-1}$) and placed in sterile whirlpak bags and snap frozen in liquid nitrogen at 13:00
145 each day (with the exception of 6, 12 and 30 hr time points). Physiological sampling occurred at
146 the following time points: 1, 2, 4, 6, 8, 12, and 16 weeks (Fig. 1D). Physiological samples were
147 immediately snap frozen in liquid nitrogen after photosynthetic and respiration rates were
148 measured (described below; n=2 $tank^{-1}$ x 3 tank $treatment^{-1}$ = 6 fragments $treatment^{-1}$ $species^{-1}$
149 $timepoint^{-1}$). All samples were stored at -80°C until subsequent processing.

150

151 *Experimental Tank Setup*

152 Treatment conditions (n=3 replicate tanks $treatment^{-1}$) were randomly assigned to twelve
153 outdoor mesocosm tanks (122 cm x 122 cm x 30 cm; 510 L). Flow rates, measured daily with a
154 graduated cylinder and timer, averaged 84.36 ± 1.20 mL $second^{-1}$ (n=826), providing full
155 mesocosm tank turnover every ~2 hours. Mesocosm tanks were 60% shaded from full irradiance,
156 and photosynthetically active radiation was measured continuously with the Apex cosine
157 corrected PAR Sensor (PMK, Neptune Systems, accuracy = ± 5%) that was cross calibrated to
158 the Li-Cor cosine corrected PAR sensor (LI-193 spherical underwater quantum sensor, LI-COR

159 Biosciences). Additionally, light values (roughly 100-700 PAR) from six different positions in each
160 tank were compared to determine spatial differences within each tank. There was no significant
161 difference in light between positions in each tank (n=4 position^{-1} tank^{-1}; Table S2). Based on these
162 results, light was measured in the center of the tank ~daily for the duration of the experiment using
163 the LI-193 spherical underwater quantum sensor. To further reduce any potential position effects
164 with respect to incoming water, heater position, or bubble stream, the positions of the coral
165 fragments in the tank were changed weekly.
166
167 *Experimental temperature conditions*
168 Temperature treatment conditions were programmed to mimic the natural daily
169 fluctuations of the environment at the collection sites in Kāneʻohe Bay, Hawaiʻi (NOAA Moku o
170 Loʻe Buoy data from September
171 2018, https://www.ndbc.noaa.gov/station_page.php?station=mokh1; Fig. 1G, Fig. S1). Based on
172 these data, high temperature treatment fluctuated between ~29-30°C to reflect previous marine
173 heatwaves in Kāneʻohe Bay, Hawaiʻi (+2°C above ambient temperature). Temperature was
174 monitored with Apex Extended Life Temperature Probes (accuracy = ± 0.05 °C, Neptune
175 Systems) and temperature loggers (HOBO Water Temp Pro v2, accuracy = ±0.21°C, resolution
176 = 0.02°C, Onset Computer Corp) that were placed in each tank at the same height as the coral
177 fragments for the duration of the experiment and logged temperature at 10 minute intervals.
178 Temperature was separately controlled by submersible heaters (ProHeat D-1500 Heater
179 Controllers, precision ± 1°C). Ambient temperature treatments reflected the natural conditions of
180 Kāneʻohe Bay.
181
182 *Experimental pCO_2 conditions*
183 Experimental pCO_2 treatment conditions were based on measurements of ambient
184 conditions in Kāneʻohe Bay, Hawaiʻi (Drupp et al. 2011) and projected future lower pH conditions

185 in embayments, which can have lower mean pH and higher diel fluctuations due to calcification,
186 photosynthesis and respiration of the benthic community and increased residence time in the
187 embayment (Jury et al. 2013; Shaw et al. 2016). The daily fluctuating pH levels in the high pCO_2
188 treatment tanks were maintained between 7.6-7.7 (pH NBS scale) with an independent pH-stat
189 feedback system in each tank and ambient conditions fluctuated between 7.9-8.0 (pH NBS scale;
190 Fig. 1F). To generate the high pCO_2 treatment, two 99.99% food-grade CO_2 cylinders were
191 connected to an automatic gas cylinder changeover system (Assurance Valve Systems,
192 Automatic Gas Changeover Eliminator Valves #6091) to prevent an abrupt shortage of CO_2
193 supply. CO_2 was added into the seawater on-demand through gas flow solenoids (Milwaukee
194 MA955), based on the pH reading (NBS) of a lab grade pH probe (Apex pH, Neptune Systems)
195 in each tank. CO_2 was delivered via airlines plumbed into a venturi injector (Forfuture-go G1/2
196 Garden Irrigation Device Venturi Fertilizer Injector), which was connected to a water circulating
197 pump (Pondmaster Pond-mag Magnetic Drive Water Pump Model 5). Gas injected into the
198 system was either CO_2 or ambient air and bubbling was constant due to the pressure driven pump
199 moving water and gas through the Venturi injector. An Apex AquaController (Neptune Systems)
200 environmental control system with a wifi base unit (Apex Controller Base Unit, Neptune Systems)
201 was linked to 12 individual monitoring units (Apex PM1 pH/ORP Probe Module, Neptune
202 Systems) with Apex lab grade pH Probes (accuracy = ±0.01 pH NBS scale, Neptune Systems),
203 which were used for microprocessor-control of a power strip (Apex Energy Bar 832, Neptune
204 Systems) containing 12 individual solenoids. This pH-stat feedback system constantly monitored
205 seawater temperature and pH conditions.
206
207 *Total Alkalinity and Carbonate Chemistry*
208 Tank parameters (temperature °C, total scale pH, and salinity in psu) were measured
209 ~twice daily using a handheld digital thermometer (Fisherbrand Traceable Platinum Ultra-
210 Accurate Digital Thermometer, accuracy = ±0.05 °C, resolution = 0.001°C) and a portable

multiparameter meter (Thermo Scientific Orion Star A series A325). A pH probe (Mettler Toledo InLab Expert Pro pH probe #51343101; accuracy = ±0.2 mV, resolution = 0.1 mV) and conductivity probe (Orion DuraProbe 4-Electrode Conductivity Cell Model 013010MD; accuracy = 0.5% of psu reading, resolution = 0.01 psu) were used with an Orion A Star meter to measured pH (mV) and salinity (psu), respectively. pH (total scale) was calculated from standard curves of pH (mV) across a range of temperature (°C) in a tris standard (Dickson Laboratory Tris Batch T27 Bottles 269, 236 and Batch T26 Bottle 198). 125 mL water samples were taken from each tank twice a week to measure total alkalinity and along with the pH on the total scale, as described above, was used to calculate carbonate chemistry. An automated titrator (Mettler Toledo T50) was used to titrate water samples with salinity adjusted 0.1M hydrochloric acid (Dickson Laboratory Titrant A3, A14). A non-linear, least-squares procedure of the Gran approach (SOP 3b; Dickson et al. 2007) was used to calculate total alkalinity (TA; μmol kg^{-1} seawater). Accuracy of the titrations was determined using certified reference material (Dickson Laboratory CO_2 CRM Batch 132 [Salinity 33.441, Total alkalinity 2229.24 ± 1.03 μmol kg^{-1}], Batch 137 [Salinity 33.607, Total alkalinity 2231.59 ± 0.62 μmol kg^{-1}], Batch 176 [Salinity 33.532, Total alkalinity 2226.38 ± 0.53 μmol kg^{-1}]; NOAA Ocean Carbon and Acidification Data System). Tank total alkalinity values were only accepted if the total alkalinity value of the CRM from that day was within 1% of the reported CRM. Carbonate values, including aragonite saturation, carbon dioxide, carbonate, dissolved inorganic carbon, bicarbonate, pCO_2, and pH, were calculated using SEACARB (v3.2.16 in R Studio; Jean-Pierre Gattuso et al. 2015) with the following parameters: calculated total pH, calculated total alkalinity, flag=8 [pH and ALK given], P=0, Pt=0, Sit=0, pHscale="T", kf="pf", k1k2="l", and ks="d". Equilibrium constant of hydrogen fluoride (mol/kg) (kf="pf") was set to "pf" for salinities ranging from 10-40 psu and temperature ranging from 9-33°C (Perez and Fraga 1987) and recommended by (Dickson et al. 2007). First (K1) and second dissociation (K2) constant of carbonic acid (mol/kg) (K1) were set to "l" (k1k2="l") for salinities ranging from 19-43 psu and temperature ranging from 2-35°C (k1k2="l"; Lueker et al. 2000). Stability constant of hydrogen sulfate (mol/kg) (Ks) was set

to "d" for using Ks (Dickson 1990) for salinities ranging from 5-45 psu and temperature ranging from 0-45°C. Salinity and temperature inputs were the measurements taken at the time of the water sample collection.

Physiological Response Variables

Survivorship, growth rates, and color score

Survivorship was tracked daily throughout the two-month exposure and two-month recovery periods using a binary score for dead versus alive. Alive was defined as any fragment with live tissue. Growth over time was determined by the buoyant weight technique (Davies 1989; Jokiel et al.1978), using air, freshwater, and saltwater standard curves as a function of temperature. Each coral fragment was buoyant weighed in its respective treatment temperature and pCO_2 conditions. Wet buoyant weight was converted to dry mass using the aragonite density of 2.03 g cm^{-3} for *Montipora spp*. (Anthony and Hoegh-Guldberg 2003) and 2.93 g $cm^{-3}$for *P. acuta* (Jokiel[6] and Maragos 1978). Rates were normalized to surface area and reported in units of mg $CaCO_3$ cm^{-2} d^{-1}. To assess tissue color change over time as a proxy for cell density and pigmentation *sensu* (Edmunds et al. 2003), each coral fragment was photographed once a week (16 timepoints across the 4 month experiment) with a red, blue, green color standards. ImageJ® was used to extract the mean red, green, and blue color score for each coral fragment and these values were normalized to the mean of the red, green, and blue color standards, respectively. The color score was quantified as Principal Component 1 (using princomp function in R) from the principal component analysis (PCA) *sensu* (Edmunds et al. 2003).

Photosynthesis and Respiration Rates

Prior to experimental exposures, 10 coral fragments (5 $species^{-1}$) were used to generate a photosynthesis-irradiance curve to determine saturating irradiance for assessing rates of photosynthesis. Fragments were exposed to 10 light levels: 0, 15, 30, 60, 91, 136, 227, 416,

529, and 756 µmol m^{-2} s^{-1} (as measured by Apex PAR sensor described above) generated by two LED lights (Aqua Illumination Hydra FiftyTwo) hung above the incubation chambers (described below). Rates of oxygen consumption or evolution were extracted using local linear regressions in the LoLinR package (Olito et al. 2017) in µmol L^{-1} s^{-1}. Rates were corrected to chamber volume including coral displacement (µmol s^{-1}). Rates of the blank chambers were subtracted from the rates of the coral fragments within each run to account for background photosynthesis or respiration due to phytoplankton, zooplankton, and bacteria. Rates of oxygen flux were normalized to surface area by the wax dipping technique (Veal et al. 2010) for final units of µmol cm^{-2} h^{-1}. Curve fitting of a non-linear least squares (NLLS) fit for a non-rectangular hyperbola (Marshall and Biscoe 1980; Heberling and Fridley 2013) was used to identify PI curve characteristics of each species, where in the following model PPFD = irradiance in µmol photons m^{-2} s^{-1}, Pnet = net photosynthetic rate (µmol O_2 cm^{-2} h^{-1}), Pmax = maximum gross photosynthetic rate (µmol O_2 cm^{-2} h^{-1}), apparent quantum yield (AQY, ϕ; mol O_2 mol $photons^{-1}$), and Rd is light enhanced dark respiration rate (LEDR; Edmunds and Spencer Davies 1988) (µmol O_2 cm^{-2} h^{-1}).

The PI curve fit equation is as follows:

$$Pnet = \frac{\phi PPFD + \sqrt{(\phi PPFD + P_{max})2 - 4\Theta\phi PPFD + P_{max}}}{2\Theta} - Rd \quad [1]$$

Photosynthesis-irradiance curves were performed four times throughout the experiment to ensure the coral fragments were not reaching photoinhibition (Fig. S4). Fragments were placed in individual respiration chambers (~610mL), with individual temperature (Pt1000 temperature sensor, PreSens Precision Sensing GmbH) and fiber-optic oxygen probes (Oxygen Dipping Probes DP-PSt7, accuracy = ± 0.05% O_2, PreSens Precision Sensing GmbH) connected to a 10-channel oxygen meter (OXY-10 ST, accuracy = ± 1.0 °C, resolution = 0.1 °C, PreSens Precision Sensing GmbH), to evaluate photosynthesis (under saturating light

289 conditions, as determined by PI curves described above) and light enhanced dark respiration
290 (LEDR; Edmunds and Spencer Davies 1988). The respirometry setup consisted of 10 chambers
291 with stirbars. Samples were measured in a series of runs that consisted of eight fragments (n=4
292 per species) and two blank chambers per run, and exposed to PAR irradiance of ~500 µmol
293 photons m^{-2} s^{-1} for 15 minutes to assess photosynthetic rates. Immediately afterwards, these
294 fragments were exposed to dark conditions (0 µmol photons m^{-2} s^{-1}) for 20 minutes to assess
295 LEDR. Following respirometry, fragments were immediately snap-frozen in liquid nitrogen and
296 stored at -80°C. Raw oxygen flux data (temperature corrected) was thinned every 40 seconds
297 and rates of oxygen flux were calculated with local linear regression as described above. Net
298 photosynthesis was calculated by subtracting the oxygen change of the dark runs (a negative
299 value) from the oxygen change of the light runs (a positive value), to isolate photosynthetic rates
300 of the symbionts from the light enhanced dark respiration (LEDR) of the coral holobiont.
301
302 *Tissue removal, surface area, and endosymbiont density*
303 Coral tissue was removed from the coral skeletons by airbrushing (Iwata Eclipse HP-BCS)
304 with ice-cold 1X Phosphate Buffer Saline (PBS) solution and the total volume was recorded. The
305 tissue slurry was then homogenized for 15 seconds at high speed (PRO Scientific Bio-Gen
306 PRO200 Homogenizer, 10 mm Homogenizer Probe). Of the total tissue slurry, aliquots of 500 µL
307 were taken for endosymbiont density, 500 µL for host soluble protein and host total antioxidant
308 capacity, 1 mL for chlorophyll-a concentration assays, and 5 mL for ash-free dry weight. The
309 skeleton was rinsed in freshwater and soaked in 20% bleach for 24 hours and dried at room
310 temperature for 24 hours. The single dip wax-dipping technique (Veal et al. 2010) was used to
311 determine surface area covered by tissue from each dried fragment skeleton. Symbiodiniaceae
312 cell concentration was quantified with 6 technical separately loaded replicate counts on a
313 haemocytometer (Hausser Scientific Bright-Line Counting Chamber) after homogenizing the

314 tissue slurry for 1 minute. The average count (cells mL^{-1}) was standardized to the airbrushed
315 homogenate volume and surface area to produce cell density values in cells cm^{-2}.
316
317 *Host soluble protein and total antioxidant capacity*
318 To quantify host soluble protein and host total antioxidant capacity, the host tissue was
319 isolated from symbionts by centrifugation at 10,000g for 10 minutes at 4°C. Soluble host protein
320 of the supernatant was measured using the Pierce BCA Protein Assay Kit (Pierce
321 Biotechnology, Waltham, Massachusetts, Catalog #23225) with two duplicates per sample
322 measured by a 96 well microplate reader (BioTek Synergy HTX Multi-Mode Reader Model
323 S1LFA) at a wavelength of 562 nm. Resulting values were calculated from a bovine serum
324 albumin standard curve and standardized to homogenate volume and surface area to obtain
325 host soluble protein values (mg cm^{-2}). Host total antioxidant capacity was quantified in duplicates
326 per sample with the Cell BioLabs OxiSelect Total Antioxidant Capacity (TAC) Assay Kit (Catalog
327 #STA-360) according to manufacturer's instructions and compared to a uric acid standard
328 curve. Antioxidants in the sample reduce Copper II to Copper I, resulting in positive correlation
329 between Copper Reducing Equivalents (CRE, mmol L^{-1}) and antioxidant levels. CRE values
330 were standardized to total soluble protein for final values in units of CRE µmol mg^{-1}.
331
332 *Chlorophyll-a concentration*
333 To isolate symbiont cells for chlorophyll concentration measurements, a 1 mL aliquot of
334 tissue homogenate was centrifuged at 13,000 g for 3 min and the supernatant was discarded. 1
335 mL of 100% acetone was added to the symbiont pellet, mixed for 15 sec on a lab vortex mixer,
336 and incubated in the dark at 4°C for 24 hours. Samples and acetone blanks were read in
337 duplicate (200 µL each) on a 96-well microplate reader at λ = 630 and 663 nanometers.
338 Chlorophyll-*a* and c_2 concentrations were calculated with the following dinoflagellate equations
339 for 100% acetone: Chlorophyll-*a* = $11.43E_{663} - 0.64E_{630}$ and Chlorophyll-c_2 $27.09E_{630} - 3.63E_{663}$

340 (Jeffrey and Humphrey 1975). Concentration values were multiplied by 0.584 to correct for the
341 path length of the plate for units of µg ml^{-1} and standardized to the airbrushed homogenate
342 volume, and normalized by surface area (µg cm^{-2}) and per symbiont cell (µg $cell^{-1}$).
343
344 *Tissue Biomass*
345 Tissue biomass was quantified using the ash-free dry weight (AFDW) method.
346 Specifically, 5 mL of tissue slurry was centrifuged at 13,000 g for 3 minutes. 4 mL of the
347 supernatant host tissue was removed and placed in pre-burned aluminum pan weighed on an
348 analytical balance (Mettler Toledo Model ML203T/00) and the symbiont pellet was resuspended
349 in 1 mL PBS solution and added to separate pre-weighed burned aluminum pans. The samples
350 were placed in a drying oven (Thermo Scientific Heratherm General Protocol Oven, Catalog
351 #51028112) for 24 hours at 60°C, weighed, and then placed in a muffle furnace for 4 hours at
352 500°C (Thermo Scientific Lindberg Blue M Muffle Furnace, Catalog #BF51728C-1). AFDW (mg
353 cm^{-2}) of the host and symbiont fractions were calculated as the post-drying oven weight (dry
354 weight) - post-muffle furnace weight and final values were standardized to the airbrushed
355 homogenate volume and normalized to surface area. Symbiont to host (S:H) biomass ratios
356 were calculated by dividing the symbiont AFDW by the host AFDW.
357
358 *Univariate statistical analysis*
359 Due to the near complete mortality during the recovery period in *P. acuta*, only the
360 exposure period was analyzed for the following physiological variables: tissue biomass,
361 chlorophyll-*a* and chlorophyll-c_2 concentration, endosymbiont density, respiration rates,
362 photosynthetic rates, host total antioxidant capacity, and host soluble protein. *M. capitata*
363 responses were analyzed in the exposure and recovery period separately to assess the effect of
364 treatment on physiological state and the effect of treatment history on physiological state during
365 a recovery period. Net photosynthetic rates per cm^{-2} from the exposure period in *M. capitata* and

366 color score for both species were square root transformed to meet assumptions of analysis.
367 Gross photosynthetic rates per cm^2 and growth rates in *M. capitata*, and growth rates and
368 chlorophyll-*a* per cell in *P. acuta* were log10 transformed for the exposure periods.
369 Endosymbiont density, symbiont AFDW per cell, host soluble protein, and host total antioxidant
370 capacity were log transformed in both *M. capitata* and *P. acuta*. All physiological responses
371 (tissue biomass, chlorophyll-*a* concentration, endosymbiont density, respiration rates,
372 photosynthetic rates, host total antioxidant capacity, and host soluble protein) were analyzed
373 with linear mixed effect models (lme4 package version 1.1-27.1; Bates et al. 2015) with time,
374 temperature, and pCO_2 as fixed factors, tank number as a random factor, and sum effect coding
375 (Kugler et al. 2018) to test for interaction effects. Color score and growth rates were analyzed
376 using linear mixed effect models with time, temperature, and pCO_2 as fixed factors and plug ID
377 nested within tank number as a random repeated measures factor. Survivorship probability was
378 calculated with a cox proportional hazards mixed-effects model fit by maximum likelihood using
379 the coxpH function in the coxme package (version 2.2-16; Therneau and Grambsch 2013) with
380 temperature and pCO_2 treatments as fixed effects and plug ID as a random factor. Type III Wald
381 χ^2 ANOVA tests were performed on all models to assess significance of fixed effects. To
382 determine baseline differences at Week 1 in physiology at between the two species, treatment
383 replicates were grouped for each response variable (n = 6 $treatment^{-1}$ x 4 treatments = 24
384 $species^{-1}$), prior to significant physiological change, and a Welch Two-Sample t-test was used for
385 each univariate measurement to assess significance.
386
387 *Multivariate statistical analysis*
388 A correlation matrix was calculated using the 'corrplot' function from the corrplot R
389 package (Wei 2021) to determine which univariate physiology variables were correlated and thus
390 what to include in multivariate analyses (Fig. S16). Gross and net photosynthetic rates were highly
391 correlated and as a result, only net photosynthetic rates were used in downstream analyses as

392 measure of symbiont photophysiology without the influence of cellular respiration. Principal
393 components analyses were performed using the 'prcomp' function from the stats package in R (R
394 Core Team 2013) to examine multivariate physiological states for each species in the exposure
395 period, as well as the recovery period for *M. capitata*. Permutational Multivariate Analysis of
396 Variance (PERMANOVA) tests were used to assess significant differences in multivariate
397 physiology with time, temperature, and pCO_2 as fixed effects ('adonis' function in the R package
398 vegan [Oksanen 2018]) separately for exposure and recovery periods for each species.
399
400 *DNA and RNA Extractions*
401 DNA and RNA were extracted simultaneously from the coral fragments that had been
402 snap frozen and stored at -80 °C. A small piece (~0.5-1 cm) was clipped off using clippers
403 sterilized in 10% bleach, deionized water, isopropanol, and RNAse free water, and then placed
404 in 2 mL microcentrifuge tube containing 0.5 mm glass beads (Fisher Scientific Catalog. #15-
405 340-152) with 1000 µL of DNA/RNA shield. A two step extraction protocol was used to extract
406 RNA and DNA for RNASeq and DNA methylation respectively, with the first step as a "soft"
407 homogenization to reduce shearing of RNA or DNA. Tubes were vortexed at high speed for 1
408 and 2 minutes for *P. acuta* and *M. capitata* fragments, respectively. The supernatant was
409 removed and designated as the "soft extraction". Second, 500 µL of DNA/RNA shield was
410 added to the bead tubes and placed in a Qiagen TissueLyser for 1 minute at 20 Hz. The
411 supernatant was removed and designated as the "hard extraction". Subsequently, 300 µL of
412 samples from both soft and hard homogenate were extracted individually with the Zymo Quick-
413 DNA/RNA Miniprep Plus Kit (Zymo Research Catalog #D7003T) Protocol instructions, with
414 following modifications. For the DNA elution step, the first elution of 10 µL of warmed 10 mM
415 Tris HCl was added to DNA columns for a 15 minute room temperature incubation and
416 centrifuged at 16,000 rcf(g) for 30 seconds. A second elution of 100 µL of warmed 10 mM Tris
417 HCl was added for a 5 minute incubation and centrifuged at 16,000xg for 30 seconds. Broad-

418 range DNA quantity (ng μL^{-1}) was measured with a ThermoFisher Qubit Fluorometer and DNA
419 quality was assessed using gel electrophoresis. Only the second elution of the “hard extraction”
420 DNA elution was used for downstream ITS2 sequencing protocols and analysis.
421
422 *Internal Transcribed Spacer 2 (ITS2) Sequencing*
423 Custom primers were ordered from Integrated DNA Technologies IDT with ITS2 region
424 locus-specific sequences based on (Lajeunesse and Trench 2000) and Illumina adapters (in
425 *italics*) to create our ITS2 forward primer (5’ GAA TTG CAG AAC TCC GTG *TCG TCG GCA*
426 *GCG TCA GAT GTG TAT AAG AGA CAG* 3’) and ITS2 reverse primer (5’ GGG ATC CAT ATG
427 CTT AAG TTC AGC GGG T*GT CTC GTG GGC TCG GAG ATG TGT ATA AGA GAC AG* 3’).
428 PCR master mix solution included (per sample values): 16.6 µL of 2X Phusion HiFi Mastermix
429 (Thermo Scientific Catalog #F531s), 14 µL of DNase/RNase free water, 0.6 µL of 10 uM ITS2
430 forward primer, 0.6 µL of 10 uM ITS2 reverse primer and 1 µL of 10 ng/µL DNA sample or 1 µL
431 of DNase/RNase free water as a negative control. To avoid PCR amplification bias, each
432 sample was run in triplicate on 96-well plates with 32 µL of master mix and 1 µL of 10 ng/µL
433 DNA sample in each well. Samples were run on the following polymerase chain reaction (PCR)
434 settings: 3 minutes at 95 °C, then 35 cycles of 30 seconds at 95 °C, 30 seconds at 52 °C, and
435 30 seconds at 72 °C, followed by 2 minutes at 72 °C and held indefinitely at 4 °C. The triplicate
436 PCR products for each sample were pooled and stored at -20°C. The PCR products were run
437 on a 2% agarose gel to confirm 360-390 bp pair fragment length (330-360 bp ITS2 region and
438 locus-specific primers + 33 bp adapter length). 45 µL of PCR product was sent to the RI-INBRE
439 Molecular Informatics Core (MIC) at the University of Rhode Island (RI, USA) for the index PCR
440 and sequencing. At the RI-INBRE MIC, PCR products were cleaned with NucleoMag beads
441 (Takara Bio, Catalog #744503) and then visualized using gel electrophoresis. A second round of
442 PCR was performed with 50 ng DNA input for 8 cycles to attach Nextera XT indices and
443 adapters using the Illumina Nextera XT Index Kit (Illumina, Catalog #FC-131-200x) and Phusion

444 HF PCR master mix (Thermo Fisher Scientific, Catalog #F531L). Products were then cleaned
445 with NucleoMag beads and visualized using gel electrophoresis (1.5% agarose gel, 110 V, 35
446 minutes). Quality of samples were run on an Agilent BioAnalyzer DNA1000 chip (Agilent
447 Catalog #5067-1505) and quantification was performed using a Qubit fluorometer with High
448 Sensitivity Kit (Invitrogen, Catalog #Q32584) prior to pooling all samples. The final pooled library
449 was quantified using qPCR (Roche LightCycler480) with the KAPA Biosystems Illumina Kit
450 (KAPA Biosystems). Samples were analyzed using 2x250 bp paired-end sequencing on an
451 Illumina MiSeq (Illumina).
452
453 *Bioinformatic analysis*
454 ITS2 sequences from raw FASTQ files were analyzed using SymPortal (symportal.org;
455 Hume et al. 2019) on University of Rhode Island's High Performance Cluster. This workflow
456 used Miniconda3 v4.9.2 and SymPortal v0.3.21-foss-2020b to assign sequences as defined
457 intragenomic variants (DIV) and 'ITS2 Type Profiles'. A raw counts matrix of the ITS2 Type
458 Profile output from SymPortal was exported and analyzed locally using R Software Version
459 4.0.3 in RStudio Version 1.4.1103. Relative abundance and a Bray-Curtis distance matrix were
460 calculated using the 'vegan' package (Dixon 2003). A PERMANOVA was performed for each
461 species to assess significant effects of time point, treatment, and their interaction.

462 **Results**

463 At the end of the ~14 day acclimation period, 89.8% of *P. acuta* and 97.8% of *M.*
464 *capitata* fragments were alive. During the exposures, treatments showed no significant variation
465 in total alkalinity between the tanks or treatments across the 16 week experiment (Table S1;
466 S13) and light conditions were not significantly different between treatments (Fig. S3; Table S2).
467 Temperature output from HOBO loggers (Fig. 1F) and carbonate chemistry (Fig. 1E; Fig. S2)
468 are reported in Supplemental Table S12 and S13, respectively.

469

470 ***High temperature drives bleaching responses and low P. acuta survivorship***

471 In high temperature treatments (HTAC and HTHC), both species displayed significant
472 color change relative to ambient, starting at four weeks in *P. acuta* and six weeks in *M. capitata*
473 (Fig. S6). High temperature and ambient CO_2 (HTAC) and high temperature high CO_2 (HTHC)
474 treatments drove this decrease in color score in the exposure period in *M. capitata* (Time x
475 Temperature p=0.0004; Time x Temperature x pCO_2 p=0.0004; Table S6) and *P. acuta* (Time x
476 Temperature p < 0.0001; Time x Temperature x pCO_2 p < 0.0001; Table S6). Additionally, *P.*
477 *acuta* color score decreased significantly through the fall season (Time p < 0.0001) and in high
478 pCO_2 treatments over time (Time x pCO_2 p < 0.0001; Table S6). Following this visual bleaching
479 response in the exposure period, both high temperature (HTHC, HTAC) and pCO_2 treatments
480 (ATHC) elicited decreased survivorship probability in both *M. capitata* (Temperature p <0.0001;
481 pCO_2 p=0.0007) and *P. acuta* (pCO_2 p < 0.0001; Temperature x pCO_2 p < 0.0001; Fig. S5, Table
482 S7). In the recovery period, *M. capitata* fragments that experienced high temperature treatments
483 (HTHC and HTAC) increased in color score to ambient color score value by week 16 (Fig.
484 S6B; Temperature p=0.0376; Time x Temperature p < 0.0001; Time x Temperature x pCO_2
485 p=0.0124). The decreases in survivorship probability for *M. capitata* stopped once treatment
486 conditions were removed (Fig. S5A). However, *P. acuta* fragments did not recover color (Fig.
487 S6B) and survivorship probability continued to sharply decrease (Fig. S5B).

488

489 ***High temperature decreased metabolic rates in both species, but* P. acuta *displays higher***
490 ***baseline photosynthetic rates***

491 There were significant decreases during the fall season (September - November) in both
492 species (Fig. S13; Fig. S14B) for Respiration (LEDR; *M. capitata* Time p=0.0005; *P. acuta* Time
493 p < 0.0001) and photosynthetic rates (*M. capitata* $P_{net}cm^{-2}$ Time p=0.0060; *P. acuta* $P_{net}cm^{-2}$ Time p
494 < 0.0001; *P. acuta* P_{net} $cell^{-1}$ Time p <0.0001). However, *P. acuta* displayed significantly higher

495 baseline (as defined by Week 1) holobiont (P_{net} cm^{-2} p=0.0002; P_{gross} cm^{-2} p=0.0013) and per cell
496 photosynthetic rates (P_{net} $cell^{-1}$ p=0.0045), as well as higher P:R ratios (P:R p=0.0023) than *M.*
497 *capitata* (Fig. 2, Table S8). During the exposure period, high temperature, rather than high pCO_2,
498 caused a decrease in respiration rates in *M. capitata* (Temperature p=0.0203) and *P. acuta*
499 (Time x Temperature p=0.0412). Similarly, high temperature drove significant decreases in net
500 photosynthetic rates in *M. capitata* (Time x Temperature p=0.0079) and *P. acuta* (Time x
501 Temperature p < 0.0001). When net photosynthetic rates were normalized per symbiont cell,
502 treatments did not affect *M. capitata* fragments (Time x Temperature x pCO_2 p=0.1833), but *P.*
503 *acuta* fragments in high temperature treatments displayed a significant decrease by week 6
504 (Time x Temperature p=0.0011; Fig. 14B). Concomitantly, by week 6, *P. acuta* fragments also
505 experienced a significant decrease in P:R ratios in high temperature treatments (Time x
506 Temperature p=0.0139) and overall changes in metabolic rates were more pronounced in *P.*
507 *acuta* fragments (Fig. S13; Table S3).
508
509 ***High pCO_2 stress depresses seasonal increase in growth rates in* M. capitata *and high***
510 ***temperature decreases growth rates in both species***
511 In both species, growth rates (mg $CaCO_3$ cm^{-2} d^{-1}) peaked in October at week 4 and
512 gradually decreased by November at week 8 of the exposure period (Fig. S15; *M. capitata* Time
513 p < 0.0001; *P. acuta* Time p < 0.0001). High temperature treatment decreased growth rates in
514 later exposure time points (Time x Temperature x pCO_2 < 0.0001) in both species. Similarly,
515 both pCO_2 and temperature treatments exhibited lower growth rates through the entire exposure
516 period (Time x pCO_2 p=0.0027; Time x Temperature x pCO_2 p < 0.0001) in *P. acuta* fragments.
517 In *M. capitata*, corals in high pCO_2 treatments displayed significantly lower growth rates over
518 time (Time x pCO_2 p=0.0003). However, during the recovery period, *M. capitata* fragments that
519 experienced only high pCO_2 (ATHC) displayed increasing growth rates through week 16 (Time x

520 pCO_2 p=0.0017), while fragments that experienced the high temperature treatments (HTAC and
521 HTHC) gradually increased to ambient levels by week 16 (Time x Temperature p < 0.0001).
522
523 ***Host physiology: biomass remained stable while temperature stress increased TAC and***
524 ***decreased protein levels***
525 On average, *M. capitata* exhibited higher baseline TAC than *P. acuta* (Fig. 2; Table S8;
526 p=0.0008). Host total antioxidant capacity, TAC, (CRE µmol mg^{-1}) remained constant in *M.*
527 *capitata* through the exposure period regardless of treatment (Fig. S10; Time x Temperature x
528 pCO_2 p=0.7028), but increased by week 8 in *P. acuta* under high temperature in HTAC and
529 HTHC (Time x Temperature p=0.0277). During recovery, *M. capitata* fragments previously
530 exposed to high temperature treatments showed reduced TAC at week 12, which returned to
531 ambient treatment values by week 16 (Fig. S10A; Time x Temperature p=0.0237). Host soluble
532 protein (mg cm^{-2}) was not significantly different between species at baseline, Week 1 (p=0.29),
533 but significantly decreased through time from September - January in both *M. capitata* (Time p <
534 0.0001) and *P. acuta* (Time p < 0.0001). At week 6, protein concentration in *M. capitata*, was
535 significantly greater in both high pCO_2 treatments (pCO_2 p=0.0002; Fig. S9) in comparison to
536 HTAC and ATAC. Additionally, corals in high temperature treatments (HTHC and HTAC in
537 comparison to ATAC and ATHC) displayed a decrease in protein over time (Temperature x
538 Time p=0.0463). In *P. acuta* fragments, high temperature treatments decreased protein in at
539 week 8 (Time x Temperature p=0.0490). Host AFDW (mg cm^{-2}) was not significantly different at
540 baseline Week 1 (p=0.22) or affected by treatment, but gradually and significantly decreased
541 from September - January in *M. capitata* (Time p=0.0050) and *P. acuta* (Time p=0.0188).
542
543 ***Symbiont and holobiont physiology: stress treatments caused an increase in symbiont***
544 ***biomass but decreased chlorophyll-a content and endosymbiont density***

545 Symbiont biomass (mg AFDW cm^{-2}) was unaffected by either temperature or pCO_2
546 treatment (Time x Temperature x pCO_2; *M. capitata* p=0.3839, *P. acuta* p=0.3790), but
547 significantly decreased through the fall season in both *M. capitata* (p=0.0013) and *P. acuta*
548 (p=0.0028; Fig. S11; Table S5). Despite no treatment effect on symbiont and host biomass (mg
549 AFDW cm^{-2}), for *P. acuta* the Symbiont:Host biomass ratio significantly decreased in high
550 temperature treatments (Temperature p=0.0180) and decreased also over time (Time
551 p=0.0090). *M. capitata* fragments exhibited significantly higher baseline Week 1 biomass (mg
552 cm^{-2} p=0.0145; mg $cell^{-1}$ p=0.0079; Fig. 2) than *P. acuta*. In *M. capitata*, symbiont cellular
553 biomass (AFDW mg $cell^{-1}$) significantly increased in corals in the high temperature treatments
554 during exposure (Temperature x pCO_2 p=0.0133) and then returned to ambient levels by week
555 16 (Time x Temperature p=0.0041). In *P. acuta*, symbiont per cell biomass decreased through
556 from September - January (p=0.0141), but significantly increased under both temperature and
557 pCO_2 exposure (Time x Temperature $p < 0.0001$; Time x pCO_2 p=0.0146; Fig. S12B). Holobiont
558 chlorophyll-*a* (cm^{-2}) increased over the fall season in *M. capitata* (Fig. S8A; p=0.0003), but high
559 temperature exposure resulted in decreased chlorophyll-*a* over time (Time x Temperature
560 p=0.0089) remained low in the recovery period (Temperature $p < 0.0001$). In *P. acuta*,
561 chlorophyll-*a* decreased over time (Fig. S8B; Time $p < 0.0001$) and in high temperature
562 treatments over time (Time x Temperature $p < 0.0001$). In *M. capitata*, only time significantly
563 affected cellular chlorophyll-*a* $cell^{-1}$ (p=0.0347), and in all fragments, regardless of treatment,
564 chlorophyll-*a* $cell^{-1}$ increased from September - January (Fig. S8C). However, in *P. acuta*,
565 chlorophyll-*a* per cell was significantly affected by temperature and time (Time x Temperature
566 p=0.0764; Fig. S8D). Endosymbiont density (cells cm^{-2}) decreased in high temperature and pCO_2
567 treatments over time in *M. capitata* (Time x Temperature p=0.0100; Time x pCO_2 p=0.0249) and
568 the decline was even more pronounced in high temperature in *P. acuta* (Temperature $p <$
569 0.0001; Time x Temperature $p < 0.0001$) (Figure S7). *P. acuta* endosymbiont density decreased
570 by week 4 in all treatments (Time $p < 0.0001$; Figure S7B), but all *M. capitata* fragments

experienced an increase in densities in the same time period followed decreased values by week 8 time points (Time $p < 0.0001$; Figure S7A). By the end of the recovery period, *M. capitata* fragments that had experienced high temperature treatments did not fully recover in symbiont cell densities (Temperature $p=0.0070$), despite being statistically indistinguishable in color score.

Multivariate physiology: high temperature exacerbates seasonal changes during stress and drives shifts during recovery

In both species, treatments exacerbated existing seasonal shifts in multivariate physiological states (Fig. 4). In *P. acuta*, physiological state shifted over time ($p < 0.001$) and in high temperature treatments (Temperature $p < 0.001$; Time x Temperature $p < 0.001$). Similarly, *M. capitata* fragments experience a shift in physiological state over time (Time $p < 0.001$), due to temperature (Temperature $p=0.005$) and differently between pCO_2 treatments through time (Time x pCO_2 $p=0.038$). PC1 explained 39.83% of the variance and separated the samples between ambient temperature and high temperature for *P. acuta*, with changes in respiration rates and host TAC levels contributing most strongly to the separation (Fig. 4A-B). The PC2 axis explains 18.40% of the variation and the separation between treatment groups is characterized by changes in endosymbiont density and cellular symbiont biomass. In *M. capitata*, the PC1 axis explains 30.51% of the variation and is characterized by changes in the host (protein, biomass, respiration) and holobiont physiology (holobiont net photosynthetic rates, aerial symbiont AFDW, and holobiont chlorophyll-a-a content) that contribute to separation primarily between time points. The PC2 axis explains 25.81% of the variation and is characterized by symbiont functions (symbiont AFDW mg $cell^{-1}$, net photosynthetic rates, and chlorophyll-a content) that separate primarily treatment groups (Fig. 4C-D). During the recovery period, both time ($p < 0.001$) and high temperature treatment ($p < 0.001$) significantly affected physiological shifts in *M. capitata* (Fig. 5C-D). PC1 explains 37.61% of the variation and is characterized by

host (biomass, protein) and holobiont traits (AFDW cm^{-2}, chlorophyll-a cm^{-2}) that separate between the history of high temperature treatment groups in *M. capitata*. PC2 explains 30.11% of the variation and changes in endosymbiont density and symbiont traits (cellular chlorophyll-a $cell^{-1}$, S:H biomass ratio, $biomass^{-1}$) contribute strongly to the separation of treatment and time groups.

M. capitata and P. acuta harbor distinctly different Symbiodiniaceae community compositions that do not change significantly during stress or recovery

The ITS2 sequencing generated 5,807,744 total raw reads from 251 samples, with an average of 22,775 reads per sample. The SymPortal analysis resulted in 4,902,971 total cleaned sequences, which excludes week 16 in *P. acuta* because of low sample sizes. *M. capitata* fragments harbored mixed Symbiodiniaceae communities composed of ITS2 Symbiont Type Profiles with majority sequences `D1/D4` and variations of `C17d/No-Name` (*Durusdinium and Cladocopium spp.*; LaJeunesse et al. 2018; Fig. 6). *P. acuta* communities were dominated by Type Profiles in Clade C with majority groups `C1d/C42.2` and `C1d`. Endosymbiont communities were significantly different by species (PERMANOVA $p < 0.001$) and differed only between two time points in *M. capitata* (12 hr vs. 24 hr $p=0.045$), but did not significantly change in exposure treatments ($p=1.000$; Table S10).

Discussion

Extended heat waves scenario induces species-specific mortality of corals and creates altered physiological legacies for the survivors

Scaling up from controlled single variable lab experiments to environmentally relevant multi-stressor experiments is essential to capture the effects of stressors in the context of

622 seasonal physiological and thus the time dependent and environmentally-relevant sensitivity of
623 corals to global change stressors. Our examination of the effects of high pCO_2 and an extended
624 heatwave at the peak of seasonal temperatures on *Montipora capitata* and *Pocillopora acuta*
625 reinforce that increased temperatures are the more substantial threat to coral physiological
626 performance (Putnam et al. 2013), survivorship (Klein et al. 2022) and physiological legacy effects
627 (Wall et al. 2021) than high pCO_2 conditions. We found that high pCO_2 concentrations alone can
628 elicit potentially beneficial effects in the more resilient M. capitata like higher endosymbiont
629 density and thus higher photosynthetic rates (cm^{-2}) during exposure, and higher growth rates
630 during recovery periods. However, these effects are not seen when high pCO_2 conditions occur
631 simultaneously with higher temperatures.

632 The extent of physiological shifts, decreased survival probability, and increased
633 bleaching were all more pronounced in *P. acuta* than *M. capitata*, reinforcing the outcome of
634 species-specific susceptibility and loss of corals on future reefs (Loya et al. 2001; R. van Woesik
635 et al. 2011). Our data indicate species-specific responses are due to a combination of
636 Symbiodiniaceae community and baseline levels of host antioxidant capacity and cellular
637 photosynthetic rates. Further, our findings of different physiology trajectories of *M. capitata*
638 during the recovery period, specifically in those exposed to high temperature, support prior work
639 that high temperature conditions leave lasting physiological legacies several months into
640 recovery (Rodríguez-Troncoso et al. 2016; Schoepf et al. 2015; Rodrigues and Grottoli 2007)
641 and those legacies can have cumulative effects that shift physiological baselines leading into a
642 subsequent stress event (Wall et al. 2021; Safaie et al. 2018; Ainsworth et al. 2016).

643

644 ***M. capitata thermal tolerance is driven by Symbiodiniaeceae communities and high levels***
645 ***of antioxidants relative to cellular photosynthetic rates***

646 Symbiodiniaceae communities aid in a coral holobiont's tolerance and survival (Baskett,
647 et al. 2009; Oliver and Palumbi 2011), specifically, studies have documented the presence of

648 *Durusdinium spp.* (Silverstein et al. 2015; Guest et al. 2016) and/or mixed endosymbiont
649 communities (Abbott et al. 2021) can be beneficial for coral holobiont survival. Our results support
650 these hypotheses, as the mixture of *Durusdinimum spp.* (D1/D4) and *Cladocopium spp.*
651 (C17/C31) in *M. capitata* was associated with higher thermal tolerance, compared to *P. acuta*'s
652 *Cladocopium spp.* (C1) dominated communities. Although there was no evidence of
653 Symbiodiniaceae community shuffling by treatment or through time, a holobiont's community prior
654 to an exposure event likely plays a crucial role in their ability to handle changing environmental
655 conditions. Through these community composition differences, symbiont physiology influences
656 holobiont tolerance (Hoadley et al. 2019; Ziegler et al. 2015), thus addressing both the host and
657 symbiont physiological states are critical to understanding the stress response of the holobiont
658 (Bellantuono et al. 2012). Differential photophysiology, carbon assimilation and translocation to
659 the host (Stat et al. 2008) and metabolite profiles (Matthews et al. 2017; Matthews et al. 2018)
660 have been seen between Symbiodiniaceae genera and thus influence holobiont tolerance (Wall
661 et al. 2020; Matthews et al. 2018; Roach et al. 2021).

662 For both host and symbiont partners, a core physiological response to stress is the activity
663 of antioxidant systems to neutralize reactive oxygen molecules (ROS) that build-up during daily
664 metabolism and in response to stressful conditions like increased temperature (Baird et al. 2009;
665 Downs et al. 2000). These excess ROS molecules can leak into the host to cause a downstream
666 cascade of cellular damage and eventually coral bleaching and apoptosis (Weis 2008). A
667 mismatch between the amount of symbiont derived ROS molecules and the host's antioxidant
668 capacity may lead to higher susceptibility for coral bleaching (e.g. Cunning and Baker 2013). We
669 hypothesize that *P. acuta*'s naturally higher cellular photosynthetic rates, but lower host
670 antioxidant capacity per unit protein, may lead to a faster build-up of reactive oxygen species
671 (ROS) damage and consequently higher mortality rates. Thus, *P. acuta* are challenged under
672 thermal stress because the symbiotic community is operating closer to the threshold between
673 productivity and damage. In comparison, *M. capitata*'s naturally lower photosynthetic rates and

674 higher host antioxidant capacity levels may be providing a greater buffer, allowing them capacity
675 to support and balance their higher endosymbiont densities during November (Fig. 3), resulting
676 in a more muted bleaching response when faced with stressful conditions. Further, *M. capitata*
677 have the benefit of thicker tissues (Loya et al. 2001; Magnusson et al. 2007) with greater energy
678 reserves (Rodrigues and Grottoli 2007) in addition to their symbiont community composition. By
679 the end of the exposure period, *P. acuta* host antioxidant capacity levels increased and cellular
680 photosynthetic rates decreased, but visual bleaching responses preceded this cellular
681 physiological change indicating the response was insufficient. *M. capitata* may be well equipped
682 to acclimatize to changing environmental conditions because of baseline holobiont physiological
683 states and existing Symbiodiniaceae communities.
684
685 ***Prior thermal stress determines bleaching recovery trajectories in M. capitata***
686 Recent studies have emphasized the importance of recovery time in between marine
687 heatwaves (Osborne et al. 2017; Neal et al. 2017). Recovery time can be highly variable, with
688 species taking 1.5 months (Rodrigues and Grottoli 2007), 2 months (Cunning et al. 2016),
689 3 months (Wall et al. 2019) up to 2 years (Matsuda et al. 2020). We found that in our experimental
690 recovery period of 2 months following exposure, physiological metrics that decreased in chronic
691 high temperature conditions stabilized as *M. capitata* fragments began to recover pigmentation
692 (color score, symbiont density, and chlorophyll-*a*). Despite full recovery in color score and growth
693 rates by week 16, chlorophyll-*a* and endosymbiont densities did not fully recover to the same
694 extent of the ambient condition corals, with differential physiological states and trajectories
695 throughout the recovery period (Fig. 5). Our results indicate that extended high temperature
696 exposure at the peak of seasonal temperature leaves a physiological legacy that lasts beyond
697 two months. Even in this resistant and resilient species, *M. capitata*, legacy effects of bleaching
698 on organismal state can be as long as 1-2 years (Wall et al. 2019, Roach et al. 2021; Thomas
699 and Palumbi 2017).

These legacy effect results are consistent with other studies that suggest environmental conditions shift coral phenotypes, ultimately eliciting a lasting legacy that could have either a beneficial or detrimental priming effect for response in future stress events (Wall et al. 2021; Hackerott et al. 2021; Putnam et al. 2017; Brown et al. 2000). However, recovery time is imperative to understand whether the lasting effects of prior thermal events can be beneficial. Sublethal temperatures that induce a bleaching response 10 days prior to a larger intensity bleaching event have been shown to be beneficial (termed a 'protective trajectory'; Ainsworth et al. 2016). Although beneficial effects were documented in long-term recovery periods of 11 months (Schoepf et al. 2015) following thermal perturbation, not all species recovery is on the same timeline, with *P. divaricata* and *O. faveolata* recovering faster than *P. astreoides* (Schoepf et al. 2015). This potential for "environmental memory" based on previous environmental conditions is clear in corals (Brown et al. 2000; Brown et al. 2022). Utilizing this to elicit purposeful stress hardening or environmental priming (Hackerott et al. 2021; Putnam et al. 2017; Brown et al. 2000; DeMerlis et al. 2022) is a proposed restoration technique (Van Oppen et al. 2015), but it is clear there are limits of recovery time. *M. capitata* is likely to survive future thermal stress events, but back-to-back bleaching events and decreased recovery time may reduce *M. capitata*'s buffer and push their physiology closer to a threshold. More multi-year studies to track differential bleaching patterns over time are needed to elucidate the threshold between eliciting beneficial 'environmental memory' versus accumulated physiological damage and energetic deficits (Schoepf et al. 2015).

Conclusion

This study highlighted the divergent thermal tolerance and recovery potential of *M. capitata* and *P. acuta*, indicating a potential for species-specific susceptibility to stress and loss of corals in future, more frequent and higher intensity bleaching events. *M. capitata* elevated stress tolerance may be due to mixed *Cladocopium* and *Durusdinium* Symbiodiniaceae

725 communities, higher antioxidant capacity and elevated photosynthetic rates at baseline, and
726 stability of metabolic and symbiont physiology during chronic high temperature conditions. In the
727 two months of ambient recovery conditions that followed two months of elevated temperature and
728 pCO_2 conditions, *M. capitata* multivariate physiology did not fully recover. High temperature
729 treatment history elicited a lasting multivariate physiological legacy that set recovering *M. capitata*
730 on a different trajectory than those that experienced ambient conditions. This study illuminates
731 and emphasizes the importance of environmentally and seasonally realistic time-series
732 experiments to further understand the impacts of pre-existing seasonal dynamics on thermal
733 stress response. Multi-year repeated bleaching event studies are needed to disentangle how a
734 physiological legacy may be adaptive or maladaptive under predicted climate change scenarios.
735

736 **Contributions**

737 HMP and ELS designed the experiment. HMP, ELS, and KW completed the experiment and
738 sampling in the field. ELS, SG, AF, and AM completed laboratory work. ELS and HMP analyzed
739 the data and wrote the manuscript. All authors commented on and confirmed the final draft.

740 **Data Availability**

741 All data and code used to produce results and complete analyses are available at
742 https://github.com/hputnam/Acclim_Dynamics. Laboratory protocols and processing can be
743 found on Emma Strand's Open Laboratory Notebook at
744 https://emmastrand.github.io/EmmaStrand_Notebook/. ITS2 Sequencing FASTQ files are
745 uploaded to NCBI under Project #PRJNA761780.

746 **Acknowledgements**

We would like to thank the Hawaiʻi Institute of Marine Biology and the Coral Resilience Laboratory for hosting us to conduct the experiment on Coconut Island, and Chris Suchoki and Adam Helbig for assistance with field work. Ariana Huffmyer provided valuable feedback on the manuscript. As guests, we recognize and give thanks for the land and water resources of the ʻāina and the traditional owners of the land, kānaka ʻōiwi, on which this experimental work was conducted in the Kāneʻohe Ahupuaʻa and the islands of Hawaiʻi. The authors acknowledge use of the computational resources of the URI Center for Computational Research for this work. This work was supported by the USDA National Institute of Food and Agriculture, Hatch Formula project accession number 1017848, and the National Science Foundation Award number 1756623.

References

Abbott, Evelyn, Groves Dixon, and Mikhail Matz. 2021. "Shuffling between Cladocopium and Durusdinium Extensively Modifies the Physiology of Each Symbiont without Stressing the Coral Host." *Molecular Ecology* 30 (24): 6585–95.

Ainsworth, Tracy D., Scott F. Heron, Juan Carlos Ortiz, Peter J. Mumby, Alana Grech, Daisie Ogawa, C. Mark Eakin, and William Leggat. 2016. "Climate Change Disables Coral Bleaching Protection on the Great Barrier Reef." *Science* 352 (6283): 338–42.

Anthony, K. R. N., and O. Hoegh-Guldberg. 2003. "Variation in Coral Photosynthesis, Respiration and Growth Characteristics in Contrasting Light Microhabitats: An Analogue to Plants in Forest Gaps and Understoreys?" *Functional Ecology* 17 (2): 246–59.

Bahr, Keisha D., Paul L. Jokiel, and Kuʻulei S. Rodgers. 2015. "The 2014 Coral Bleaching and Freshwater Flood Events in Kāneʻohe Bay, Hawaiʻi." *PeerJ* 3 (August): e1136.

Bahr, Keisha D., Paul L. Jokiel, and Ku'ulei S. Rodgers. 2016. "Relative Sensitivity of Five Hawaiian Coral Species to High Temperature under High-pCO2 Conditions." *Coral Reefs* 35 (2): 729–38.

Baird, Andrew H., Ranjeet Bhagooli, Peter J. Ralph, and Shunichi Takahashi. 2009. "Coral Bleaching: The Role of the Host." *Trends in Ecology & Evolution*. https://doi.org/10.1016/j.tree.2008.09.005.

Barshis, Daniel J., Jason T. Ladner, Thomas A. Oliver, François O. Seneca, Nikki Traylor-Knowles, and Stephen R. Palumbi. 2013. "Genomic Basis for Coral Resilience to Climate Change." *Proceedings of the National Academy of Sciences of the United States of America* 110 (4): 1387–92.

Baskett, Marissa L., Steven D. Gaines, and Roger M. Nisbet. 2009. "Symbiont Diversity May Help Coral Reefs Survive Moderate Climate Change." *Ecological Applications: A Publication of the Ecological Society of America* 19 (1): 3–17.

Bates, Douglas, Martin Mächler, Ben Bolker, and Steve Walker. 2015. “Fitting Linear Mixed-Effects Models Using**lme4**.” *Journal of Statistical Software*. https://doi.org/10.18637/jss.v067.i01.

Bellantuono, Anthony J., Ove Hoegh-Guldberg, and Mauricio Rodriguez-Lanetty. 2012. “Resistance to Thermal Stress in Corals without Changes in Symbiont Composition.” *Proceedings. Biological Sciences / The Royal Society* 279 (1731): 1100–1107.

Boilard, Aurélie, Caroline E. Dubé, Cécile Gruet, Alexandre Mercière, Alejandra Hernandez-Agreda, and Nicolas Derome. 2020. “Defining Coral Bleaching as a Microbial Dysbiosis within the Coral Holobiont.” *Microorganisms* 8 (11). https://doi.org/10.3390/microorganisms8111682.

Bourne, David G., Kathleen M. Morrow, and Nicole S. Webster. 2016. “Insights into the Coral Microbiome: Underpinning the Health and Resilience of Reef Ecosystems.” *Annual Review of Microbiology*. https://doi.org/10.1146/annurev-micro-102215-095440.

Brown, B. E., R. P. Dunne, M. S. Goodson, and A. E. Douglas. 2000. “Bleaching Patterns in Reef Corals.” *Nature* 404 (6774): 142–43.

Brown, Kristen T., Matheus A. Mello-Athayde, Eugenia M. Sampayo, Aaron Chai, Sophie Dove, and Katie L. Barott. 2022. “Environmental Memory Gained from Exposure to Extreme pCO Variability Promotes Coral Cellular Acid-Base Homeostasis.” *Proceedings. Biological Sciences / The Royal Society* 289 (1982): 20220941.

Claar, Danielle C., Samuel Starko, Kristina L. Tietjen, Hannah E. Epstein, Ross Cunning, Kim M. Cobb, Andrew C. Baker, Ruth D. Gates, and Julia K. Baum. 2020. “Dynamic Symbioses Reveal Pathways to Coral Survival through Prolonged Heatwaves.” *Nature Communications* 11 (1): 6097.

“Correction for Matthews et Al., Optimal Nutrient Exchange and Immune Responses Operate in Partner Specificity in the Cnidarian-Dinoflagellate Symbiosis.” 2017. *Proceedings of the National Academy of Sciences of the United States of America* 114 (51): E11058.

Cunning, Ross, and Andrew C. Baker. 2013. “Excess Algal Symbionts Increase the Susceptibility of Reef Corals to Bleaching.” *Nature Climate Change*. https://doi.org/10.1038/nclimate1711.

Cunning, R., R. Ritson-Williams, and R. D. Gates. 2016. “Patterns of Bleaching and Recovery of Montipora Capitata in Kāneʻohe Bay, Hawaiʻi, USA.” *Marine Ecology Progress Series*. https://doi.org/10.3354/meps11733.

Cziesielski, Maha J., Sebastian Schmidt-Roach, and Manuel Aranda. 2019. “The Past, Present, and Future of Coral Heat Stress Studies.” *Ecology and Evolution* 9 (17): 10055–66.

DeMerlis, Allyson, Amanda Kirkland, Madeline L. Kaufman, Anderson B. Mayfield, Nathan Formel, Graham Kolodziej, Derek P. Manzello, Diego Lirman, Nikki Traylor-Knowles, and Ian C. Enochs. 2022. “Pre-Exposure to a Variable Temperature Treatment Improves the Response of Acropora Cervicornis to Acute Thermal Stress.” *Coral Reefs*. https://doi.org/10.1007/s00338-022-02232-z.

Dickson, A. G. 1990. Standard potential of the reaction: AgCl (s)+ 12H2 (g)= Ag (s)+ HCl (aq), and the standard acidity constant of the ion HSO4− in synthetic sea water from 273.15 to 318.15 K. *The Journal of Chemical Thermodynamics*, *22*(2), 113-127.

Dickson, Andrew Gilmore, Christopher L. Sabine, and James Robert Christian. 2007. *Guide to Best Practices for Ocean CO2 Measurements*.

Dixon, Philip. 2003. “VEGAN, a Package of R Functions for Community Ecology.” *Journal of Vegetation Science*. https://doi.org/10.1111/j.1654-1103.2003.tb02228.x.

Downs, C. A., E. Mueller, S. Phillips, J. E. Fauth, and C. M. Woodley. 2000. “A Molecular Biomarker System for Assessing the Health of Coral (Montastraea Faveolata) during Heat Stress.” *Marine Biotechnology* 2 (6): 533–44.

Drupp, Patrick, Eric Heinen De Carlo, Fred T. Mackenzie, Paul Bienfang, and Christopher L. Sabine. 2011. “Nutrient Inputs, Phytoplankton Response, and CO2 Variations in a Semi-

Enclosed Subtropical Embayment, Kaneohe Bay, Hawaii." *Aquatic Geochemistry* 17 (4-5): 473–98.

Edmunds, Peter J., and Hollie M. Putnam. 2020. "Science-Based Approach to Using Growth Rate to Assess Coral Performance and Restoration Outcomes." *Biology Letters* 16 (7): 20200227.

Edmunds, P. J., R. D. Gates, and D. F. Gleason. 2003. "The Tissue Composition of Montastraea Franksi during a Natural Bleaching Event in the Florida Keys." *Coral Reefs* 22 (1): 54–62.

Edmunds, P. J., and P. Spencer Davies. 1988. "Post-Illumination Stimulation of Respiration Rate in the Coral Porites Porites." *Coral Reefs*. https://doi.org/10.1007/bf00301975.

Frölicher, Thomas L., and Charlotte Laufkötter. 2018. "Emerging Risks from Marine Heat Waves." *Nature Communications* 9 (1): 650.

Gardner, Stephanie G., Jean-Baptiste Raina, Matthew R. Nitschke, Daniel A. Nielsen, Michael Stat, Cherie A. Motti, Peter J. Ralph, and Katherina Petrou. 2017. "A Multi-Trait Systems Approach Reveals a Response Cascade to Bleaching in Corals." *BMC Biology* 15 (1): 117.

Gates, R. D., G. Baghdasarian, and L. Muscatine. 1992. "Temperature Stress Causes Host Cell Detachment in Symbiotic Cnidarians: Implications for Coral Bleaching." *The Biological Bulletin* 182 (3): 324–32.

Gattuso, Jean-Pierre, Jean-Marie Epitalon, Heloise Lavigne, J. Orr, B. Gentili, A. Hofmann, A. Proye, K. Soetaert, and J. Rae. 2015. "Seacarb: Seawater Carbonate Chemistry." *R Package Version* 3 (8).

Gattuso, J-P, A. Magnan, R. Billé, W. W. L. Cheung, E. L. Howes, F. Joos, D. Allemand, et al. 2015. "Contrasting Futures for Ocean and Society from Different Anthropogenic CO2 Emissions Scenarios." *Science* 349 (6243). https://doi.org/10.1126/science.aac4722.

Gibbin, Emma M., Hollie M. Putnam, Simon K. Davy, and Ruth D. Gates. 2014. "Intracellular pH and Its Response to CO2-Driven Seawater Acidification in Symbiotic versus Non-Symbiotic Coral Cells." *The Journal of Experimental Biology* 217 (Pt 11): 1963–69.

Gibbin, Emma M., Hollie M. Putnam, Ruth D. Gates, Matthew R. Nitschke, and Simon K. Davy. 2015. "Species-Specific Differences in Thermal Tolerance May Define Susceptibility to Intracellular Acidosis in Reef Corals." *Marine Biology* 162 (3): 717–23.

Guest, J. R., J. Low, K. Tun, B. Wilson, C. Ng, D. Raingeard, K. E. Ulstrup, et al. 2016. "Coral Community Response to Bleaching on a Highly Disturbed Reef." *Scientific Reports* 6 (February): 20717.

Hackerott, Serena, Harmony A. Martell, and Jose M. Eirin-Lopez. 2021. "Coral Environmental Memory: Causes, Mechanisms, and Consequences for Future Reefs." *Trends in Ecology & Evolution* 36 (11): 1011–23.

Heberling, J. Mason, and Jason D. Fridley. 2013. "Resource-Use Strategies of Native and Invasive Plants in Eastern North American Forests." *The New Phytologist* 200 (2): 523–33.

Heron, Scott F., Jeffrey A. Maynard, Ruben van Hooidonk, and C. Mark Eakin. 2016. "Warming Trends and Bleaching Stress of the World's Coral Reefs 1985–2012." *Scientific Reports* 6 (1): 1–14.

Hoadley, Kenneth D., Allison M. Lewis, Drew C. Wham, D. Tye Pettay, Chris Grasso, Robin Smith, Dustin W. Kemp, Todd C. LaJeunesse, and Mark E. Warner. 2019. "Host–symbiont Combinations Dictate the Photo-Physiological Response of Reef-Building Corals to Thermal Stress." *Scientific Reports* 9 (1): 9985.

Hume, Benjamin C. C., Edward G. Smith, Maren Ziegler, Hugh J. M. Warrington, John A. Burt, Todd C. LaJeunesse, Joerg Wiedenmann, and Christian R. Voolstra. 2019. "SymPortal: A Novel Analytical Framework and Platform for Coral Algal Symbiont Next-generation Sequencing ITS2 Profiling." *Molecular Ecology Resources* 19 (4): 1063–80.

Jeffrey, S. W., and G. F. Humphrey. 1975. "New Spectrophotometric Equations for Determining Chlorophylls A, B, c1 and c2 in Higher Plants, Algae and Natural Phytoplankton." *Biochemie Und Physiologie Der Pflanzen*. https://doi.org/10.1016/s0015-3796(17)30778-3.

Jokiel, P. L., and J. E. Maragos. 1978. “Coral Growth: Buoyant Weight Technique.” https://www.researchgate.net/profile/Paul_Jokiel/publication/285472773_Coral_growth_buoyant_weight_technique_In_Stoddart_DR_Johannes_RE_eds_Coral_reefs_research_methods/links/568b229608aebccc4e1a3a5c.pdf.

Jurriaans, S., and M. O. Hoogenboom. 2020. “Seasonal Acclimation of Thermal Performance in Two Species of Reef-Building Corals.” *Marine Ecology Progress Series* 635 (February): 55–70.

Jury, Christopher P., Florence I. M. Thomas, Marlin J. Atkinson, and Robert J. Toonen. 2013. “Buffer Capacity, Ecosystem Feedbacks, and Seawater Chemistry under Global Change.” *WATER* 5 (3): 1303–25.

Klein, Shannon G., Nathan R. Geraldi, Andrea Anton, Sebastian Schmidt-Roach, Maren Ziegler, Maha J. Cziesielski, Cecilia Martin, et al. 2022. “Projecting Coral Responses to Intensifying Marine Heatwaves under Ocean Acidification.” *Global Change Biology* 28 (5): 1753–65.

Kugler, Kari C., John J. Dziak, and Jessica Trail. 2018. “Coding and Interpretation of Effects in Analysis of Data from a Factorial Experiment.” *Optimization of Behavioral, Biobehavioral, and Biomedical Interventions*. https://doi.org/10.1007/978-3-319-91776-4_6.

Lajeunesse, T. C., and R. K. Trench. 2000. “Biogeography of Two Species of Symbiodinium (Freudenthal) Inhabiting the Intertidal Sea Anemone Anthopleura Elegantissima (Brandt).” *The Biological Bulletin* 199 (2): 126–34.

LaJeunesse, Todd C., John Everett Parkinson, Paul W. Gabrielson, Hae Jin Jeong, James Davis Reimer, Christian R. Voolstra, and Scott R. Santos. 2018. “Systematic Revision of Symbiodiniaceae Highlights the Antiquity and Diversity of Coral Endosymbionts.” *Current Biology: CB* 28 (16): 2570–80.e6.

Le Nohaïc, Morane, Claire L. Ross, Christopher E. Cornwall, Steeve Comeau, Ryan Lowe, Malcolm T. McCulloch, and Verena Schoepf. 2017. “Marine Heatwave Causes Unprecedented Regional Mass Bleaching of Thermally Resistant Corals in Northwestern Australia.” *Scientific Reports* 7 (1): 14999.

Lesser, Michael P. 2011. “Coral Bleaching: Causes and Mechanisms.” *Coral Reefs: An Ecosystem in Transition*. https://doi.org/10.1007/978-94-007-0114-4_23.

Lueker, T. J., Dickson, A. G., & Keeling, C. D. (2000). Ocean pCO2 calculated from dissolved inorganic carbon, alkalinity, and equations for K1 and K2: validation based on laboratory measurements of CO2 in gas and seawater at equilibrium. *Marine chemistry*, *70*(1-3), 105-119.

Loya, Y., K. Sakai, K. Yamazato, Y. Nakano, H. Sambali, and R. van Woesik. 2001. “Coral Bleaching: The Winners and the Losers.” *Ecology Letters*. https://doi.org/10.1046/j.1461-0248.2001.00203.x.

Magnusson, S. H., Fine, M., & Kühl, M. (2007). Light microclimate of endolithic phototrophs in the scleractinian corals Montipora monasteriata and Porites cylindrica. *Marine Ecology Progress Series*, *332*, 119-128.

Marshall, B., and P. V. Biscoe. 1980. “A Model for C_3Leaves Describing the Dependence of Net Photosynthesis on Irradiance.” *Journal of Experimental Botany*. https://doi.org/10.1093/jxb/31.1.29.

Masson-Delmotte, T. W. V., P. Zhai, H. O. Pörtner, D. Roberts, J. Skea, P. R. Shukla, A. Pirani, et al. 2018. “IPCC, 2018: Summary for Policymakers. In: Global Warming of 1.5 C. An IPCC Special Report on the Impacts of Global Warming of 1.5 C above Pre-Industrial Levels and Related Global Greenhouse Gas Emission Pathways, in the Context of Strengthening the Global.” *World Meteorological Organization, Geneva, Tech. Rep*.

Matsuda, Shayle, Ariana Huffmyer, Elizabeth A. Lenz, Jen Davidson, Joshua Hancock, Ariana Przybylowski, Teegan Innis, Ruth D. Gates, and Katie L. Barott. n.d. “Coral Bleaching Susceptibility Is Predictive of Subsequent Mortality within but Not between Coral Species.” https://doi.org/10.1101/2019.12.17.880161.

Matthews, Jennifer L., Clinton A. Oakley, Adrian Lutz, Katie E. Hillyer, Ute Roessner, Arthur R. Grossman, Virginia M. Weis, and Simon K. Davy. 2018. “Partner Switching and Metabolic Flux in a Model Cnidarian–dinoflagellate Symbiosis.” *Proceedings of the Royal Society B: Biological Sciences*. https://doi.org/10.1098/rspb.2018.2336.

McLachlan, Rowan H., James T. Price, Agustí Muñoz-Garcia, Noah L. Weisleder, Christopher P. Jury, Robert J. Toonen, and Andréa G. Grottoli. 2021. “Environmental Gradients Drive Physiological Variation in Hawaiian Corals.” *Coral Reefs* , July. https://doi.org/10.1007/s00338-021-02140-8.

McLachlan, Rowan H., James T. Price, Sarah L. Solomon, and Andréa G. Grottoli. 2020. “Thirty Years of Coral Heat-Stress Experiments: A Review of Methods.” *Coral Reefs*. https://doi.org/10.1007/s00338-020-01931-9.

Mollica, Nathaniel R., Weifu Guo, Anne L. Cohen, Kuo-Fang Huang, Gavin L. Foster, Hannah K. Donald, and Andrew R. Solow. 2018. “Ocean Acidification Affects Coral Growth by Reducing Skeletal Density.” *Proceedings of the National Academy of Sciences of the United States of America* 115 (8): 1754–59.

Mydlarz, Laura D., Elizabeth S. McGinty, and C. Drew Harvell. 2010. “What Are the Physiological and Immunological Responses of Coral to Climate Warming and Disease?” *The Journal of Experimental Biology* 213 (6): 934–45.

Neal, Benjamin Paul, Adi Khen, Tali Treibitz, Oscar Beijbom, Grace O’Connor, Mary Alice Coffroth, Nancy Knowlton, David Kriegman, B. Greg Mitchell, and David I. Kline. 2017. “Caribbean Massive Corals Not Recovering from Repeated Thermal Stress Events during 2005–2013.” *Ecology and Evolution*. https://doi.org/10.1002/ece3.2706.

Oakley, C. A., and S. K. Davy. 2018. “Cell Biology of Coral Bleaching.” *Ecological Studies*. https://doi.org/10.1007/978-3-319-75393-5_8.

Oksanen J, Blanchet FG, Friendly M, Kindt R, Legendre P, McGlinn D, Minchin PR, O'Hara RB, Simpson GL, Solymos P, Stevens MHH, Szoecs E, Wagner H (2018) vegan: Community Ecology Package. R package version 2.5-2

Olito, Colin, Craig R. White, Dustin J. Marshall, and Diego R. Barneche. 2017. “Estimating Monotonic Rates from Biological Data Using Local Linear Regression.” *The Journal of Experimental Biology* 220 (Pt 5): 759–64.

Oliver, Eric C. J., Jessica A. Benthuysen, Sofia Darmaraki, Markus G. Donat, Alistair J. Hobday, Neil J. Holbrook, Robert W. Schlegel, and Alex Sen Gupta. 2021. “Marine Heatwaves.” *Annual Review of Marine Science* 13 (January): 313–42.

Oliver, Eric C. J., Markus G. Donat, Michael T. Burrows, Pippa J. Moore, Dan A. Smale, Lisa V. Alexander, Jessica A. Benthuysen, et al. 2018. “Longer and More Frequent Marine Heatwaves over the Past Century.” *Nature Communications* 9 (1): 1324.

Oliver, T. A., and S. R. Palumbi. 2011. “Many Corals Host Thermally Resistant Symbionts in High-Temperature Habitat.” *Coral Reefs*. https://doi.org/10.1007/s00338-010-0696-0.

Oppen, Madeleine J. H. van, and Janice M. Lough. 2018. *Coral Bleaching: Patterns, Processes, Causes and Consequences*. Springer.

Osborne, Kate, Angus A. Thompson, Alistair J. Cheal, Michael J. Emslie, Kerryn A. Johns, Michelle J. Jonker, Murray Logan, Ian R. Miller, and Hugh P. A. Sweatman. 2017. “Delayed Coral Recovery in a Warming Ocean.” *Global Change Biology*. https://doi.org/10.1111/gcb.13707.

Pendleton, Linwood H., Ove Hoegh-Guldberg, Chris Langdon, and Adrien Comte. 2016. “Multiple Stressors and Ecological Complexity Require a New Approach to Coral Reef Research.” *Frontiers in Marine Science*. https://doi.org/10.3389/fmars.2016.00036.

Perez, F. F., & Fraga, F. (1987). Association constant of fluoride and hydrogen ions in seawater. *Marine Chemistry*, *21*(2), 161-168.

Putnam, H. M., A. B. Mayfield, T. Y. Fan, C. S. Chen, and R. D. Gates. 2013. “The Physiological and Molecular Responses of Larvae from the Reef-Building Coral Pocillopora Damicornis

Exposed to near-Future Increases in Temperature and pCO2." *Marine Biology*. https://doi.org/10.1007/s00227-012-2129-9.

Putnam, Hollie M. 2021. "Avenues of Reef-Building Coral Acclimatization in Response to Rapid Environmental Change." *The Journal of Experimental Biology* 224 (Pt Suppl 1). https://doi.org/10.1242/jeb.239319.

Putnam, Hollie M., Katie L. Barott, Tracy D. Ainsworth, and Ruth D. Gates. 2017. "The Vulnerability and Resilience of Reef-Building Corals." *Current Biology: CB* 27 (11): R528–40.

R Core Team (2013). R: A language and environment for statistical computing. R Foundation for Statistical Computing, Vienna, Austria. ISBN 3-900051-07-0, URL http://www.R-project.org/.

Rodrigues, Lisa J., and Andréa G. Grottoli. 2007. "Energy Reserves and Metabolism as Indicators of Coral Recovery from Bleaching." *Limnology and Oceanography*. https://doi.org/10.4319/lo.2007.52.5.1874.

Rodríguez-Troncoso, Alma P., Eugenio Carpizo-Ituarte, and Amílcar L. Cupul-Magaña. 2016. "Physiological Response to High Temperature in the Tropical Eastern Pacific Coral *Pocillopora Verrucosa*." *Marine Ecology*. https://doi.org/10.1111/maec.12392.

Rohwer, F., V. Seguritan, F. Azam, and N. Knowlton. 2002. "Diversity and Distribution of Coral-Associated Bacteria." *Marine Ecology Progress Series* 243: 1–10.

Ross, Claire L., Andrew Warnes, Steeve Comeau, Christopher E. Cornwall, Michael V. W. Cuttler, Melissa Naugle, Malcolm T. McCulloch, and Verena Schoepf. 2022. "Coral Calcification Mechanisms in a Warming Ocean and the Interactive Effects of Temperature and Light." *Communications Earth & Environment* 3 (1): 1–11.

Safaie, Aryan, Nyssa J. Silbiger, Timothy R. McClanahan, Geno Pawlak, Daniel J. Barshis, James L. Hench, Justin S. Rogers, Gareth J. Williams, and Kristen A. Davis. 2018. "High Frequency Temperature Variability Reduces the Risk of Coral Bleaching." *Nature Communications* 9 (1): 1671.

Scheufen, Tim, Wiebke E. Krämer, Roberto Iglesias-Prieto, and Susana Enríquez. 2017. "Seasonal Variation Modulates Coral Sensibility to Heat-Stress and Explains Annual Changes in Coral Productivity." *Scientific Reports* 7 (1): 4937.

Schoepf, Verena, Andréa G. Grottoli, Stephen J. Levas, Matthew D. Aschaffenburg, Justin H. Baumann, Yohei Matsui, and Mark E. Warner. 2015. "Annual Coral Bleaching and the Long-Term Recovery Capacity of Coral." *Proceedings of the Royal Society B: Biological Sciences*. https://doi.org/10.1098/rspb.2015.1887.

Schoepf, Verena, Hermione Sanderson, and Ellis Larcombe. 2022. "Coral Heat Tolerance under Variable Temperatures: Effects of Different Variability Regimes and Past Environmental History vs. Current Exposure." *Limnology and Oceanography*. https://doi.org/10.1002/lno.12000.

Shaw, Emily C., Sarah M. Hamylton, and Stuart R. Phinn. 2016. "Incorporating Benthic Community Changes into Hydrochemical-Based Projections of Coral Reef Calcium Carbonate Production under Ocean Acidification." *Coral Reefs* 35 (2): 739–50.

Silverstein, Rachel N., Ross Cunning, and Andrew C. Baker. 2015. "Change in Algal Symbiont Communities after Bleaching, Not Prior Heat Exposure, Increases Heat Tolerance of Reef Corals." *Global Change Biology*. https://doi.org/10.1111/gcb.12706.

Stat, Michael, Emily Morris, and Ruth D. Gates. 2008. "Functional Diversity in Coral–dinoflagellate Symbiosis." *Proceedings of the National Academy of Sciences* 105 (27): 9256–61.

Sweet, Michael J., and Barbara E. Brown. 2016. "Coral Responses to Anthropogenic Stress in the Twenty-First Century: An Ecophysiological Perspective." *Oceanography and Marine Biology: An Annual Review*, 279–322.

Therneau, Terry M., and Patricia M. Grambsch. 2013. *Modeling Survival Data: Extending the Cox Model*. Springer Science & Business Media.

Thomas, Luke, and Stephen R. Palumbi. 2017. “The Genomics of Recovery from Coral Bleaching.” *Proceedings. Biological Sciences / The Royal Society* 284 (1865). https://doi.org/10.1098/rspb.2017.1790.

Thornhill, Daniel J., Randi D. Rotjan, Brian D. Todd, Geoff C. Chilcoat, Roberto Iglesias-Prieto, Dustin W. Kemp, Todd C. LaJeunesse, et al. 2011. “A Connection between Colony Biomass and Death in Caribbean Reef-Building Corals.” *PloS One* 6 (12): e29535.

Tresguerres, Martin, Katie L. Barott, Megan E. Barron, Dimitri D. Deheyn, David I. Kline, and Lauren B. Linsmayer. 2017. “Cell Biology of Reef-Building Corals: Ion Transport, Acid/Base Regulation, and Energy Metabolism.” In *Acid-Base Balance and Nitrogen Excretion in Invertebrates: Mechanisms and Strategies in Various Invertebrate Groups with Considerations of Challenges Caused by Ocean Acidification*, edited by Dirk Weihrauch and Michael O’Donnell, 193–218. Cham: Springer International Publishing.

Veal, C. J., M. Carmi, M. Fine, and O. Hoegh-Guldberg. 2010. “Increasing the Accuracy of Surface Area Estimation Using Single Wax Dipping of Coral Fragments.” *Coral Reefs* 29 (4): 893–97.

Wall, Christopher B., Mario Kaluhiokalani, Brian N. Popp, Megan J. Donahue, and Ruth D. Gates. 2020. “Divergent Symbiont Communities Determine the Physiology and Nutrition of a Reef Coral across a Light-Availability Gradient.” *The ISME Journal* 14 (4): 945–58.

Wall, Christopher B., Contessa A. Ricci, Alexandra D. Wen, Bren E. Ledbetter, Delania E. Klinger, Laura D. Mydlarz, Ruth D. Gates, and Hollie M. Putnam. 2021. “Shifting Baselines: Physiological Legacies Contribute to the Response of Reef Corals to Frequent Heatwaves.” *Functional Ecology* 35 (6): 1366–78.

Wei T, Simko V (2021). *R package 'corrplot': Visualization of a Correlation Matrix*. (Version 0.92)

Weis, Virginia M. 2008. “Cellular Mechanisms of Cnidarian Bleaching: Stress Causes the Collapse of Symbiosis.” *The Journal of Experimental Biology* 211 (Pt 19): 3059–66.

Woesik, Robert van, and Chelsey Kratochwill. 2022. “A Global Coral-Bleaching Database, 1980-2020.” *Scientific Data* 9 (1): 20.

Woesik, Robert van, Tom Shlesinger, Andréa G. Grottoli, Rob J. Toonen, Rebecca Vega Thurber, Mark E. Warner, Ann Marie Hulver, et al. 2022. “Coral-bleaching Responses to Climate Change across Biological Scales.” *Global Change Biology*. https://doi.org/10.1111/gcb.16192.

Woesik, R. van, K. Sakai, A. Ganase, and Y. Loya. 2011. “Revisiting the Winners and the Losers a Decade after Coral Bleaching.” *Marine Ecology Progress Series*. https://doi.org/10.3354/meps09203.

Wolfe, Kennedy, and George Roff. 2022. “Global Predictions of Coral Reef Dissolution in the Anthropocene.” *Communications Earth & Environment* 3 (1): 1–4.

Ziegler, Maren, Andrea Anton, Shannon G. Klein, Nils Rädecker, Nathan R. Geraldi, Sebastian Schmidt-Roach, Vincent Saderne, et al. 2021. “Integrating Environmental Variability to Broaden the Research on Coral Responses to Future Ocean Conditions.” *Global Change Biology* 27 (21): 5532–46.

Ziegler, Maren, Cornelia M. Roder, Claudia BÃ¼chel, and Christian R. Voolstra. 2015. “Mesophotic Coral Depth Acclimatization Is a Function of Host-Specific Symbiont Physiology.” *Frontiers in Marine Science*. https://doi.org/10.3389/fmars.2015.00004.

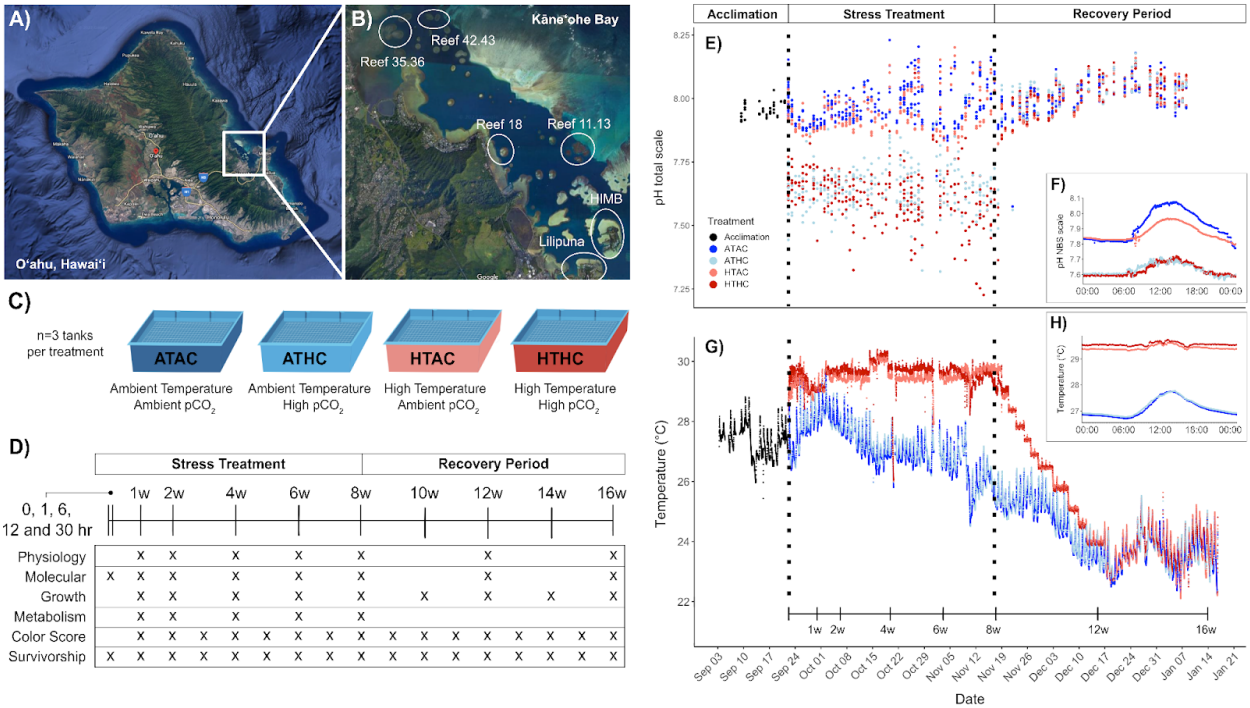

Fig 1. Experimental design for an environmentally and seasonally realistic extended heat wave scenario. (A) A map of O‘ahu, Hawai‘i with a highlight box around the study site. (B) A map of Kane‘ohe Bay with six circled collection sites. (C) Twelve tanks (n=3 per treatment) were assigned a treatment with the following color and acronym code: ATAC (dark blue), ATHC (light blue), HTAC (salmon), HTHC (dark red). (D) Sampling timeline with a ‘X’ to indicate when sampling occurred for each response category. Physiology includes: antioxidant capacity, soluble protein, AFDW, chlorophyll-a content, and endosymbiont density. Metabolism includes: photosynthetic and respiration rates. (E) Discrete measurements for pH treatment conditions (pH total scale) for the full experimental period. (F) Average daily pH treatment conditions modeled after natural fluctuations that occur in Kane‘ohe Bay. Data comes from continuous measurements from an Apex System set-up during the first 2 weeks of exposure period. (G) Discrete measurements for temperature treatment conditions (°C) for the full experimental period. A timeline of physiological sampling dates is indicated above the x-ais. (H) Average daily temperature treatment conditions modeled after natural fluctuations that occur in Kane‘ohe Bay.

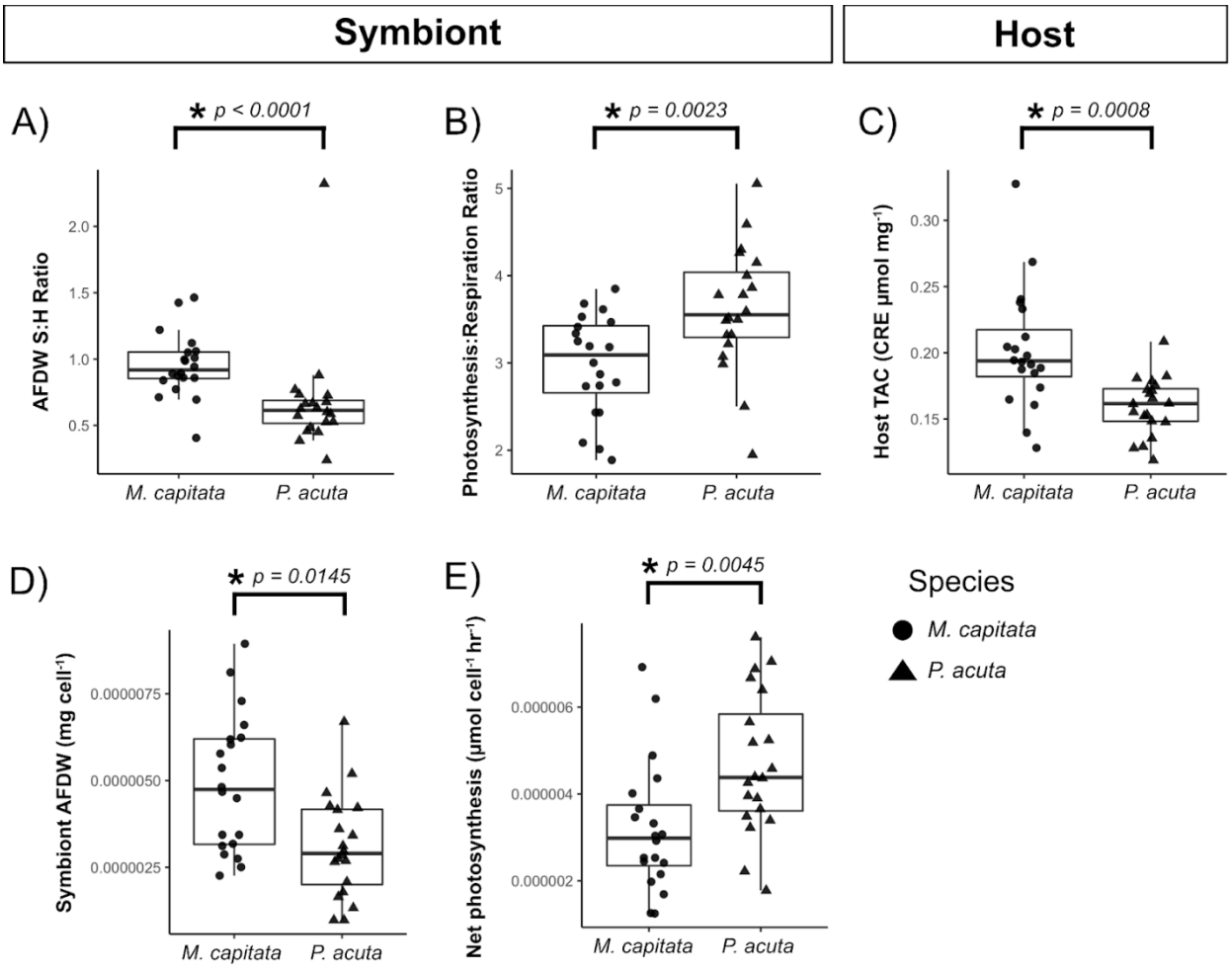

Fig 2. Baseline physiological measurements measured at week 1 ordered by most significant differences to least. (A) Ash-free dry weight symbiont:host ratio, (B) Photosynthesis:Respiration ratio, (C) Host total antioxidant capacity (CRE µmol mg^{-1}), (D) Symbiont cellular AFDW (mg $cell^{-1}$), and (E) Holobiont net photosynthetic rates (µmol cm^{-2} hr^{-1}).

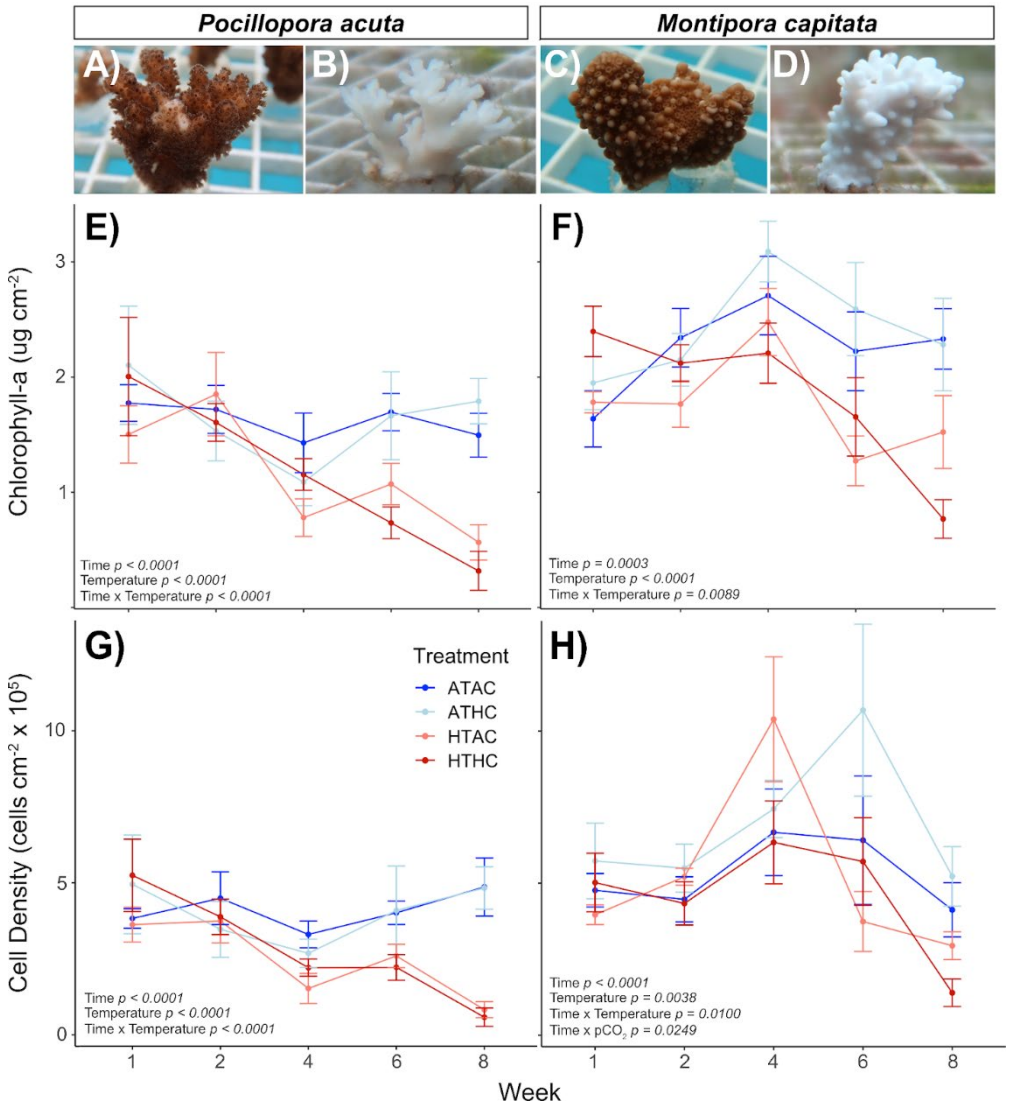

Fig 3. Holobiont chlorophyll-a-a content (µg cm-2) and endosymbiont cell density (cells cm^{-2} x 10^5) levels during the exposure period (week 1-8). The x-axis of panel E, F, G, and H is time in weeks with sampling at week 1, 2, 4, 6, and 8 weeks. Color indicates the four treatments. Significant effects for each response are labeled with corresponding p-value. (A) Example of a healthy *P. acuta* fragment. (B) Example of a bleached *P. acuta* fragment. (C) Example of a healthy *M. capitata* fragment. (D) Example of a bleached *M. capitata* fragment. (E) *P. acuta* chlorophyll-*a* content (µg cm^{-2}). (F) *M. capitata* chlorophyll-*a* content (µg cm^{-2}). (G) *P. acuta* cell density levels (cells cm^{-2} x 10^5). (H) *M. capitata* cell density levels (cells cm^{-2} x 10^5).

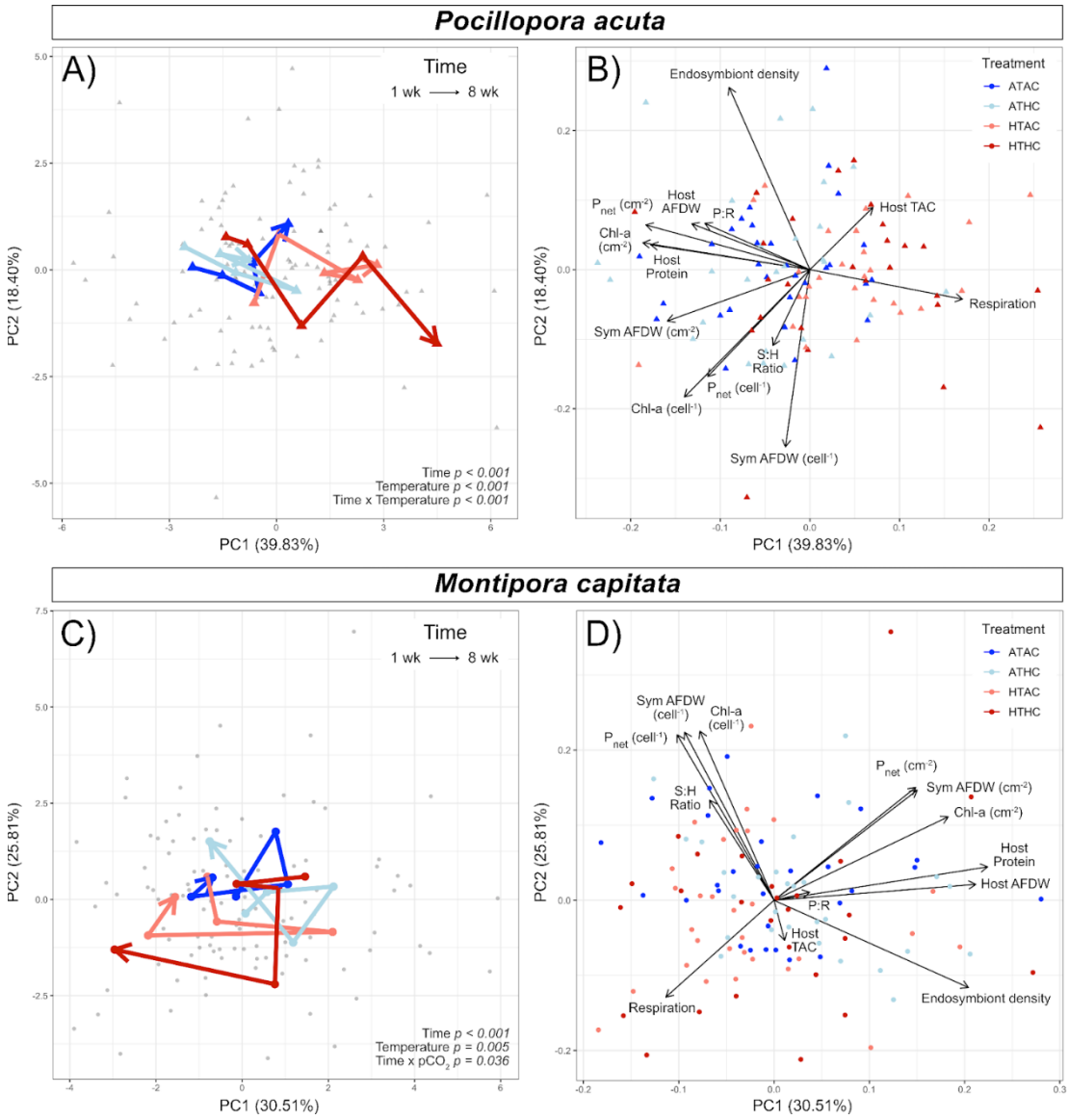

Fig. 4. Principal components analyses of multivariate physiological state during the exposure period (week 1-8) for both species. (A,B) *P. acuta* fragments. (C,D) *M. capitata* fragments. Each point represents an individual coral fragment's multivariate physiological state composed of 13 host and symbiont response variables and colored by treatment. Significant effects for each species are included within Panels A and C (bottom right of each panel). PC axis labels indicate the percent variance explained by that axis. (A,C) Centroid multivariate state for each treatment at each time period is indicated by a bold, treatment-colored point. All mean points are connected within each treatment to show the shifts in the through time (week 1 → 8). (B,D) Biplots of the response variables are shown on the multivariate plots. Each black arrow represents a physiological response variable. The direction and length of each arrow indicates the relative strength of that variable to the PC axes.

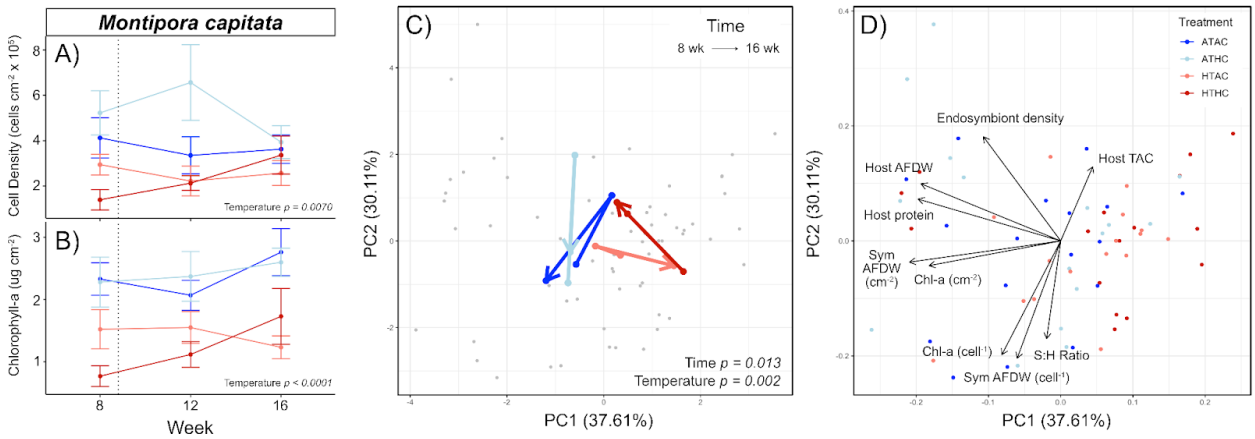

Fig. 5. Bleaching assessment and Principal components analysis for multivariate physiological state of *M. capitata* fragments during the recovery period (week 8-16). (A) Endosymbiont densities (cells cm^{-2} x 10^5) and (B) Holobiont chlorophyll-a-a content (µg cm^{-2}) for the recovery period. (C,D) Each point represents an individual fragment's multivariate physiological state composed of 9 host and symbiont response variables (respiration and photosynthetic rates were not measured during the recovery period). (C) Centroid multivariate physiological state through time (week 8 → 16). (D) Biplot of individual physiological variable contributions to PCA separation. Each point (individual fragment) is colored by treatment.

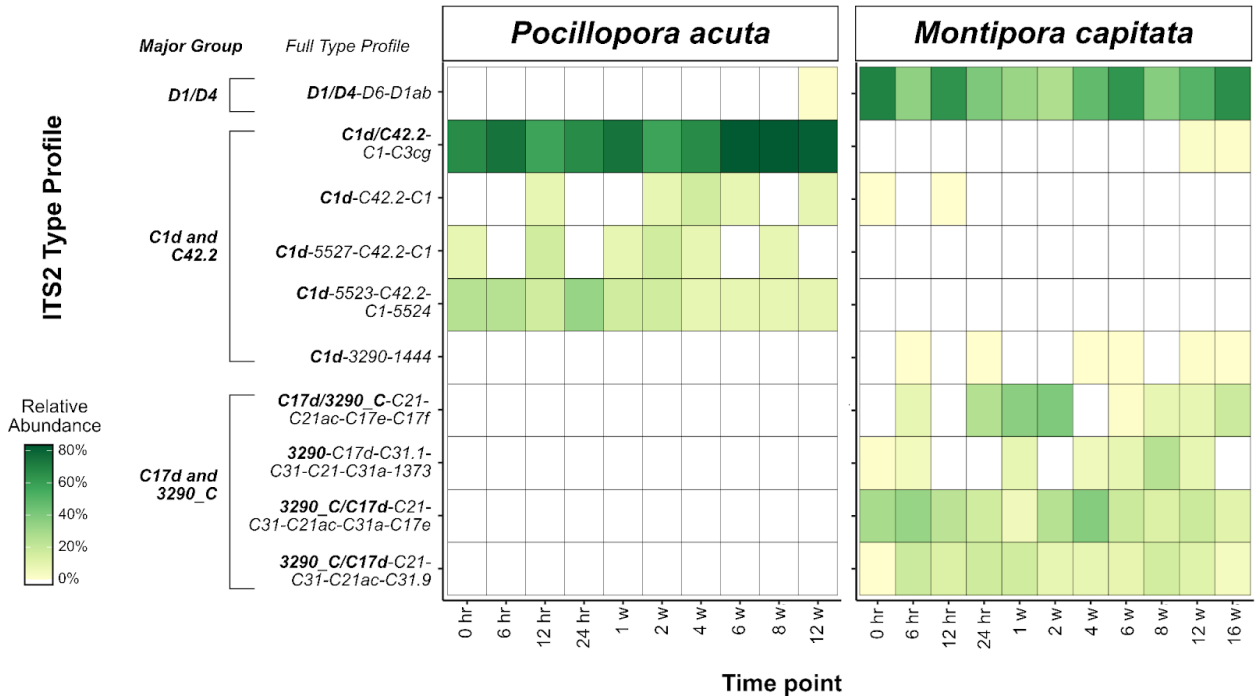

Fig. 6. Relative abundance of Symbiodiniaceae 'Type Profiles' identified by ITS2 sequencing for both species during exposure **and recovery periods.** The y-axis includes each Type Profile, composed of a Major Sequence ID (in bold italics) and subsequent Full Type Profile ID (in italics). Relative abundance is indicated by 0-100% continuous color-scale, with the darkest green coloring equals 100% abundance of that full Type Profile. The exposure period includes 0, 6, and 12 hour, 1, 2, 4, 6, 8, and 12 weeks. The recovery period includes 12 and 16 weeks, but there was not a high enough sample size for *P. acuta* fragments at 16 weeks.

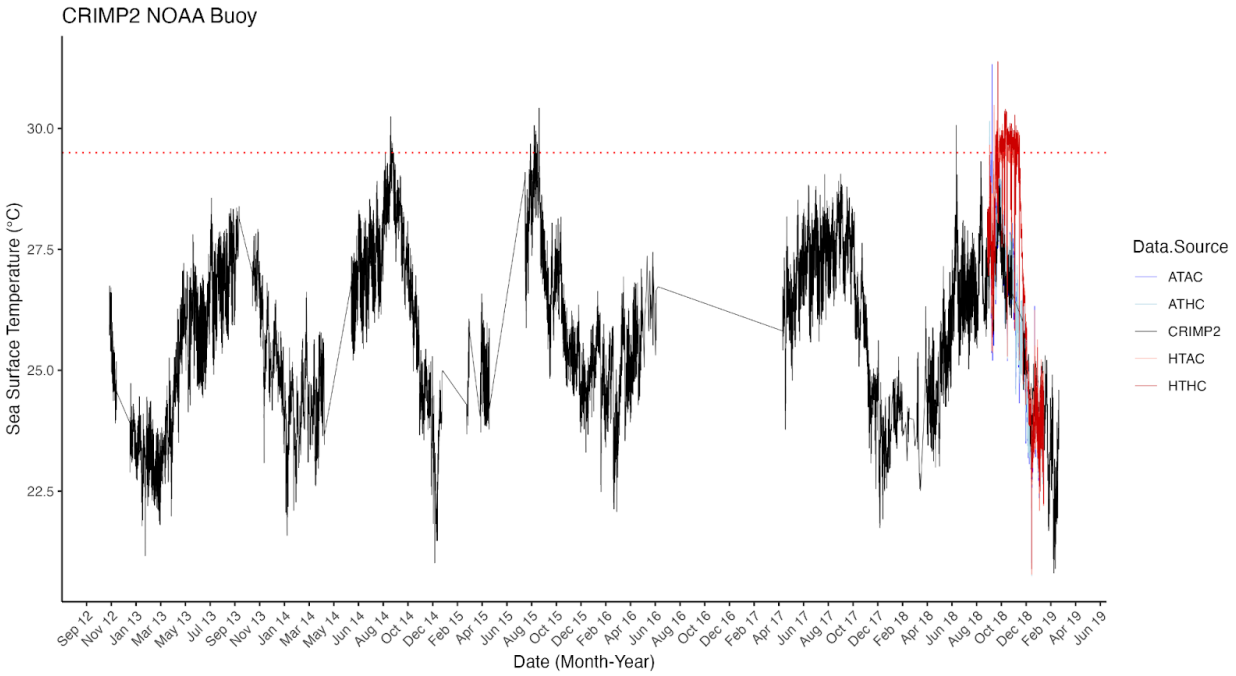

Fig. S1. NOAA Moku o Loʻe Buoy data (CRIMP2) from September 2012 - June 2019 with treatment conditions overlayed. CRIMP2 buoy data (sea surface temperature °C) was used to determine an environmentally realistic range of temperatures for the experimental exposure period. The red dotted line represents the average high temperature treatment condition.

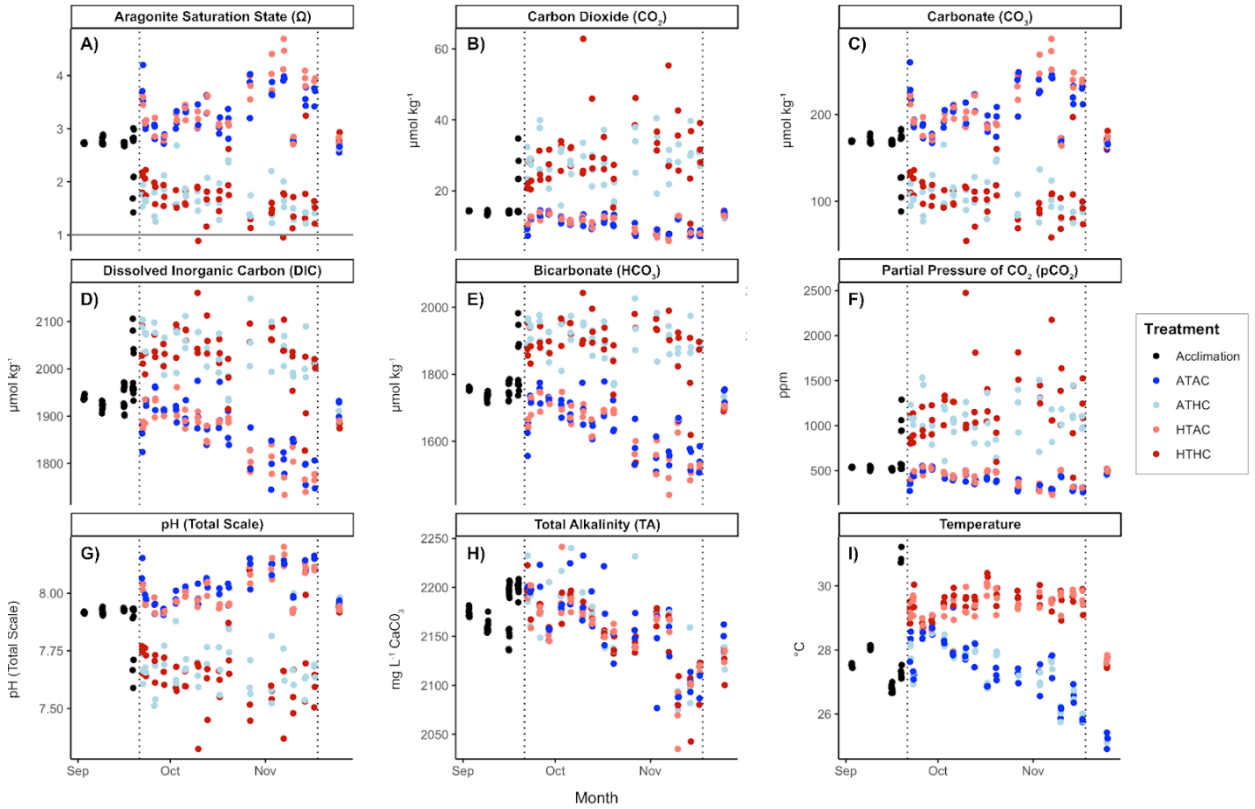

Fig. S2. Carbonate chemistry parameters during the acclimation, exposure, and beginning of the recovery period for all treatments. Treatment is indicated by color and vertical dotted lines mark the start and end of the treatment period. All x-axes represent time by month. Parameters include the following: (A) Aragonite Saturation State (Ω). (B) Carbon dioxide (CO_2; µmol kg^{-1}). (C) Carbonate (CO_3; µmol kg^{-1}). (D) Dissolved inorganic carbon (DIC; µmol kg^{-1}). (E) Bicarbonate (HCO_3; µmol kg^{-1}). (F) Partial pressure of CO_2 (pCO_2; ppm). (G) pH (total scale). (H) Total alkalinity (TA; mg L^{-1} $CaCO_3$) (I). Temperature (°C).

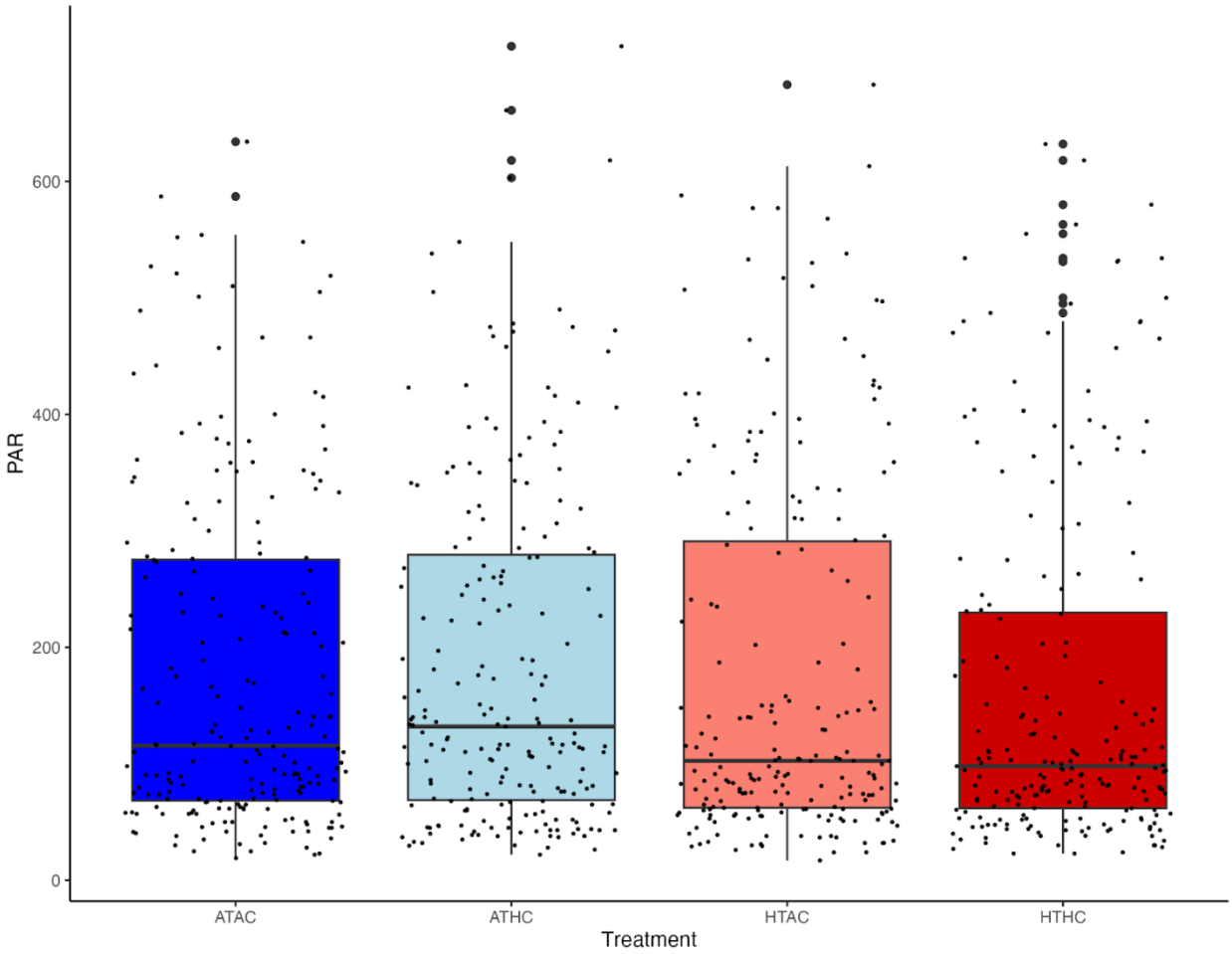

Fig. S3. Light data from the exposure period for all treatments. Light reported in PAR measured with a LICOR-193 as described in methods. Color indicates treatment (light blue = ATAC, dark blue = ATHC, light red = HTAC, and dark red = HTHC).

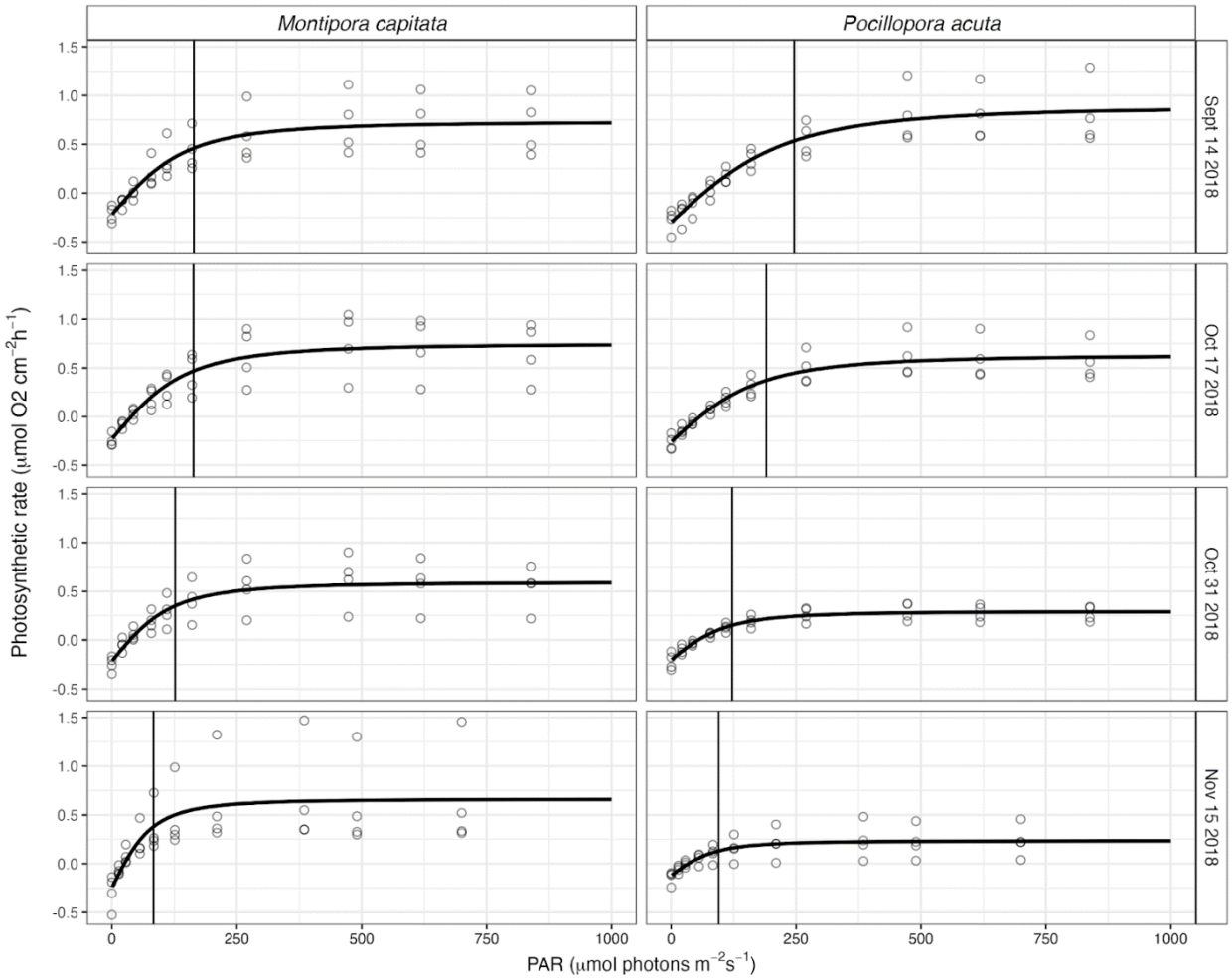

Fig. S4. Photosynthetic Irradiance (PI) Curves for four time points during the exposure period for both species. Photosynthetic rates (µmol oxygen cm^{-2} h^{-1}) measured at a range of irradiance (µmol photons m^{-2} s^{-1}) levels plotted for four time points: September 14 2018, October 17 2018, October 31 2018, and November 15 2018. PI curves were conducted to identify saturating irradiance (I_k; solid vertical line in each plot) and ensure coral fragments were not reaching photoinhibition during respiration and photosynthesis measurements.

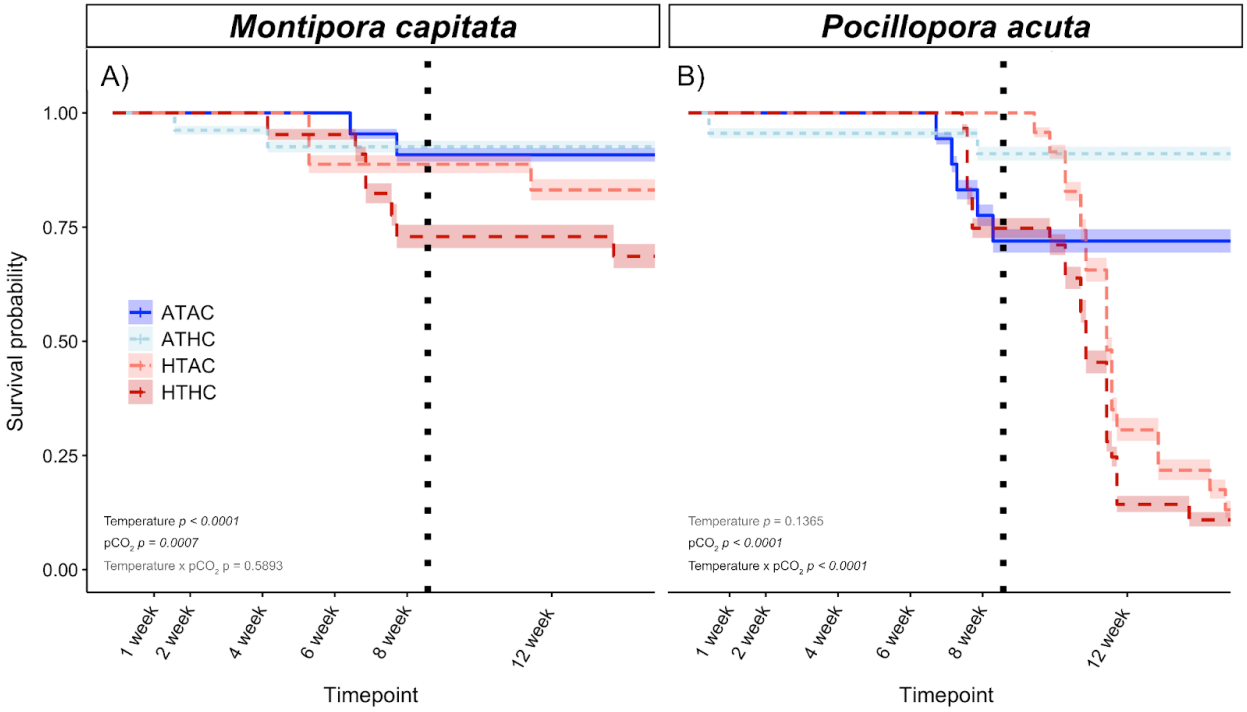

Fig. S5. Survival probability calculated from a cox-mixed effects model for each species. Treatment is indicated by color, significant effects are in black text, and non-significant effects are in gray text. The dotted line is the point when all treatment returns to ambient level conditions. Survival probability is on a scale of 0-1.00 for both (A) *Montipora capitata* fragments. (B) *Pocillopora acuta* fragments across both exposure (day 1 - week 8) and recovery (week 8-16) periods.

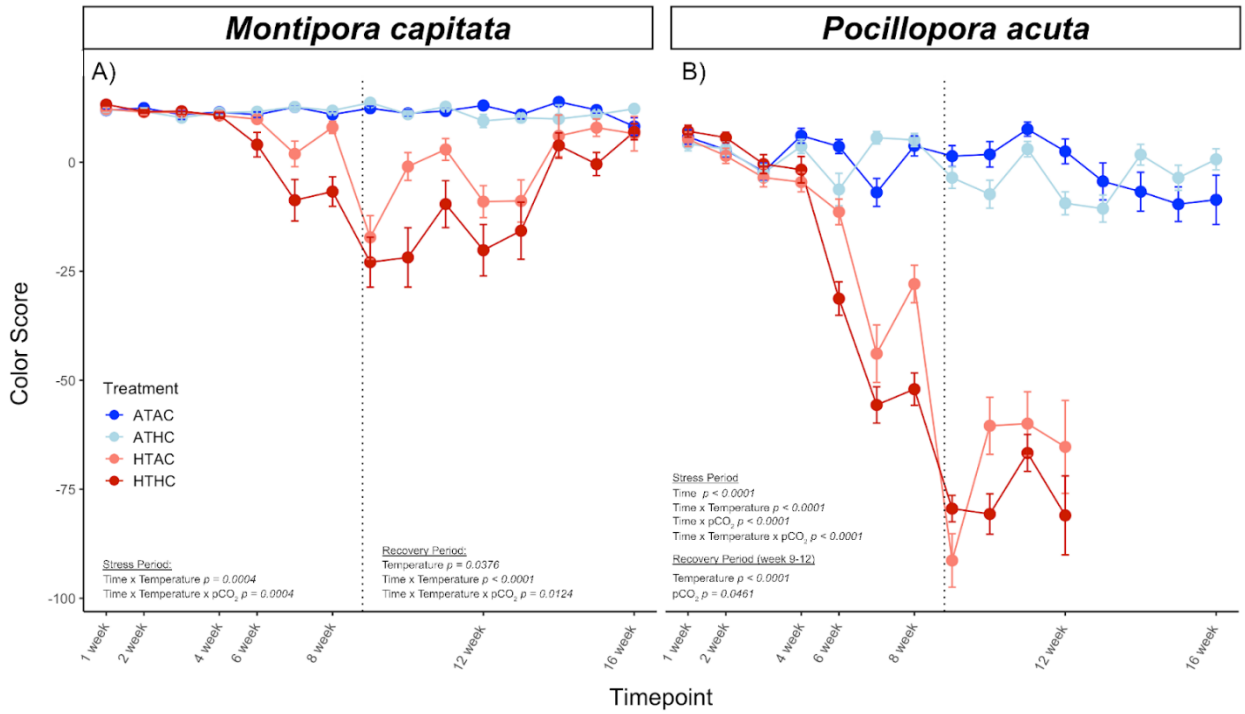

Fig. S6. Mean weekly color score measurements through both exposure (week 1-8) and recovery (week 9-16) periods for each species. (A) *M. capitata* fragments. (B) *P. acuta* fragments. Significant effects from the model output are listed on each panel. Treatments are indicated by colored mean points for each time point. The dotted line is when treatment conditions return to fully ambient values (week 9).

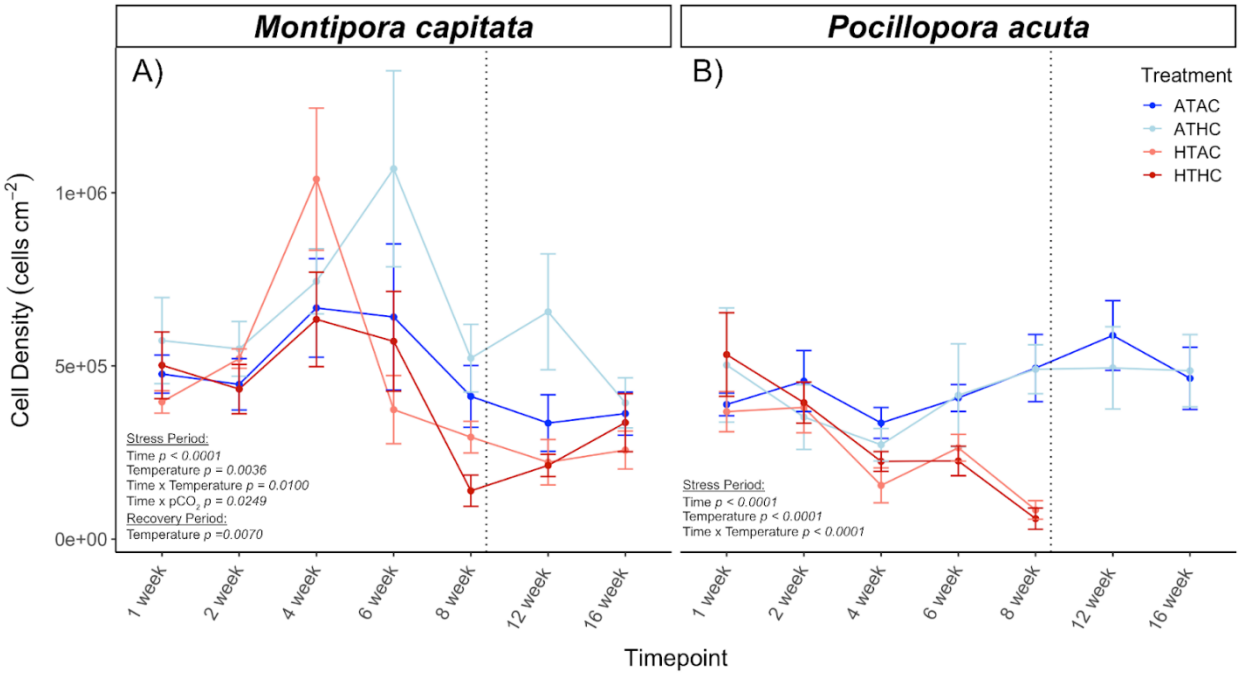

Fig. S7. Mean endosymbiont cell density levels (cells cm^{-2}) through both exposure and recovery periods for (A) *M. capitata* and (B) *P. acuta*. Treatments are indicated by color and significant effects for each species are labeled on the corresponding panel. The dotted line marks when all treatments returned to ambient level conditions at week 9. In *P. acuta*, high temperature treatments did not yield enough sample sizes to complete physiological measurements for weeks 12 and 16.

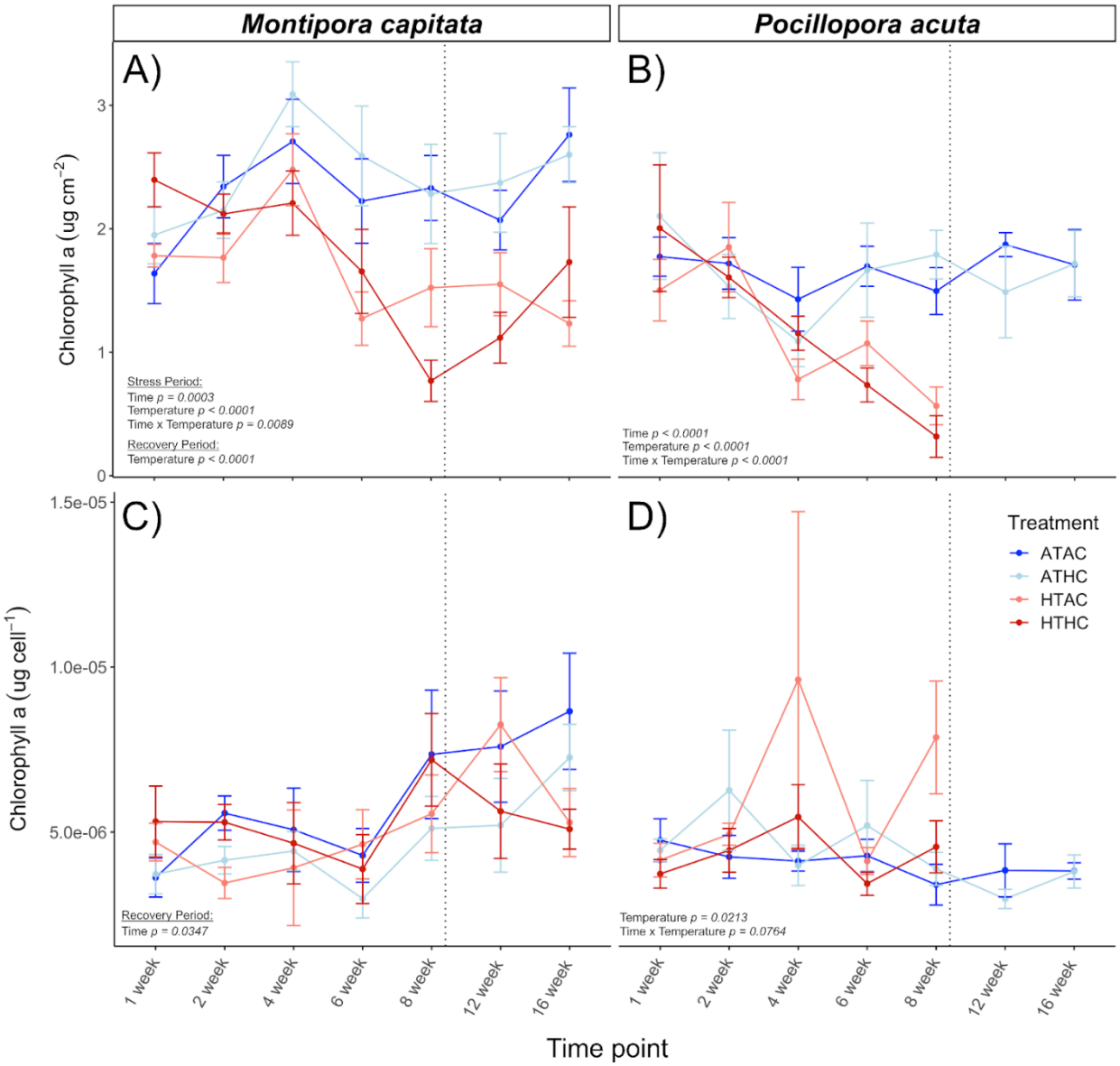

Fig. S8. Mean chlorophyll-a-a content levels normalized to both surface area (µg cm^{-2}) and endosymbiont cell density (µg cell^{-1}) for (A, C) *M. capitata* and (B, D) *P. acuta*. Treatments are indicated by color and significant effects for each species are labeled on the corresponding panel. The dotted line marks when all treatments returned to ambient level conditions at week 9. In all *P. actua* panels, high temperature treatments did not yield enough sample sizes to complete physiological measurements for weeks 12 and 16.

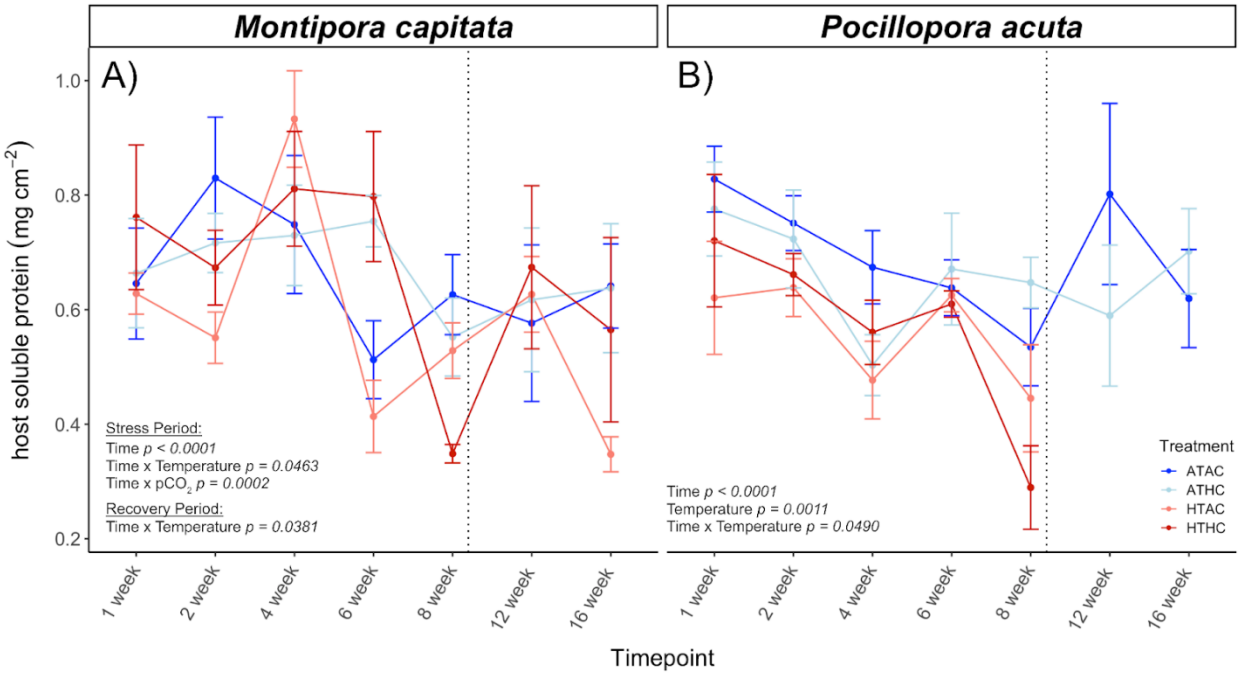

Fig. S9. Mean host soluble protein levels normalized to surface area (mg cm^{-2}) for both (A) *M. capitata* and (B) *P. acuta* in exposure and recovery periods. Treatments are indicated by color and significant effects for each species are labeled on the corresponding panel. The dotted line marks when all treatments returned to ambient level conditions at week 9. In *P. acuta*, high temperature treatments did not yield enough sample sizes to complete physiological measurements for weeks 12 and 16.

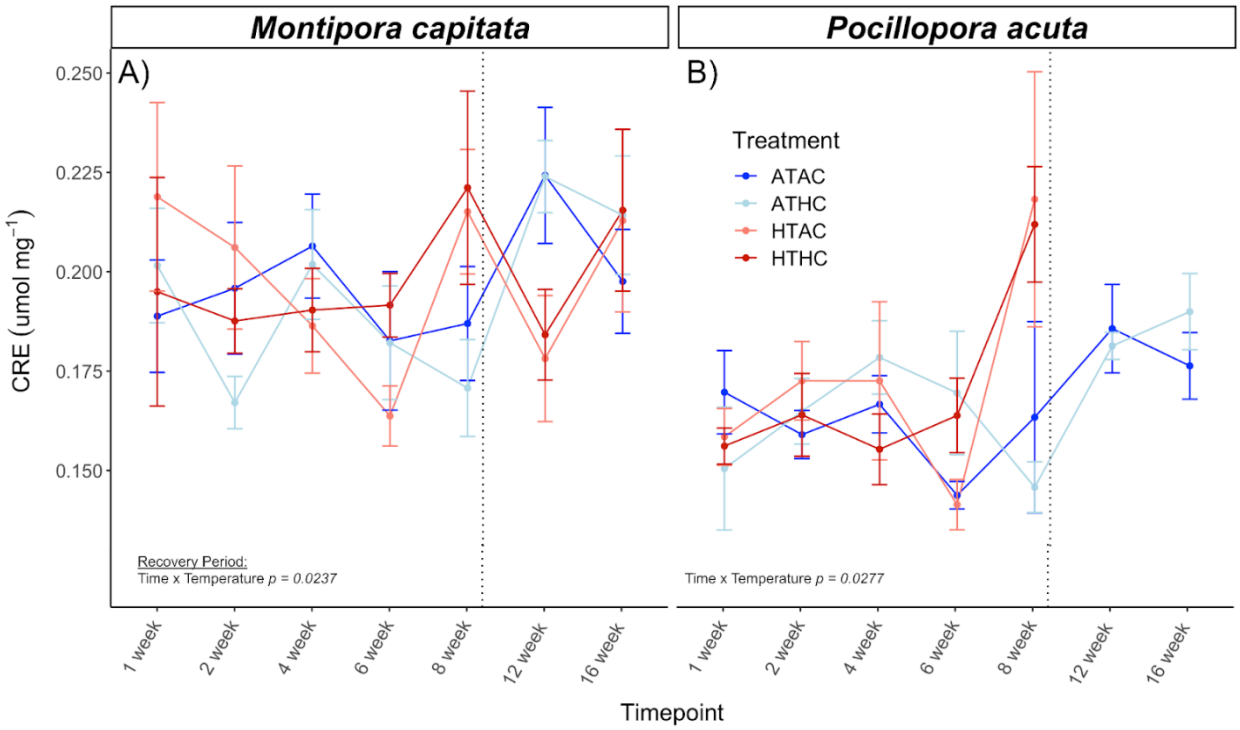

Fig. S10. Mean host total antioxidant capacity (TAC) levels normalized to host soluble protein (CRE µmol mg^{-1}) for both (A) *M. capitata* and (B) *P. acuta* through exposure and recovery periods. Treatments are indicated by color and significant effects for each species are labeled on the corresponding panel. The dotted line marks when all treatments returned to ambient level conditions at week 9. In *P. acuta*, high temperature treatments did not yield enough sample sizes to complete physiological measurements for weeks 12 and 16.

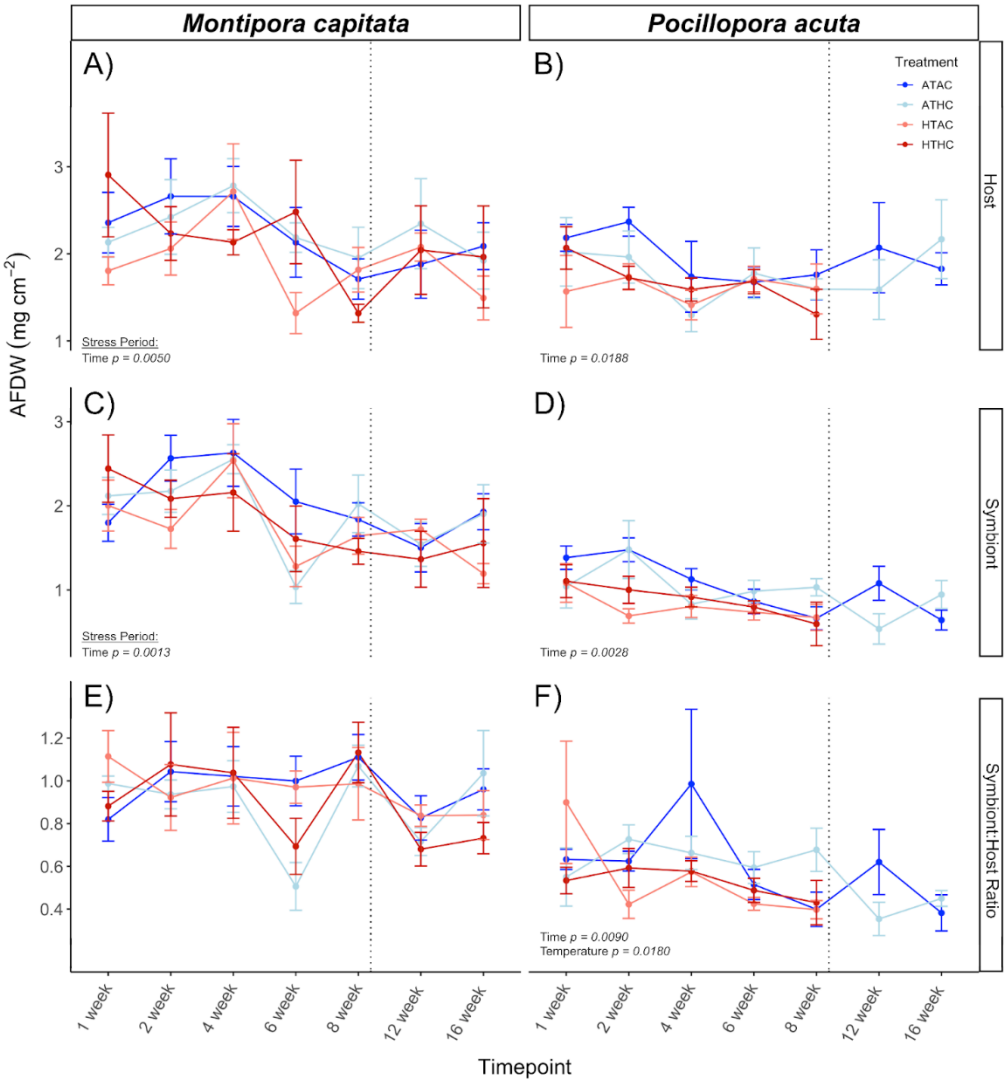

Fig. S11. Mean tissue biomass levels measured in Ash-Free Dry Weight normalized to surface area (AFDW mg cm^{-2}) for host, symbiont, and the ratio of symbiont:host for both (A, C, E) *M. capitata* and (B, D, F) *P. acuta*. Treatments are indicated by color and significant effects are labeled on the corresponding panel. The dotted line represents when treatments returned to ambient level conditions. (A,B) Host AFDW (mg cm^{-2}). (C,D) Symbiont AFDW (mg cm^{-2}). (E,F) Symbiont:Host AFDW Ratio. For all *P. acuta* panels, high temperature treatments did not yield enough sample sizes to complete physiological measurements for weeks 12 and 16.

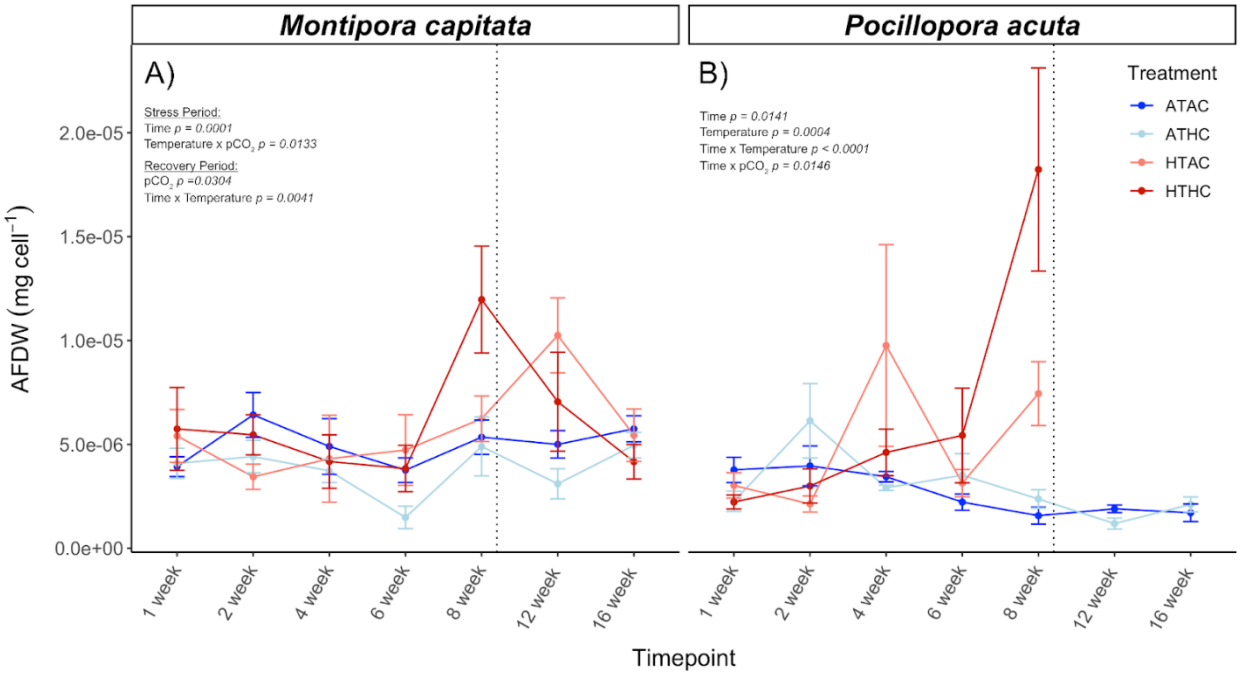

Fig. S12. Mean symbiont cellular Ash-Free Dry Weight levels normalized to cell densities (AFDW; mg cell^{-1}) for (A) *M. capitata* and (B) *P. acuta*. Treatments are indicated by color and significant effects are labeled on the corresponding panel. The dotted line represents when treatments returned to ambient level conditions. In *P. acuta*, high temperature treatments did not yield enough sample sizes to complete physiological measurements for weeks 12 and 16.

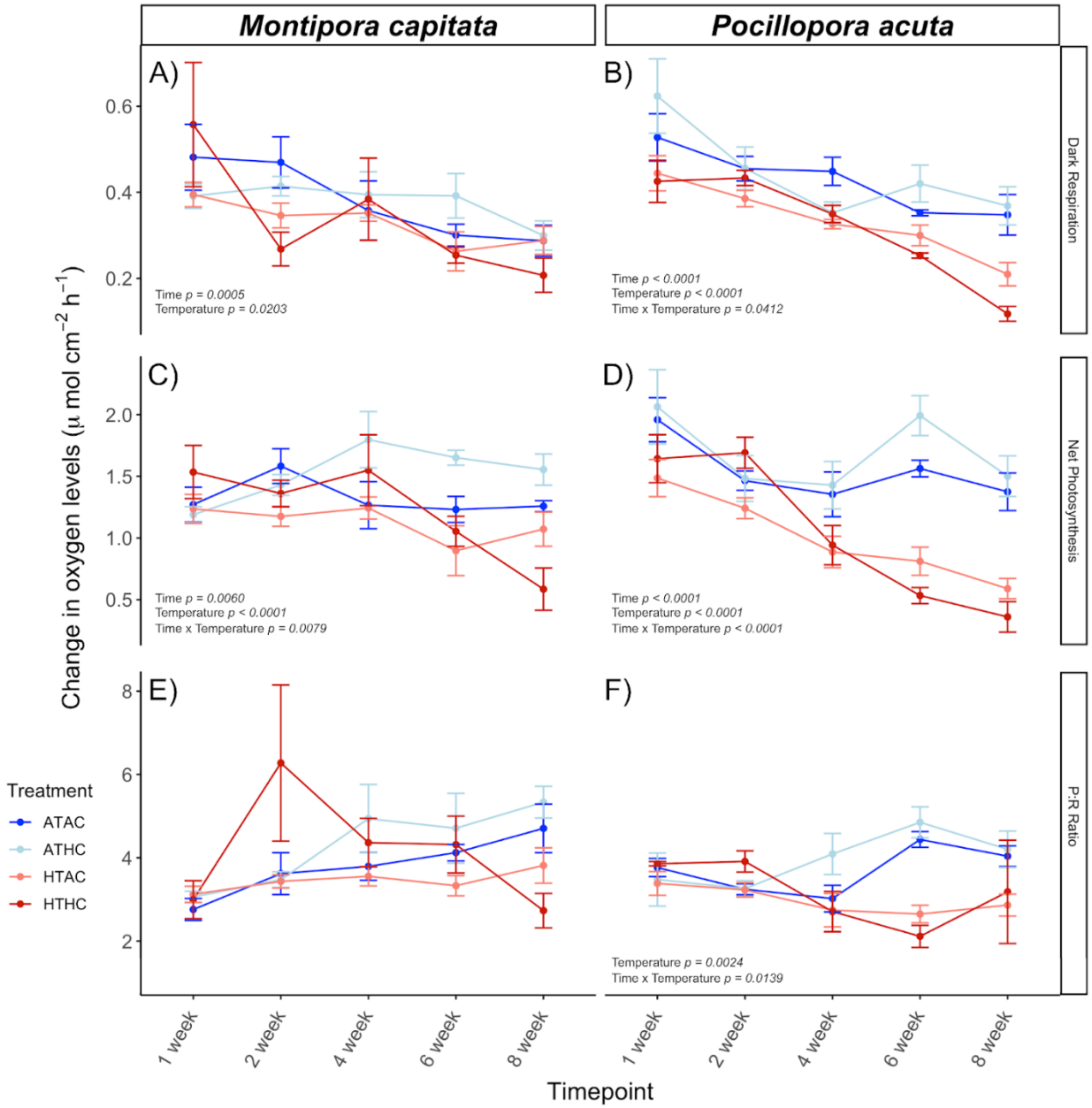

Fig. S13. Mean dark respiration and net photosynthetic rates during the exposure period for both (A, C, E) *M. capitata* and (B, D, F) *P. acuta*. Treatments are indicated by color and significant effects are labeled on the corresponding panel. Both respiration (A,B) and photosynthetic rates (C,D) are reported in units of change in oxygen levels (μmol cm^{-2} hr^{-1}). Respiration rates are the absolute value of the rate of change so that a decrease in rates is equal to lower respiration happening within the coral holobiont. Both respiration and photosynthetic rates were not measured for the recovery period. (E,F) Net photosynthetic rates (μmol cm^{-2} hr^{-1}) to dark respiration rates (μmol cm^{-2} hr^{-1}) ratio reported in unitless values.

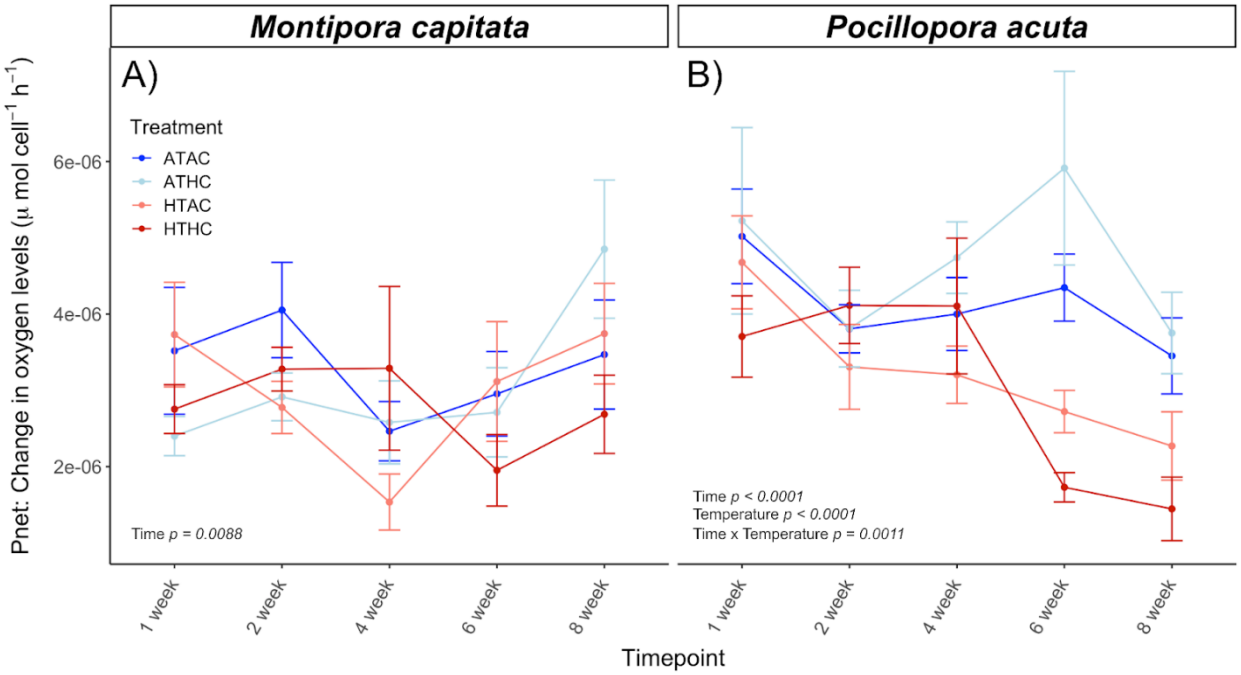

Fig. S14. Mean cellular net photosynthetic rates measured via change in oxygen levels µmol cell^{-1} hr^{-1}) and normalized to cell densities for each species (A) *M. capitata*. (B) *P. acuta*. Treatments are indicated by color and significant effects are labeled on the corresponding panel. Both respiration and photosynthetic rates were not measured for the recovery period.

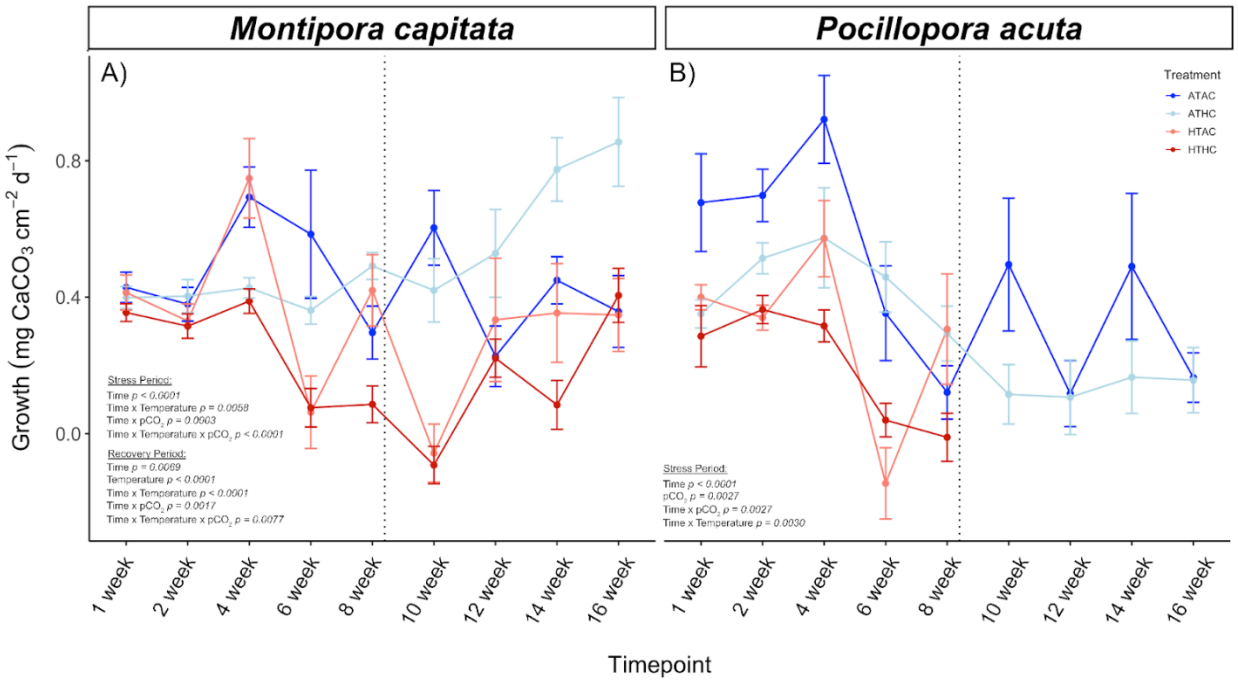

Fig. S15. Weekly mean holobiont growth rates measured in mg $CaCO_3$ cm^{-2} d^{-1} for both (A) *M. capitata* and (B) *Pocilopora acuta*. Treatments are indicated by color and significant effects are labeled on the corresponding panel. The dotted line indicates when treatment returned to ambient levels. *P. acuta* fragments did not survive in enough quantities for sufficient sample sizes during the recovery period.

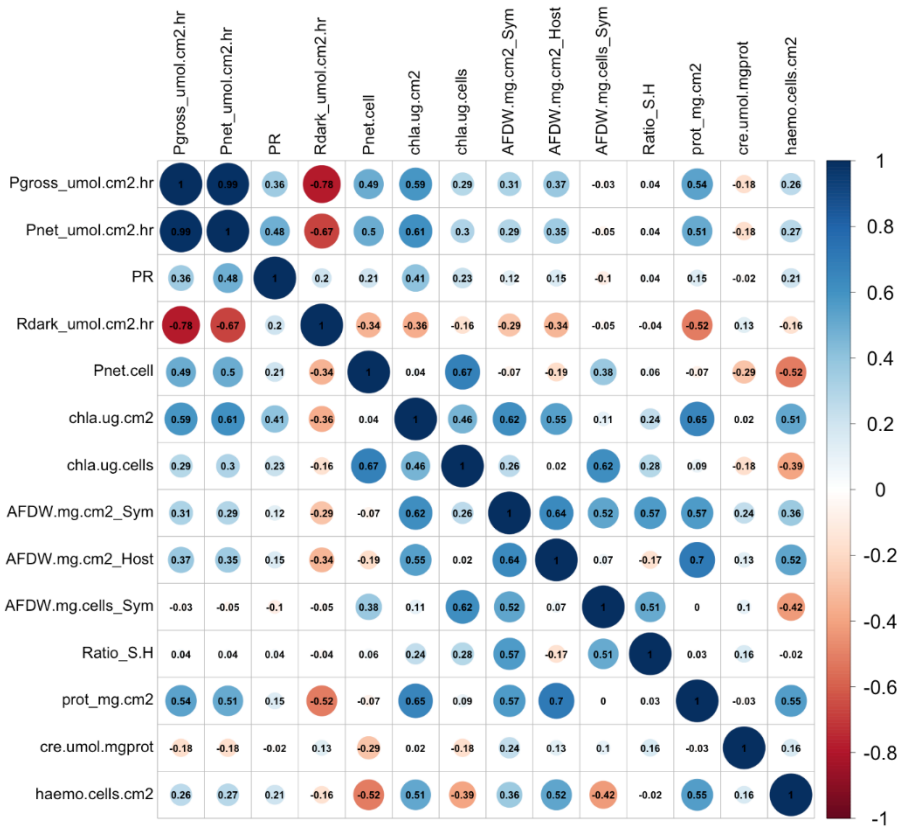

Fig. S16. Correlation plot between all measured physiological variables (14 total). All treatments, species, and timepoints are collapsed into one figure to assess which variables are highly correlated and redundant to include in multivariate analyses. Dark blue indicates highly positively correlated (value of 1) and dark red indicates highly negatively correlated (value of -1). The size of the dot in each cell indicates the degree of correlation so that a larger dot is a higher correlation. Gross photosynthetic rates and net photosynthetic rates were highly positively correlated and therefore only net photosynthetic rates were included in multivariate analyses.

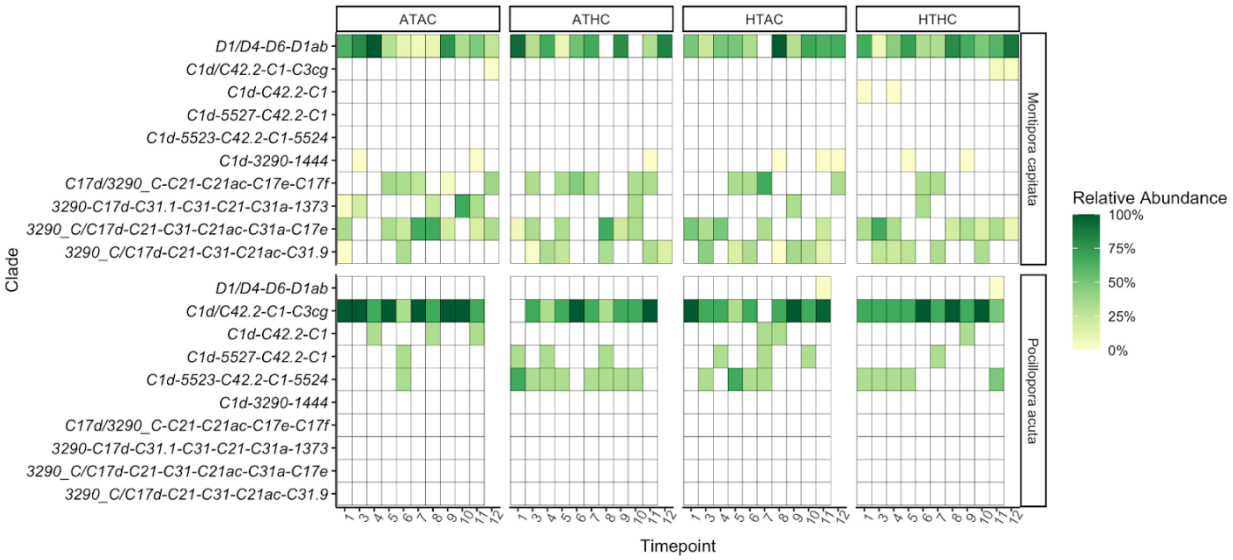

Fig. S17. Relative abundance (%) of ITS2 Symbiodiniaceae Type Profiles. Each individual square is the average percent relative abundance per treatment per time point per species (n=3). The four column sections indicate treatments (ATAC, ATHC, HTAC, and HTHC) and the two row sections indicate host species (*Montipora capitata* and *Pocillopora acuta*). The following time points are included in the exposure period: 0 hour, 6 hour, 12 hour, 30 hour, 1, 2, 4, 6, and 8 weeks. The vertical dotted line indicates the start of the recovery period, which includes 12 and 16 weeks. *P. acuta* samples were only collected through week 12. Each square is colored by percentage relative abundance, with 100% as the darkest green and 0% as white. In the ITS2 Type Profile name, the major sequence is bolded, followed by the rest of the full type profile name.

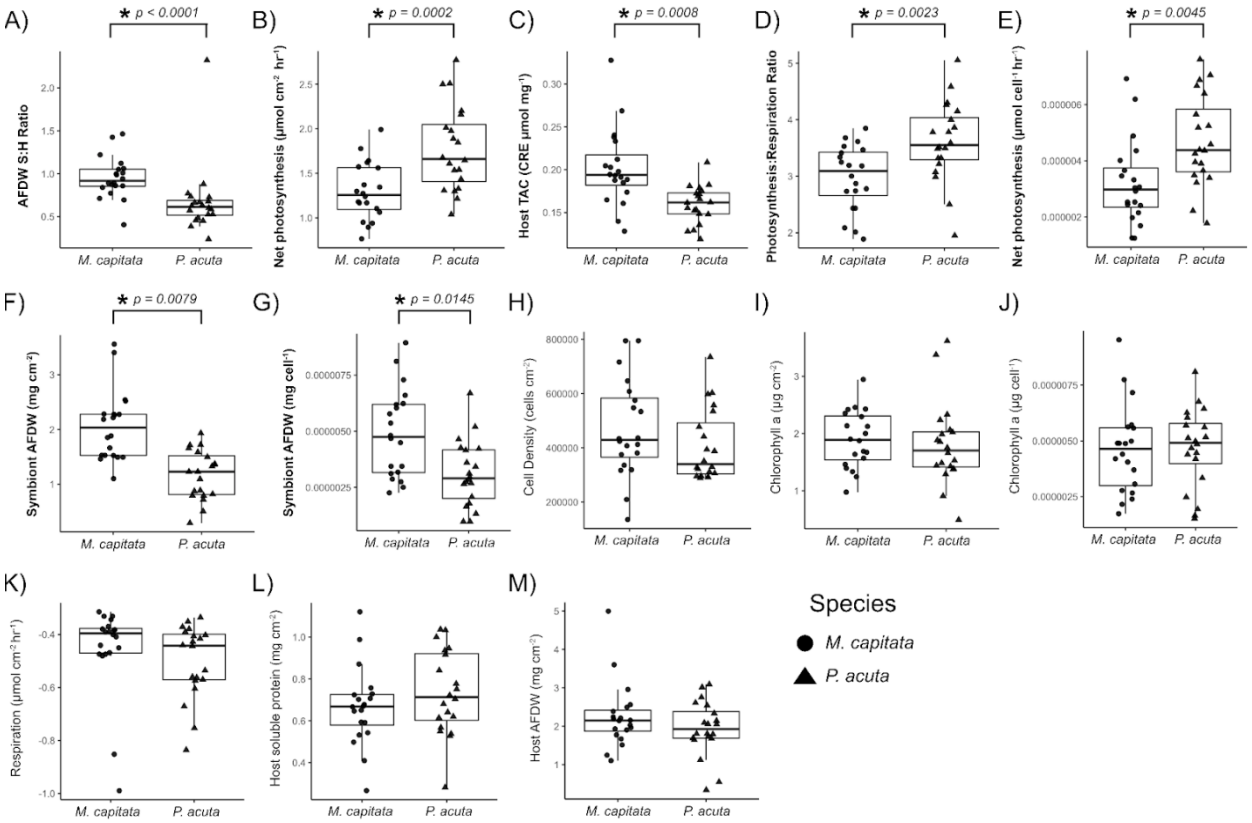

Fig S18. Baseline physiological measurements from week 1 ordered by most significant differences to least. (A) Ash-free dry weight symbiont:host ratio, (B) Holobiont net photosynthetic rates (µmol cm^{-2} hr^{-1}), (C) Host total antioxidant capacity (CRE µmol mg^{-1}), (D) Photosynthesis:Respiration ratio, (E) Cellular net photosynthetic rates (µmol $cell^{-1}$ hr^{-1}), (F) Symbiont AFDW (mg cm^{-2}), (G) Symbiont cellular AFDW (mg $cell^{-1}$), (H) Endosymbiont cell density (cells cm^{-2}), (I) Holobiont chlorophyll-a-a content (µg cm^{-2}), (J) Symbiont cellular chlorophyll-a-a content (µg $cell^{-1}$), (K) Host respiration rates (µmol cm^{-2} hr^{-1}), (L) Host soluble protein (mg cm^{-2}), (M) Host AFDW (mg cm^{-2}). *M. capitata* indicated by circles and *P. acuta* samples indicated by triangles.

Total Alkalinity: Stress Period

Treatment	*N*	*Mean*	*St. Error*
ATAC	48	2159.06	5.89
ATHC	48	2162.74	5.49
HTAC	48	2155.58	5.25
HTHC	48	2156.79	5.31

*Timepoint * Treatment + (1 | Tank)*

Effect	X^2	*df*	*P*
Timepoint	170.0467	15	**< 0.0001**
Treatment	1.1034	3	0.7762
Timepoint:Treatment	43.8277	45	0.5126

Table S1. Total Alkalinity sample size (N), mean, and standard error (St. Error) output from the exposure period for each treatment. A linear mixed model was run to determine the effects of treatment and time point on tank conditions.

*aov: PAR ~ Position * Tank*

Effect	*df*	*Sum of Sq*	*Mean Sq*	*F*	*Pr(>F)*
Position	5	23764	4753	0.155	0.978
Tank	11	498085	45280	1.475	0.143
Position:Tank	55	120265	2187	0.071	1.000

Light Summary Data: Stress Period

Treatment	*N*	*Mean*	*St. Error*
ATAC	212	179.70	9.97
ATHC	211	186.54	10.20
HTAC	210	176.64	10.84
HTHC	211	165.12	10.41

lmer: Treatment + (1 | Date) + (1 | Tank)

Effect	X^2	*df*	*P*
Treatment	2.0687	3	0.5583

Table S2. Light (PAR) output: sample size (N), mean, and standard error (St. Error) output from the exposure period for each treatment. A linear mixed model was run to determine the effects of treatment on tank conditions.

Stress Treatment Period

Montipora capitata

Dependent Variable	Effect	X^2	*df*	*P*
Respiration	**Timepoint**	19.7897	4	**0.0005**
(µmol cm^{-2} h^{-1})	**Temperature**	5.3829	1	**0.0203**
	CO2	0.2874	1	0.5919
	Timepoint:Temperature	3.5403	4	0.4718
	Timepoint:CO2	2.8987	4	0.5749
	Temperature:CO2	0.1348	1	0.7135
	Timepoint:Temperature:CO2	3.7495	4	0.4410
Net Photosynthesis	**Timepoint**	14.4620	4	**0.0060**
(µmol cm^{-2} h^{-1})	**Temperature**	18.1524	1	**< 0.0001**
	CO2	1.9896	1	0.1584
	Timepoint:Temperature	13.8077	4	**0.0079**
	Timepoint:CO2	9.1105	4	0.0584
	Temperature:CO2	1.5185	1	0.2178
	Timepoint:Temperature:CO2	9.0938	4	0.0588
Net Photosynthesis	**Timepoint**	13.5702	4	**0.0088**
(µmol cell^{-1} h^{-1})	Temperature	1.8312	1	0.1760
	CO2	0.3743	1	0.5407
	Timepoint:Temperature	1.6383	4	0.8019
	Timepoint:CO2	4.1280	4	0.3890
	Temperature:CO2	0.0064	1	0.9360
	Timepoint:Temperature:CO2	6.2204	4	0.1833
Gross Photosynthesis	**Timepoint**	21.1984	4	**0.0003**
(µmol cm^{-2} h^{-1})	**Temperature**	22.3058	1	**< 0.0001**
	CO2	0.3925	1	0.5310
	Timepoint:Temperature	15.5217	4	**0.0037**
	Timepoint:CO2	11.9872	4	**0.0174**
	Temperature:CO2	2.2441	1	0.1341
	Timepoint:Temperature:CO2	11.0932	4	**0.0255**
P:R Ratio	Timepoint	8.5378	4	0.0738
	Temperature	0.0187	1	0.8913
	CO2	3.4479	1	0.0633
	Timepoint:Temperature	2.2871	4	0.6831
	Timepoint:CO2	0.3761	4	0.9844
	Temperature:CO2	0.3484	1	0.5550
	Timepoint:Temperature:CO2	1.0685	4	0.8992

Pocillopora acuta

Dependent Variable	Effect	X^2	*df*	*P*
Respiration	**Timepoint**	87.4169	4	**< 0.0001**
(µmol cm^{-2} h^{-1})	**Temperature**	40.3078	1	**< 0.0001**
	CO2	0.3721	1	0.5419
	Timepoint:Temperature	9.9564	4	**0.0412**
	Timepoint:CO2	2.2023	4	0.6986
	Temperature:CO2	0.4268	1	0.5136
	Timepoint:Temperature:CO2	7.8998	4	0.0953
Net Photosynthesis	**Timepoint**	51.8737	4	**< 0.0001**
(µmol cm^{-2} h^{-1})	**Temperature**	61.5502	1	**< 0.0001**
	CO2	0.0146	1	0.9038
	Timepoint:Temperature	34.5005	4	**< 0.0001**
	Timepoint:CO2	2.3684	4	0.6684
	Temperature:CO2	0.7537	1	0.3853
	Timepoint:Temperature:CO2	7.6865	4	0.1038
Net Photosynthesis	**Timepoint**	29.9940	4	**< 0.0001**
(µmol cell^{-1} h^{-1})	**Temperature**	29.7790	1	**< 0.0001**
	CO2	2.8160	1	0.5957
	Timepoint:Temperature	18.3100	4	**0.001073**
	Timepoint:CO2	3.7644	4	0.4388
	Temperature:CO2	2.4520	1	0.1174
	Timepoint:Temperature:CO2	5.6688	4	0.2253
Gross Photosynthesis	**Timepoint**	58.0206	4	**< 0.0001**
(µmol cm^{-2} h^{-1})	**Temperature**	60.0036	1	**< 0.0001**
	CO2	0.3337	1	0.5635
	Timepoint:Temperature	24.9031	4	**< 0.0001**
	Timepoint:CO2	1.7910	4	0.7741
	Temperature:CO2	0.3442	1	0.5574
	Timepoint:Temperature:CO2	7.1393	4	0.1287
P:R Ratio	Timepoint	1.8573	4	0.7620
	Temperature	9.1988	1	**0.0024**
	CO2	0.8475	1	0.3573
	Timepoint:Temperature	12.5200	4	**0.0139**
	Timepoint:CO2	0.5815	4	0.9651
	Temperature:CO2	0.0370	1	0.8475
	Timepoint:Temperature:CO2	2.3578	4	0.6703

Table S3. Statistical output for metabolic (photosynthetic and respiration) rates normalized to both surface area (cm^{-2}) and cell density (cell^{-1}). Left: *M. capitata*. Right: *P. acuta*.

Stress Treatment Period

Montipora capitata

Dependent Variable	Effect	X^2	*df*	*P*
Host soluble protein	**Timepoint**	28.6767	4	**< 0.0001**
mg cm^{-2}	Temperature	1.6554	1	0.1982
	CO2	1.4948	1	0.2215
	Timepoint:Temperature	9.6751	4	**0.0463**
	Timepoint:CO2	22.1155	4	**0.0002**
	Temperature:CO2	0.2089	1	0.6476
	Timepoint:Temperature:CO2	3.8747	4	0.4232
Host total antioxidant capacity (TAC)	Timepoint	3.3971	4	0.4937
	Temperature	1.2026	1	0.2728
CRE µmol (mg prot)$^{-1}$	CO2	0.2111	1	0.6459
	Timepoint:Temperature	5.7398	4	0.2194
	Timepoint:CO2	2.3971	4	0.6632
	Temperature:CO2	0.2418	1	0.6229
	Timepoint:Temperature:CO2	2.1796	4	0.7028
Chlorophyll-a	**Timepoint**	21.1924	4	**0.0003**
ug cm^{-2}	**Temperature**	15.8058	1	**< 0.0001**
	CO2	0.7297	1	0.3930
	Timepoint:Temperature	13.5381	4	**0.0089**
	Timepoint:CO2	5.0723	4	0.2800
	Temperature:CO2	0.1355	1	0.7128
	Timepoint:Temperature:CO2	3.5923	4	0.4640
Chlorophyll-a	Timepoint	7.2542	4	0.1231
ug $cell^{-1}$	Temperature	3.0607	1	0.0802
	CO2	2.2806	1	0.1310
	Timepoint:Temperature	4.2774	4	0.3698
	Timepoint:CO2	1.9902	4	0.7376
	Temperature:CO2	0.2751	1	0.5999
	Timepoint:Temperature:CO2	4.2725	4	0.3704
Endosymbiont density	**Timepoint**	34.9996	4	**< 0.0001**
cells cm^{-2}	**Temperature**	8.4654	1	**0.0036**
	CO2	0.0533	1	0.8173
	Timepoint:Temperature	13.2732	4	**0.0100**
	Timepoint:CO2	8.4822	4	0.0754
	Temperature:CO2	5.0336	1	**0.0249**
	Timepoint:Temperature:CO2	5.3255	4	0.2555

Pocillopora acuta

Dependent Variable	Effect	X^2	*df*	*P*
Host soluble protein	**Timepoint**	31.4707	4	**< 0.0001**
mg cm^{-2}	**Temperature**	10.7168	1	**0.0011**
	CO2	0.1423	1	0.7060
	Timepoint:Temperature	9.5372	4	**0.0490**
	Timepoint:CO2	0.6262	4	0.9601
	Temperature:CO2	0.0761	1	0.7827
	Timepoint:Temperature:CO2	8.6149	4	0.0715
Host total antioxidant capacity (TAC)	Timepoint	5.5116	4	0.2387
	Temperature	1.5631	1	0.2387
CRE µmol (mg prot)$^{-1}$	CO2	0.0277	1	0.8679
	Timepoint:Temperature	11.2675	4	**0.0237**
	Timepoint:CO2	2.9275	4	0.5700
	Temperature:CO2	0.0066	1	0.9351
	Timepoint:Temperature:CO2	1.3579	4	0.8515
Chlorophyll-a	**Timepoint**	27.8694	4	**< 0.0001**
ug cm^{-2}	**Temperature**	18.5191	1	**< 0.0001**
	CO2	0.6615	1	0.4160
	Timepoint:Temperature	25.1913	4	**< 0.0001**
	Timepoint:CO2	2.8095	4	0.5902
	Temperature:CO2	0.1432	1	0.7051
	Timepoint:Temperature:CO2	6.3085	4	0.1773
Chlorophyll-a	Timepoint	9.3925	4	0.0520
ug $cell^{-1}$	**Temperature**	5.3056	1	**0.0213**
	CO2	0.1696	1	0.6804
	Timepoint:Temperature	8.4497	4	**0.0764**
	Timepoint:CO2	1.9180	4	0.7508
	Temperature:CO2	0.0055	1	0.9408
	Timepoint:Temperature:CO2	1.8844	4	0.7570
Endosymbiont density	**Timepoint**	28.9709	4	**< 0.0001**
cells cm^{-2}	**Temperature**	25.8864	1	**< 0.0001**
	CO2	0.0001	1	0.9905
	Timepoint:Temperature	36.2584	4	**< 0.0001**
	Timepoint:CO2	3.6063	4	0.4619
	Temperature:CO2	0.7820	1	0.3765
	Timepoint:Temperature:CO2	4.6170	4	0.3289

Recovery Period

Montipora capitata

Dependent Variable	Effect	X^2	*df*	*P*
Host soluble protein	Timepoint	1.2029	1	0.2727
mg cm^{-2}	Temperature	1.2085	1	0.2716
	CO2	0.4967	1	0.4810
	Timepoint:Temperature	4.3028	1	**0.0381**
	Timepoint:CO2	0.1406	1	0.7077
	Temperature:CO2	0.2735	1	0.6010
	Timepoint:Temperature:CO2	0.4454	1	0.5045
Host total antioxidant capacity (TAC)	Timepoint	0.446	1	0.5043
	Temperature	2.7182	1	0.0992
CRE µmol (mg prot)$^{-1}$	CO2	0.4044	1	0.5248
	Timepoint:Temperature	4.8473	1	**0.0277**
	Timepoint:CO2	0.0354	1	0.8507
	Temperature:CO2	0.0317	1	0.8586
	Timepoint:Temperature:CO2	0.2589	1	0.6109
Chlorophyll-a	Timepoint	1.7639	1	0.1841
ug cm^{-2}	**Temperature**	20.1042	1	**< 0.0001**
	CO2	0.0496	1	0.8237
	Timepoint:Temperature	0.458	1	0.4986
	Timepoint:CO2	0.2575	1	0.6118
	Temperature:CO2	0.0059	1	0.9389
	Timepoint:Temperature:CO2	2.2585	1	0.1329
Chlorophyll-a	**Timepoint**	4.4612	1	**0.0347**
ug $cell^{-1}$	Temperature	0.869	1	0.3512
	CO2	2.2783	1	0.1312
	Timepoint:Temperature	0.929	1	0.3351
	Timepoint:CO2	0.7022	1	0.4020
	Temperature:CO2	0.0001	1	0.9907
	Timepoint:Temperature:CO2	0.2732	1	0.6012
Endosymbiont density	Timepoint	1.5153	1	0.2183
cells cm^{-2}	**Temperature**	7.2667	1	**0.0070**
	CO2	2.2871	1	0.1305
	Timepoint:Temperature	1.3407	1	0.2469
	Timepoint:CO2	0.1552	1	0.6936
	Temperature:CO2	0.1244	1	0.7244
	Timepoint:Temperature:CO2	0.9057	1	0.3413

Table S4. Statistical output for host soluble protein, host total antioxidant capacity, chlorophyll-a-a content, and endosymbiont densities during the exposure period for both *M. capitata* and *P. acuta* and the recovery period for *M. capitata.*

Stress Treatment Period

Montipora capitata

Dependent Variable	Effect	X^2	*df*	*P*
Host AFDW	**Timepoint**	14.8616	4	**0.0050**
mg cm^{-2}	Temperature	1.9343	1	0.1643
	CO2	0.6814	1	0.4091
	Timepoint:Temperature	1.0511	4	0.9020
	Timepoint:CO2	4.3846	4	0.3564
	Temperature:CO2	0.7694	1	0.3804
	Timepoint:Temperature:CO2	7.4577	4	0.1136
Symbiont AFDW	**Timepoint**	17.8198	4	**0.0013**
mg cm^{-2}	Temperature	1.2744	1	0.2589
	CO2	0.0635	1	0.8010
	Timepoint:Temperature	2.2496	4	0.6900
	Timepoint:CO2	2.105	4	0.7165
	Temperature:CO2	0.8867	1	0.3464
	Timepoint:Temperature:CO2	4.1668	4	0.3839
Symbiont AFDW	**Timepoint**	23.2685	4	**0.0001**
mg $cell^{-1}$	Temperature	2.064	1	0.1508
	CO2	0.6042	1	0.4370
	Timepoint:Temperature	8.7003	4	0.0690
	Timepoint:CO2	8.6447	4	0.0706
	Temperature:CO2	6.1314	1	**0.0133**
	Timepoint:Temperature:CO2	1.9128	4	0.7518
Symbiont:Host Ratio	Timepoint	9.1648	4	0.0571
	Temperature	0.3193	1	0.5720
	CO2	1.2031	1	0.2727
	Timepoint:Temperature	0.4943	4	0.9741
	Timepoint:CO2	6.4993	4	0.1648
	Temperature:CO2	0.2733	1	0.6011
	Timepoint:Temperature:CO2	3.1485	4	0.5333

Pocillopora acuta

Dependent Variable	Effect	X^2	*df*	*P*
Host AFDW	**Timepoint**	11.8141	4	**0.0188**
mg cm^{-2}	Temperature	3.3048	1	0.0691
	CO2	0.4392	1	0.5075
	Timepoint:Temperature	2.2453	4	0.6907
	Timepoint:CO2	1.8383	4	0.7655
	Temperature:CO2	1.6816	1	0.1947
	Timepoint:Temperature:CO2	2.5394	4	0.6376
Symbiont AFDW	**Timepoint**	16.1781	4	**0.0028**
mg cm^{-2}	Temperature	1.5581	1	0.2120
	CO2	1.6089	1	0.2046
	Timepoint:Temperature	6.0128	4	0.1982
	Timepoint:CO2	5.5813	4	0.2327
	Temperature:CO2	0.9101	1	0.3401
	Timepoint:Temperature:CO2	4.2046	4	0.3790
Symbiont AFDW	**Timepoint**	12.4879	4	**0.0141**
mg $cell^{-1}$	**Temperature**	12.4936	1	**0.0004**
	CO2	1.2175	1	0.2699
	Timepoint:Temperature	54.2688	4	**< 0.0001**
	Timepoint:CO2	12.4029	4	**0.0146**
	Temperature:CO2	0.0764	1	0.7822
	Timepoint:Temperature:CO2	1.0241	4	0.9061
Symbiont:Host Ratio	**Timepoint**	13.5081	4	**0.0090**
	Temperature	5.5936	1	**0.0180**
	CO2	0.3185	1	0.5725
	Timepoint:Temperature	4.2439	4	0.3740
	Timepoint:CO2	6.6815	4	0.1537
	Temperature:CO2	0.2966	1	0.5860
	Timepoint:Temperature:CO2	4.1574	4	0.3851

Recovery Period

Montipora capitata

Dependent Variable	Effect	X^2	*df*	*P*
Host AFDW	Timepoint	0.5857	4	0.4441
mg cm^{-2}	Temperature	0.3283	1	0.5666
	CO2	0.4115	1	0.5212
	Timepoint:Temperature	0.1518	4	0.6968
	Timepoint:CO2	0.0118	4	0.9136
	Temperature:CO2	0.0139	1	0.9061
	Timepoint:Temperature:CO2	0.9804	4	0.3221
Symbiont AFDW	Timepoint	3.0004	4	0.0832
mg cm^{-2}	Temperature	2.3528	1	0.1251
	CO2	1.0417	1	0.3074
	Timepoint:Temperature	1.8469	4	0.1741
	Timepoint:CO2	0.6433	4	0.4225
	Temperature:CO2	0.6127	1	0.4338
	Timepoint:Temperature:CO2	0.2205	4	0.6386
Symbiont AFDW	Timepoint	0.3926	4	0.5309
mg $cell^{-1}$	Temperature	2.8253	1	0.0928
	CO2	4.6844	1	**0.0304**
	Timepoint:Temperature	8.2396	4	**0.0041**
	Timepoint:CO2	1.0486	4	0.3058
	Temperature:CO2	0.0088	1	0.9254
	Timepoint:Temperature:CO2	0.1601	4	0.6891
Symbiont:Host Ratio	Timepoint	0.2829	4	0.5948
	Temperature	1.5012	1	0.2205
	CO2	0.0007	1	0.9794
	Timepoint:Temperature	1.7413	4	0.1870
	Timepoint:CO2	0.5863	4	0.4438
	Temperature:CO2	0.0001	1	0.9926
	Timepoint:Temperature:CO2	0.8463	4	0.3576

Table S5. Statistical output for tissue biomass measurements: host AFDW, symbiont AFDW normalized to both surface area (cm^{-2}) and cell density ($cell^{-1}$), and symbiont:host AFDW Ratio for both species during the exposure and the recovery period for *M. capitata*.

Buoyant Weight

Montipora capitata

Time Period	Effect	X^2	*df*	*P*
Stress	**Timepoint**	32.815	4	**< 0.0001**
	Temperature	0.2465	1	0.6195
	CO2	0.0469	1	0.8285
	Timepoint:Temperature	14.516	4	**0.0058**
	Timepoint:CO2	21.1175	4	**0.0003**
	Temperature:CO2	0.022	1	0.8820
	Timepoint:Temperature:CO2	32.3638	4	**< 0.0001**
Recovery	**Timepoint**	12.1538	4	**0.0069**
	Temperature	12.1538	1	**< 0.0001**
	CO2	1.1876	1	0.2758
	Timepoint:Temperature	28.2451	4	**< 0.0001**
	Timepoint:CO2	15.1806	4	**0.0017**
	Temperature:CO2	1.9284	1	0.1649
	Timepoint:Temperature:CO2	11.9167	4	**0.0077**

Pocillopora acuta

Time Period	Effect	X^2	*df*	*P*
Stress	**Timepoint**	47.5441	4	**< 0.0001**
	Temperature	3.2183	1	0.0728
	CO2	9.0017	1	**0.0027**
	Timepoint:Temperature	16.0271	4	**0.0030**
	Timepoint:CO2	16.2463	4	**0.0027**
	Temperature:CO2	2.3846	1	0.1225
	Timepoint:Temperature:CO2	4.5003	4	0.3425

Color Score

Montipora capitata

Time Period	Effect	X^2	*df*	*P*
Stress	Timepoint	3.3689	7	0.8489
	Temperature	0.0019	1	0.9655
	CO2	0.0001	1	0.9916
	Timepoint:Temperature	26.3114	7	**0.0004**
	Timepoint:CO2	1.8481	7	0.9678
	Temperature:CO2	0.0753	1	0.7837
	Timepoint:Temperature:CO2	26.5600	7	**0.0004**
Recovery	Timepoint	4.4963	3	0.7212
	Temperature	4.3216	1	**0.0376**
	CO2	0.0016	1	0.9680
	Timepoint:Temperature	87.9628	3	**< 0.0001**
	Timepoint:CO2	10.1081	3	0.1825
	Temperature:CO2	3.242	1	0.0718
	Timepoint:Temperature:CO2	17.8984	3	**0.0124**

Pocillopora acuta

Time Period	Effect	X^2	*df*	*P*
Stress	**Timepoint**	41.936	7	**< 0.0001**
	Temperature	0.0074	1	0.9312
	CO2	0.052	1	0.8196
	Timepoint:Temperature	57.1031	7	**< 0.0001**
	Timepoint:CO2	95.8169	7	**< 0.0001**
	Temperature:CO2	0.0231	1	0.8792
	Timepoint:Temperature:CO2	49.8236	7	**< 0.0001**
Recovery *(week 9-12)*	Timepoint	5.8895	3	0.1171
	Temperature	34.8274	1	**< 0.0001**
	CO2	3.9797	1	**0.0461**
	Timepoint:Temperature	1.2276	3	0.7464
	Timepoint:CO2	6.781	3	0.0792
	Temperature:CO2	0.0042	1	0.9485
	Timepoint:Temperature:CO2	0.509	3	0.9169

Table S6. Statistical output for calcification growth rates and color score for both species during the exposure and recovery period.

Survivorship Probability

Montipora capitata

Type III Anova	Effect	*df*	X^2	*P*
	Temperature	1	21.004	**< 0.0001**
	CO2	1	11.4891	**0.0007**
	Temperature:CO2	1	0.2914	0.5893

Cox mixed-effects model fit by maximum likelihood	Effect	*coef*	*exp(coef)*	*se(coef)*	*z*	*p*
Surv(lifespan, status) ~ Temperature * CO2 + (1|PLUG.ID/Tank)	**High Temperature**	1.1421189	3.133401	0.2492068	4.58	**< 0. 0001**
	High CO2	0.7981529	2.221434	0.2354737	3.39	**0.0007**
	High Temp: High CO2	0.1732892	1.18921	0.3210069	0.54	0.5900

	NULL	*Integrated*	*Fitted*
Log-likelihood	-7359.299	-5183.304	-4472.52

Pocillopora

Type III Anova	Effect	*df*	X^2	*P*
	Temperature	1	2.2173	0.1365
	CO2	1	40.5412	**< 0.0001**
	Temperature:CO2	1	79.9506	**< 0.0001**

Cox mixed-effects model fit by maximum likelihood	Effect	*coef*	*exp(coef)*	*se(coef)*	*z*	*p*
Surv(lifespan, status) ~ Temperature * CO2 + (1|PLUG.ID/Tank)	**High Temperature**	-0.9585059	0.383	0.6436949	-1.49	**0.1400**
	High CO2	-4.4442835	0.012	0.6979973	-6.37	**< 0.0001**
	High Temp: High CO2	7.8613358	2594.984	0.8791956	8.94	**< 0.0001**

	NULL	*Integrated*	*Fitted*
Log-likelihood	-24130.77	NaN	-18100.5

Table S7. Statistical output from survival probability models for both *M. capitata* and *P. acuta* throughout the entire experiment.

Species Comparison (all samples at Week 1)

Dependent Variable	*t*	*df*	*P*
Host total antioxidant capacity (TAC) CRE µmol (mg prot)$^{-1}$	3.7566	27.413	**0.0008**
Host soluble protein mg cm^{-2}	-1.0843	37.811	0.2851
Respiration (µmol cm^{-2} h^{-1})	1.2234	44.266	0.2276
Gross Photosynthesis (µmol cm^{-2} h^{-1})	-3.4385	44.001	**0.0013**
Net Photosynthesis (µmol cm^{-2} h^{-1})	-4.0388	40.851	**0.0002**
Net Photosynthesis (µmol cell^{-1} h^{-1})	-3.0230	37.777	**0.0045**
P:R Ratio	-3.2361	45.631	**0.0023**
Endosymbiont Density cells cm^{-2}	1.8842	229.730	0.0608
Chlorophyll-a concentration ug cm^{-2}	0.4576	33.717	0.6502
Chlorophyll-a concentration ug cell^{-1}	-0.1252	37.549	0.9011
Host AFDW mg cm^{-2}	1.2561	36.851	0.2170
Symbiont AFDW mg cell^{-1}	2.5909	30.642	**0.0145**
Symbiont AFDW mg cm^{-2}	2.8515	28.989	**0.0079**
Symbiont:Host Ratio AFDW	5.0694	34.066	**< 0.0001**

Table S8. Statistical output for baseline physiological measurement comparison between *M. capitata* and *P. acuta* fragments at the initial week 1 measurement.

STRESS PERIOD

PERMANOVA: Timepoint * Temperature * CO2 * Species

Effect	*df*	*Sum of Squares*	*R2*	*F*	*Pr(>F)*
Timepoint	4	203.56	0.07022	5.4788	**0.001**
Temperature	1	130.16	0.04490	14.0127	**0.001**
CO2	1	13.74	0.00474	1.4789	0.166
Species	1	298.93	0.10311	32.1831	**0.001**
Timepoint:Temperature	4	115.98	0.04001	3.1218	**0.001**
Timepoint:CO2	4	69.68	0.02404	1.8755	**0.008**
Temperature:CO2	1	9.13	0.00315	0.9830	0.403
Timepoint:Species	4	145.09	0.05005	3.9051	**0.001**
Temperature:Species	1	21.56	0.00744	2.3213	**0.029**
CO2:Species	1	13.25	0.00457	1.4270	0.209
Timepoint:Temperature:CO2	4	62.88	0.02169	1.6926	**0.033**
Timepoint:Temperature:Species	4	32.22	0.01111	0.8672	0.652
Timepoint:CO2:Species	4	36.75	0.01268	0.9892	0.456
Temperature:CO2:Species	1	3.11	0.00107	0.3350	0.936
Timepoint:Temperature:CO2:Species	4	33.88	0.01169	0.9119	0.545

Montipora capitata PERMANOVA: Timepoint * Temperature * CO2

Effect	*df*	*Sum of Squares*	*R2*	*F*	*Pr(>F)*
Timepoint	4	184.65	0.12682	4.2291	**0.001**
Temperature	1	39.29	0.02699	3.5995	**0.005**
CO2	1	20.27	0.01393	1.8574	0.091
Timepoint:Temperature	4	60.73	0.04171	1.3909	0.099
Timepoint:CO2	4	71.81	0.04932	1.6447	**0.036**
Temperature:CO2	1	5.78	0.00397	0.5298	0.792
Timepoint:Temperature:CO2	4	58.28	0.04003	1.3349	0.135

Pocillopora acuta PERMANOVA: Timepoint * Temperature * CO2

Effect	*df*	*Sum of Squares*	*R2*	*F*	*Pr(>F)*
Timepoint	4	171.63	0.12002	4.3344	**0.001**
Temperature	1	139.81	0.09777	14.1231	**0.001**
CO2	1	4.67	0.00326	0.4716	0.824
Timepoint:Temperature	4	117.25	0.082	2.9611	**0.001**
Timepoint:CO2	4	42.69	0.02985	1.0781	0.377
Temperature:CO2	1	8.25	0.00577	0.8334	0.487
Timepoint:Temperature:CO2	4	44.86	0.03137	1.133	0.314

RECOVERY PERIOD

Montipora capitata PERMANOVA: Timepoint * Temperature * CO2

Effect	*df*	*Sum of Squares*	*R2*	*F*	*Pr(>F)*
Timepoint	4	40.95	0.0711	2.5587	**0.013**
Temperature	1	46.70	0.0811	5.8358	**0.002**
CO2	1	5.56	0.0097	0.6945	0.621
Timepoint:Temperature	4	29.98	0.0521	1.8732	0.060
Timepoint:CO2	4	14.18	0.0246	0.8861	0.507
Temperature:CO2	1	2.39	0.0042	0.2987	0.921
Timepoint:Temperature:CO2	4	12.08	0.0210	0.7550	0.661

Table S9. Statistical output from a permutational multivariate ANOVA (PERMANOVA) on the multivariate physiology states for each species during the exposure and the recovery period for M. capitata.

ITS2

PERMANOVA: Timepoint * Temperature * CO2 * Species

Effect	*df*	*Sum of Squares*	*R2*	*F*	*Pr(>F)*
Timepoint	10	119.18	0.04767	1.3438	**0.023**
Temperature	1	4.44	0.00178	0.5008	0.898
CO2	1	9.38	0.00375	1.0575	0.394
Species	1	329.71	0.13188	37.1762	**0.001**
Timepoint:Temperature	10	92.17	0.03687	1.0392	0.384
Timepoint:CO2	10	81.46	0.03258	0.9184	0.699
Temperature:CO2	1	13.62	0.00545	1.5361	0.121
Timepoint:Species	10	95.53	0.03821	1.1968	0.119
Temperature:Species	1	4.52	0.00181	0.5100	0.859
CO2:Species	1	9.32	0.00373	1.0505	0.407
Timepoint:Temperature:CO2	10	45.77	0.01831	0.5160	1.000
Timepoint:Temperature:Species	10	88.20	0.03528	1.1050	0.230
Timepoint:CO2:Species	10	69.92	0.02797	0.8760	0.776
Temperature:CO2:Species	1	13.35	0.00534	1.5057	0.138
Timepoint:Temperature:CO2:Species	10	42.32	0.01693	0.5302	1.000

Montipora capitata PERMANOVA: Timepoint * Temperature * CO2

Effect	*df*	*Sum of Squares*	*R2*	*F*	*Pr(>F)*
Timepoint	10	107.80	0.10286	1.3377	**0.030**
Temperature	1	7.88	0.00752	0.9782	0.457
CO2	1	6.37	0.00608	0.7903	0.593
Timepoint:Temperature	10	94.42	0.09010	1.1717	0.161
Timepoint:CO2	10	68.68	0.06554	0.8523	0.810
Temperature:CO2	1	10.94	0.01044	1.3573	0.215
Timepoint:Temperature:CO2	10	42.76	0.04080	0.5306	1.000

Pocillopora acuta PERMANOVA: Timepoint * Temperature * CO2

Effect	*df*	*Sum of Squares*	*R2*	*F*	*Pr(>F)*
Timepoint	10	44.00	0.07458	0.9719	0.501
Temperature	1	2.25	0.00381	0.4469	0.795
CO2	1	7.63	0.01292	1.5159	0.191
Timepoint:Temperature	10	55.42	0.09394	1.2242	0.177
Timepoint:CO2	10	40.50	0.06865	0.8946	0.630
Temperature:CO2	1	10.59	0.01795	2.1055	0.068
Timepoint:Temperature:CO2	10	32.21	0.05460	0.7115	0.916

Table S10. Statistical output from a permutational multivariate ANOVA (PERMANOVA) on the ITS2 full type profiles for each species for the entire time series.

Species	Metric	Sept 18 2018	Oct 17 2018	Oct 31 2018	Nov 15 2018
Montipora capitata	Am	0.95 ± 0.196	0.98 ± 0.178	0.81 ± 0.150	0.91 ± 0.328
	AQY	0.01 ± 0.001	0.01 ± 0.001	0.01 ± 0.001	0.01 ± 0.003
	Ic	40.40 ± 5.467	40.96 ± 5.092	38.02 ± 5.459	25.38 ± 2.962
	Ik	164.08 ± 14.970	163.35 ± 22.658	126.51 ± 6.308	83.19 ± 7.270
	Rd	0.22 ± 0.041	0.23 ± 0.028	0.22 ± 0.034	0.25 ± 0.066
Pocillopora acuta	Am	1.19 ± 0.257	0.89 ± 0.144	0.50 ± 0.079	0.36 ± 0.120
	AQY	0.005 ± 0.001	0.005 ± 0.001	0.004 ± 0.001	0.004 ± 0.001
	Ic	64.40 ± 8.240	58.28 ± 4.172	54.16 ± 4.208	50.12 ± 20.932
	Ik	246.29 ± 26.716	190.53 ± 9.757	121.90 ± 5.651	95.21 ± 7.303
	Rd	0.30 ± 0.069	0.26 ± 0.038	0.21 ± 0.040	0.12 ± 0.031

Table S11. Photosynthetic curve output (mean ± standard error, n=4) for maximal photosynthetic rate (Am; µmol O_2 cm^{-2} h^{-1}), apparent quantum yield (AQY, ф; mol O_2 mol $photons^{-1}$), Compensation irradiance (IC; PAR), saturating irradiance (I_k; PAR), and light enhanced dark respiration rate (Rd; µmol O_2 cm^{-2} h^{-1}).